Filters in Nuclear Medicine

Rafael Puchal Añé

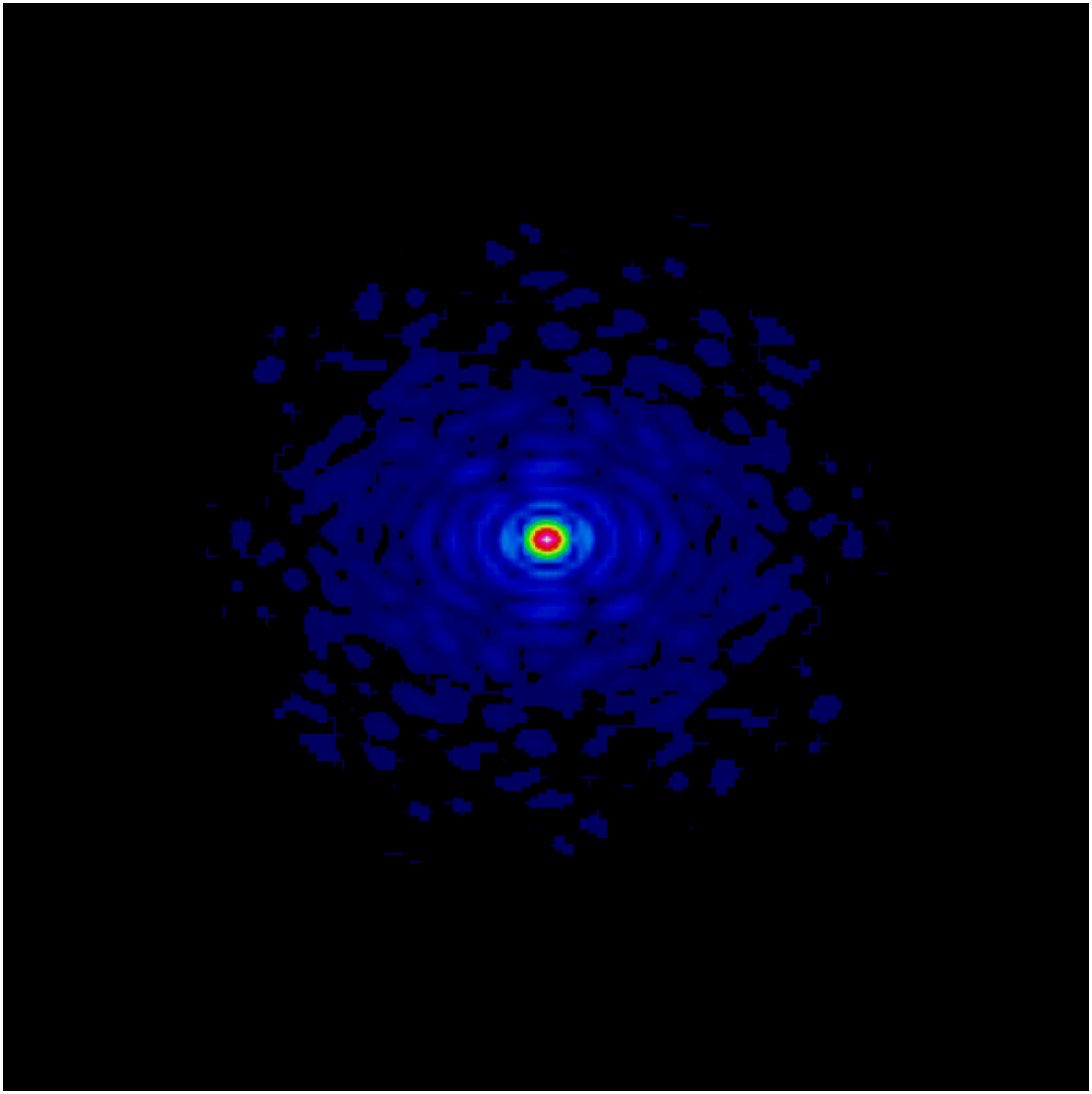

Barcelona-2019

This book is an adapted and revised English translation from the original "Filtros en Medicina Nuclear" submitted to https://archive.org/ in June 2017.

Author´s e-mail: rafelpuchal@gmail.com

To Cuquina

Contents

1 Preface 6

2 What is "a filter"?

2.1 Introduction 9

2.2 Nature of Nuclear Medicine Images 9

2.3 Direct representation of filters 10

3. Frequency representation of images

3.1 Introduction 16

3.2 Spatial Frequency 16

3.3 Sine functions 18

3.4 Frequency analysis in one dimension 20

3.5 Frequency analysis of images 24

3.6 Nuclear Medicine images 29

3.7 SPECT and PET images 36

3.7.1 Dependence on the number of counts 40

3.7.2 Distance between the collimator and the patient 41

3.7.3 Relationship between distance and matrix size 43

3.7.4 Effect of the number of projections 44

3.7.5 Reorientation of images 45

4. Imaging in Nuclear Medicine

4.1 Introduction 48

4.2 Limitations of the detection equipment 48

4.3 Planar gamma camera 50

4.3.1 Bar-phantom 51

4.3.2 Interference of collimators 56

4.4 Tomograph of positrons 56

4.5 Digitization dependence 62

4.6 Distance pacient-collimator dependence 66

4.7 Signal-to-noise dependence 67

5. Frequency filters

5.1 Introduction 70

5.2 Representation of frequency filters 70

5.3 Equivalence of filter representations 73

5.4 Types of filters 74

5.4.1 Ideal filters 75
5.4.2. Smoothing filters 77
5.4.3 Restoration filters 78
6. Tomographic reconstruction and filters
6.1 Introduction 82
6.2 Acquisition of tomographic studies 82
6.3 Reconstruction of tomographic studies 85
6.3.1 Filtered backprojection 86
6.3.2 Iterative Reconstruction 90
6.3.3 Iterations and frequency spectra 93
6.4 Pre-filtering and Post-filtering 97
6.4.1 Pre-filtering 97
6.4.2 Post-filtering 98
6.5 Quantitative aspects 99
6.5.1 Factors from the patient 100
6.5.2 Factors from the imaging devices 100
6.5.3 Factors from processing 101
6.5.4 Dependence of values with filters. An example. 101
Appendix 1 Filters implemented for SPECT and PET 106
Appendix 2 Note on units of frequencies 114
Bibliography 115

1 Preface

The correct application of filters to Nuclear Medicine images is not an easy subject. The difficulties inherent in the filtering added to the ones due to the radioactive origin of the images make filtering a problematic task. To filter means to enter into the field of things unclear. All people that have processed Nuclear Medicine studies have applied different filters in SPECT or PET by varying their parameters to see what happened: They have seen how different filters produce visually identical results and also how in changing a setting slightly, at times, very different images result. It may also happen that the recommended filters and those that appear in the literature produced disappointing results. On many occasions, people adhere to the preset filters by the manufacturers without knowing if they are optimal, trusting in their work.

The filters are not an invention of the SPECT or PET. In the first Nuclear Medicine computers already existed the possibility, albeit very limited, of filtering images and curves to decrease the statistical fluctuations. The incorporation of the tomographic techniques to the clinical routine has made the filters, which are a powerful and sophisticated mathematical tool, to acquire a particular relevance in several aspects, first, because of their ability to transform a whole study using a single command. Second, by being obliged to use them because without their application, the reconstructed studies are often incomprehensible. In third place because there is not a "unique filter with unique parameters" for every kind of study since the filters must be adapted to each imaging equipment. Each manufacturer has chosen to recommend a particular filter ("default") leaving the door open to be able to use other filters, each of them with one or more parameters, which generates a high number of possibilities and considerable uncertainty. This offer makes to use of the "option by default" very frequently, even knowing that better results could be achieved using other options.

New reconstruction methods are used to compensate for the degradations caused by the detection devices and by the physical processes involved. These corrections are the first step to obtain a correct quantitative estimation of the radioactivity distribution. The second step is to systematize the filters and processing procedures due to their influence on the values and images, which lead to a diagnose.

To understand how the filters act and how they are characterized and which consequences can be, it is needed to use concepts that, although they are not complicated, people are not used to them. Therefore this work aims to present to the Nuclear Medicine specialists the basic concepts to work appropriately within the scope of the filters. It is not intended to be exhaustive; it only wants to introduce a series of ideas that result ultimately in the quality of the diagnostic. The only thing that is trying to do is to answer three questions. What is filtering? How is a filter characterized? What types of filters SPECT and PET use? And thus facilitate their use.

Filters are procedures that are easy to explain using mathematical expressions. However, since in many cases this formalism is difficult to understand for people not familiar with mathematics, this work tries to describe and explain filters using a common language, although rigorous and precise. The only mathematical tool used profusely has been graphics, as they are of frequent use. The effects of the filters are easily described using the "frequency language." This language, apparently abstruse, is something usual in ordinary life, which allows using analogies based on the musical notation to explain it.

Two types of images are used to make more accessible the interpretation and comparison of results of the various filters. One type is the set of images obtained from a bar-phantom, which by its very nature, allows following the effects of manipulations. The other type corresponds to a brain phantom, which enables us to observe these effects in an image that is similar to a clinical one. It has been opted for this type of planar imaging to prevent the dependence with the reconstruction methods and to be able to observe their effects of varying some parameters. Another aspect that has been thought advisable to deal with is that of the different units of frequency that different computer manufacturers use in the filters. These differences are not banal since the same numeric value in a parameter can have different effects depending on the units of frequency used in the computer in question.

This work is the result of an in-depth review, update, and translation of previous work[1]. A new section includes a brief description of two methods of

[1] R.Puchal. Filtros de imagen en medicina nuclear.Ediciones Eurobook, S.L. 1997

tomographic reconstruction. Some comments are also made on the behavior of the iterative algorithms from the frequency point of view.

Some filters frequently used in clinical practice are presented in an appendix, as well as the different ways to express the spatial frequency in this context.

Finally, this text is not intended in any way to be an operations manual or a textbook. It is assumed that readers already have some experience and training in Nuclear Medicine and therefore the book does not go into issues that need to be known such as the operation of a gamma camera or the interaction of radiation with matter. Its objective is to inform all those who process Nuclear Medicine studies- physicians, technologists - an aspect of their work that usually is not detailed enough in the books of text or it is explained using some mathematical background which makes it difficult for their understanding. The book is also aimed at physicists who come into contact with Nuclear Medicine to inform them of specific topics that may not have seen in his or her qualifications or to focus on "nuclear medicine" ideas. This disparity of potential readers will no doubt make that some of them find the text difficult while others may find it sometimes trivial. The book intends, in some way, to revert to an improvement in some aspects of Nuclear Medicine processing. The final result of a PET or SPECT study depends not only on the quality of the equipment and on its use but also on the ability to using the appropriate processing, particularly filters. To do that is very important to have a minimal knowledge of their fundamentals, which is just another aspect of the quality assurance in Nuclear Medicine that this small book tries to fulfill.

I want to express my gratitude to all of the people that helped me to make this book, to the current members of the Nuclear Medicine Service at the Hospital Universitari de Bellvitge, in particular to Dr. Jaume Mora, Pablo Saldaña and Gabriel Reynes - for technical data and support to generate new examples. Finally, I would like to acknowledge the assistance provided by Joaquima Miralpeix for her criticism of the manuscript and the constructive discussions that they led to the final version.

2-What is "a filter"?

2.1 Introduction

A filter, in a first approximation, is a means of transforming a signal according to a preset pattern. There are numerous examples of filters: from sunglasses to the controls of bass and treble of the musical equipment. The filters modify the signals (light, sound) in a way set in advance: sunglasses always reduce in the same proportion the intensity of the radiation of specific wavelengths, a treble filter always reduces the same range of frequencies. In Nuclear Medicine every specialist has applied a "smoothing" to minimize random fluctuations in the activity ("noise"), making it more pleasing to the eye, on some images or curves: also in this case he has applied a filter. The programs that automatically detect contours use another type of filter. These "highlight" the differences to locate the edges of the organs. They are the so-called edge enhancement filters.

To understand what filters in Nuclear Medicine are and how they act is necessary to know first of all, how are the signals on which they work.

2.2 Nature of Nuclear Medicine Images

The images generated by equipment composed by a rotating gamma camera and a computer in SPECT represent the position, and the activity of the radiation detected. The representations (projections) are distributions of memory cells called matrices in which the value stored in each cell corresponds to the number of detections recorded in an area of the detector which, in turn, corresponds to a small volume of the patient. There is a correspondence between the position on the image (matrix) and the position in the patient. This type of representation is called the spatial domain.

In PET the images are obtained by reconstruction of the sinograms acquired with a tomograph for positrons (see section 6.2). Although not generated directly, the images produced in PET are also matrices whose cells represent the activity detected from inside the patient.

These matrices are two-dimensional arrays of numbers that, by codification (through color tables), we visualize as images in which each of its elements has a color associated with its numerical value. The same distribution of radioactivity (object) supports many representations, changing the color table or

the mathematical relationship between the level of counts and the associated color. It is important to note that this process does not alter the content of the cells, only its visual representation that is a pixel (a term that comes from the contraction of "picture element").

Radioactive decay is a random process, which means that if you make repeated measurements of the same source of radiation, the values obtained are different but spread around a particular value. These "oscillations" constitute the so-called noise which is intrinsic to the radioactivity, and that makes each measure to have uncertainty that reflects these "oscillations."

The measures from the radioactive decay follow a Poisson statistical distribution which means that if there is only a single measure, as is the case in the obtainment of clinical images, it is considered that the uncertainty of the number of counts is the square root of this number. It is important to note that this is only correct in the case of direct values or without mathematical manipulations that make to lose their "Poissonian" character.

In front of a uniform source of radiation, the uncertainty of each number of counts (noise) makes the value of each cell slightly different when it should be the same on all of them (these differences may result in changes of color in the image). The changes in the activity due to the patient are therefore corrupted by the variations due to the noise.

The relative importance of the signal from the noise measures the "statistical" quality of the images. When the counts come from direct images of a gamma camera, this signal-to-noise ratio depends only on the number of counts recorded in the area of interest, while in the reconstructions of SPECT and PET also depends on the size of the reconstructed area, the reconstruction method, and the filter used.

However, the higher the statistical quality of the original data, the higher the quality of the reconstructed images.

2.3 Direct representation of filters

A filter in the spatial domain is a transformation of one image into a new one. The values of the new image are calculated by adding and multiplying the values of the original image by weights or factors which constitute the filter. The result is another image, derived from cell to cell (pixel by pixel).

The number and the values of the weights determine the character of the filter. Given that the images are arrays of numbers, the filters for images also are arrays of numbers but smaller ("masks"). This way of applying filters is called convolution and consists of several steps:

Following the diagram in Figure 2.3.1, consider an area in the image "original" that we are going to filter. The values of their cells are a, b, c, ..., i, ... On the other hand, we will apply a mask of 3x3 values, and the result values will be a', b', c', ..., i',...

The way to obtain these values are:

1) center the filter mask in one pixel of the image (for example, the value-e).

2) multiply each cell covered by the mask by the weight of the filter according to its position and add up all the values. The result, in this case, is e'.

3) place the value obtained in the new image, at the same coordinates as in step #1, (e' in the same position as e).

4) go to the next pixel (In this example, f)

5) Repeat all the sequence until the end of the image (return to step #1 to calculate the new value f').

The values of the filtered image are obtained one by one.

Let's look at some examples of smoothing and enhancement. In both cases, the starting image is the image of a bar-phantom[2] obtained using a high-resolution collimator and at 0 cm distance (Figure 2.3.3).

[2] A bar-phantom consists of a perspex block with inserted bars of lead in such a way that the distance between them is equal to their thickness. A common bar-phantom has the bars arranged in 4 quadrants according to the thickness. The images allow estimating approximately the spatial resolution of the gamma cameras. There are also versions in 3 dimensions for the tomographic equipment check.(See section 4.3.1)

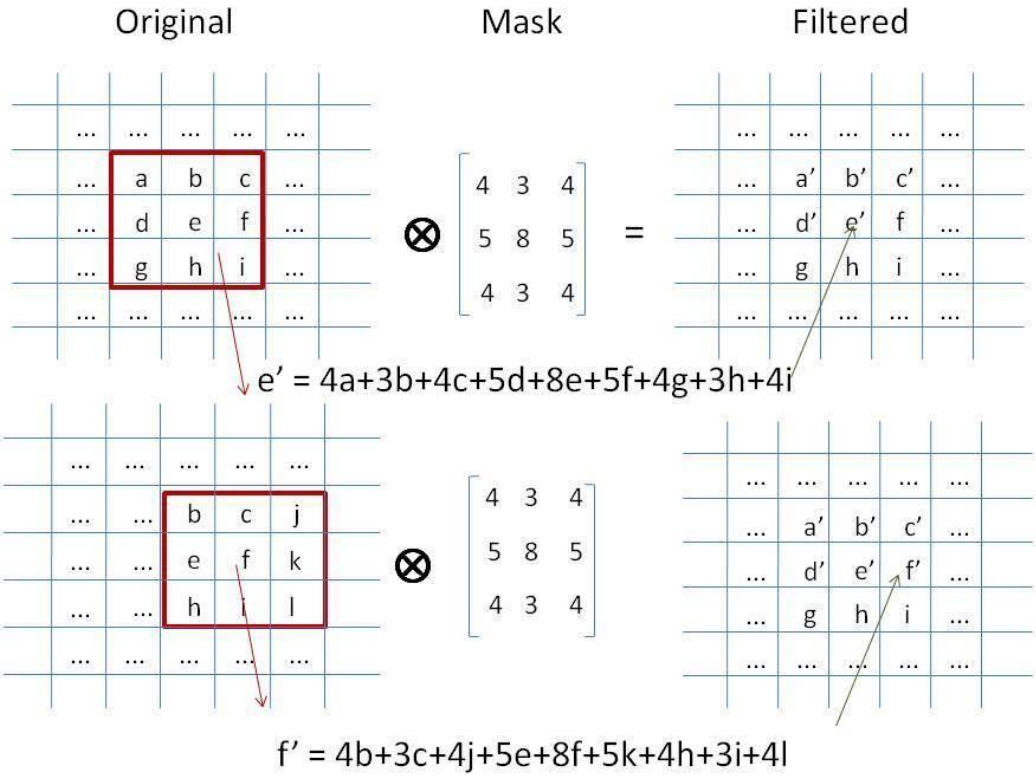

Fig 2.3.1: scheme of the convolution product of an image with a mask

Smoothing: To smooth a picture is to reduce the fluctuations due to the noise by trying to alter the signal the least possible (since it is not possible to separate the signal from the noise). One way is to decrease the differences between a pixel and its neighbors by replacing each pixel with a weighted average of itself with its neighbors. The decrease in these differences leads inescapably to decrease contrast and resolution. A smoothing filter very often used is defined by the weights 1,2,1;2,4,2;1,2,1 ordered according to the 3x3 matrix (Figure 2.3.2):

$$1/16\begin{pmatrix}1 & 2 & 1\\ 2 & 4 & 2\\ 1 & 2 & 1\end{pmatrix}$$

Fig.2.3.2: array or mask of a smoothing filter.

Figure 2.3.4 shows the effect of applying this filter to the image of the bar-phantom of Figure 2.3.3. The filtered image presents a more uniform appearance, having decreased the statistical fluctuations as well as the spatial

resolution since it is only distinguished the bars of the first and second quadrants that correspond to the bars of greater thickness while in the original are identified all the bars.

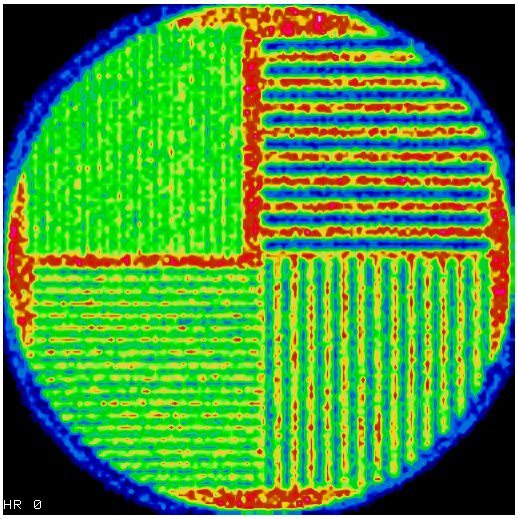

Fig.2.3.3: the original image of the phantom.

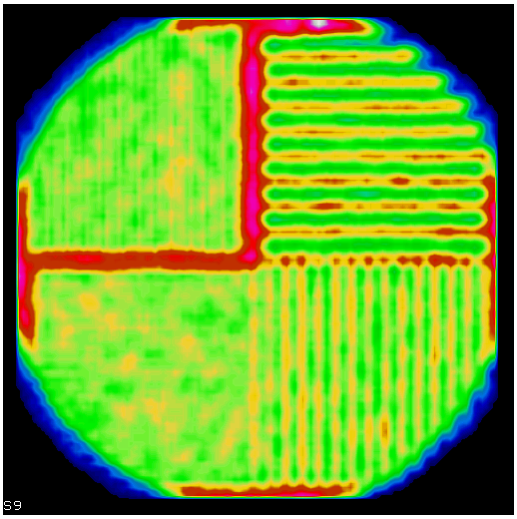

Fig.2.3.4: image after applying the smoothing filter

Edge detection: the filters used in the automatic detection of a contour, instead of reducing the differences between pixels, they highlight the sharp changes in the number of counts, that may correspond to the edges of organs or lesions. Figure 2.3.5 shows the mask of one of these filters.

$$\begin{pmatrix} 0 & -1 & 0 \\ -1 & 4 & -1 \\ 0 & -1 & 0 \end{pmatrix}$$

Fig.2.3.5: array or a filter mask.

If the noise level is high (which is very common in Nuclear Medicine) before applying a filter such as the latter that enhances outlines as variations due to the noise, it must be used first a smoothing: First, it reduces the noise, in the second place, it detects the contour. However, both types of filtering can be combined so that a single operation achieves both effects, for example, with the following mask (Figure 2.3.6):

$$\begin{pmatrix} -1 & -1 & -1 \\ -1 & 8 & -1 \\ -1 & -1 & -1 \end{pmatrix}$$

Fig.2.3.6: array or a filter mask contour detector.

Figure 2.3.7 shows the result of applying this filter to the same image as before (Figure 2.3.3). We note that the background has disappeared almost entirely and that the lines are sharper than before. As can be seen, the difference to the smoothing is striking.

The relationship between the size and weights of a filter in matrix form with the effect that produces is complicated. It is not easy to determine, in advance, for example, the degree of smoothing when varying the weights of the filter.

The use of use frequency filters is an alternative and an utterly equivalent way of filtering images. To understand what this means is necessary, first, to know what is meant by the frequency representation of images.

Fig.2.3.7: image result of applying a filter to detect edges in the image of the phantom.

Note: for the curious reader, the mathematical expression of the convolution in 2 dimensions using the smoothing filter of Figure 2.3.2 has the following expression:

$$S(i,j) = \frac{1}{16}\left\{\begin{matrix} 1 \cdot O(i-1,j-1) + 2 \cdot O(i,j-1) + 1 \cdot O(i+1,j-1) + \\ 2 \cdot O(i-1,j) + 4 \cdot O(i,j) + 2 \cdot O(i+1,j) + \\ 1 \cdot O(i-1,j+1) + 2 \cdot O(i,j+1) + 1 \cdot O(i+1,j+1) \end{matrix}\right\}$$

Where *O(i,j)* represents the values of the original matrix, *S(i,j)* of the image result (smoothed). The pixels are calculated by row and column. Using the classic matrix notation, the symbol "i" means the vertical position (rows) and the "j" the horizontal position (columns) being the first element (1,1) in the upper left-hand corner. According to that, the expression (i-1,j-1) refers to the point "up and to the left of the center point of the mask which is in (i, j), that is, in the previous row and the previous column. The (i,j-1) points to that of "above" (upper line), etc, until the (i+1,j+1) that points "to the right" (bottom row and next column).

Note that this mask is divided by 16, which is the sum of the nine values of the filter (1+2+1+2+4+2+1+2+1=16), to prevent the total number of counts of the filtered image is different from the original; what this filter does is to redistribute the counts while maintaining the total number of them. If not, it would increase the number of counts of the images in a completely artificial way.

The mathematical expression is fully applicable to any weights and dimensions (filters for edge detection or enhancement don't retain the number of counts because their purpose is purely to remove or to enhance information which is in the image).

3 Frequency representation of images

3.1 Introduction

Everyone knows that we can hear a piece of music as well as we can read it in a musical score. A musical score is a transcript of what we hear: notes, intensities, durations, silences, i.e., all those parameters that allow generating the sounds you hear. Similarly, the frequency representation of an image is the "score" of the image that we see. In it are also represented frequencies and intensities.

The "score" of an image corresponds, using the musical analogy, to what is heard at a given time by the static nature of an image.

3.2 Spatial Frequency

When a phenomenon is repeated from time to time, this time interval is the period and the inverse, frequency, because it indicates the number of times this event occurs per unit of time.

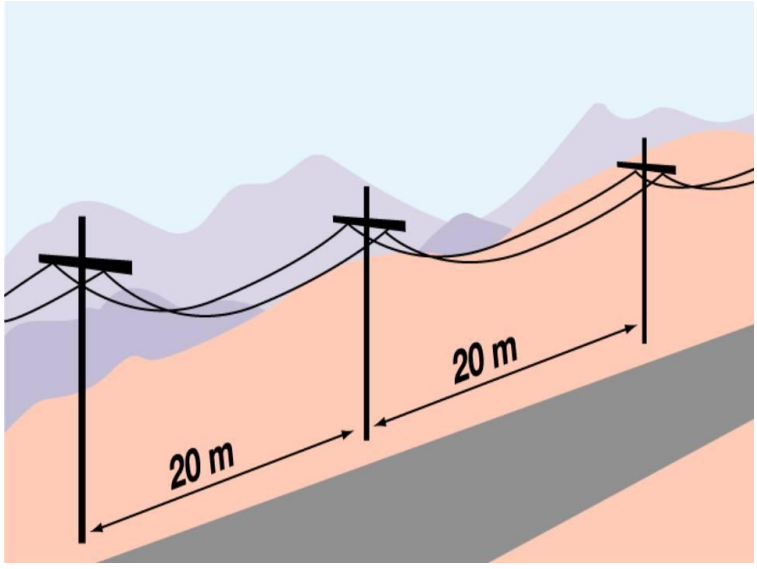

Fig.3.2.1: sequence in one dimension.

The same happens in space. When "something" happens each a regular length (period), the frequency indicates the number of times that this "something" occurs per unit of length. For example, if the telephone poles along a road (Figure 3.2.1) are situated every 20 meters, the period is 20 meters and its frequency is 1 post each 20 meters, which mathematically is expressed by the

ratio 1/(20 m)=0.05 m^{-1} (remember that a superscript "-1 " is a mathematical nomenclature which means a magnitude that is dividing).

In two dimensions, as could it be a plantation of fruit trees, there are two different directions of spatial frequencies, one in each direction of the plane (X, Y) , for example, a tree every 10 meters in the X direction (f_x=1/(10 m)=0.1 m^{-1}) and one each 8 meters in the Y direction and (f_y=1/(8 m)=0,125 m^{-1}) (Figure 3.2.2).

Please note that f_y is higher than f_x since the trees are closer according to the Y direction that according to the X direction and that, consequently, if we move according to the direction Y is more frequent to observe trees that if the movement is according to X.

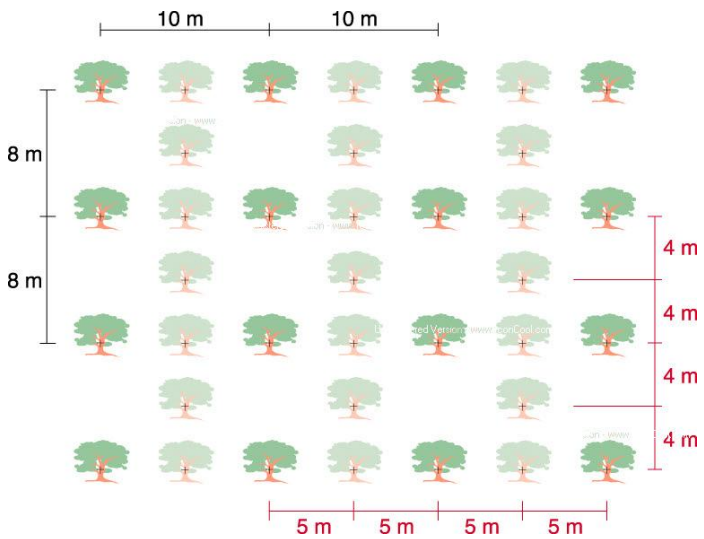

Fig.3.2.2: Two-dimensional distribution.

We can describe the planting of trees in two forms: one, by specifying the coordinates of each tree, which requires 2 numbers (X, Y) per tree, and another, more general, giving the coordinates of a corner (Ox,Oy) and say that from this point on the trees are planted with frequencies f_x and f_y. Both forms are entirely equivalent, that is to say, we can move from one representation to the other without loss of information.

If, for example, it is decided to insert new trees between the already existing ones, so that there is one every 5 meters according to X and one every 4 meters along Y, the new set can be represented by 2 new frequencies (f_x'=1/(5 m) =0.2 m^{-1}, f_y' =1/(4 m) =0.25 m^{-1}) (Figure 3.2.2). If we wanted to represent

some magnitude that change with the frequency, for example, the height of the trees or the telegraph poles, it would be necessary a second parameter called amplitude to represent it. There is also a third parameter that is called phase and that it is required to describe a periodic magnitude completely. That is, one thing is that "something" varies regularly with a specific frequency, and another is that at the initial measurement (t=0 or x=0) its value does match what it should be. This difference is taken into account using an offset (shift in origin) that must be set at the beginning of the measurement. In this way, the magnitude will repeat with a specific frequency. In the case of the poles separated 20 m between, if we start to count them to 5m of one of them, there will be a misalignment of 15m (initial displacement) and then follow one every 20 m. The phase would be of 15 m (or -5m).

3.3 Sine functions

A usual mathematical form that brings together the three parameters (amplitude, frequency, and phase) to represent a simple periodic variation are the sine or sinusoidal functions[3]:

$$F(x) = A \cdot \sin(f_x \cdot x + \Phi)$$

Where A symbolizes the amplitude, f_x the frequency, x the position, and Φ the phase. Figures 3.3.1 illustrate the variations in the shape of a sinusoidal function (Figure 3.3.1(a)) when each of its three parameters varies: amplitude in Figure 3.3.1(b), frequency in the Figure 3.3.1(c) and phase in the 3.3.1 (d).

[3] The sine functions or sinusoids are a way of representing in a compact form some magnitude that varies periodically. Instead of showing each one of its values explicitly as a list, they give a compact manner to generate and to represent them. An example of a sinusoidal function is the sound produced by a tuning fork. The pitch of the note "A" generates periodic oscillations in the air with a frequency of 440 Hz (oscillations per second). Its amplitude and duration depend on how hard you hit the fork to make it vibrate, but the frequency remains constant.

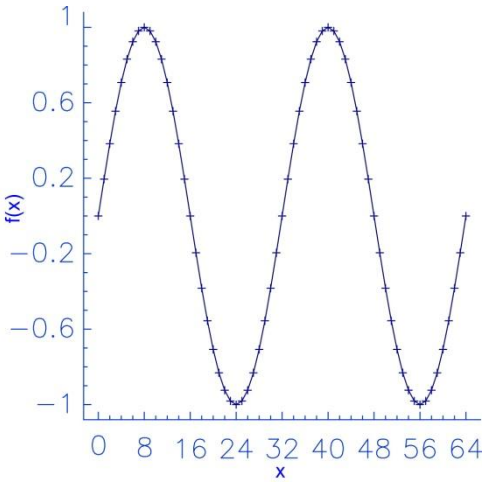

Fig.3.3.1 (a): original function

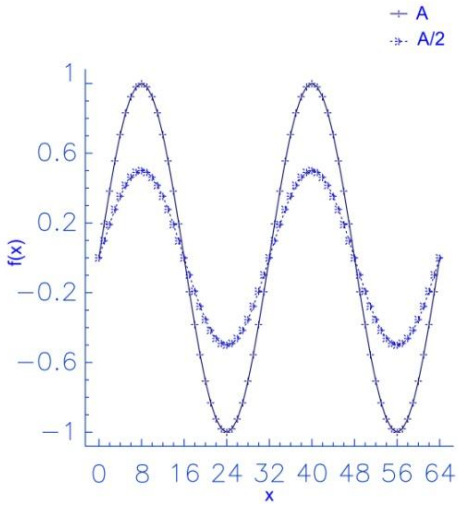

Fig. 3.3.1(b): change in amplitude (half).

The reader used to interpret cardiac motility studies can not miss these concepts. Recall that they generate parametric images of the amplitude and phase, one that represents the degree of motility (amplitude of the movement) and another that indicates the degree of synchronicity of movement (phase image) between different areas of the myocardium.

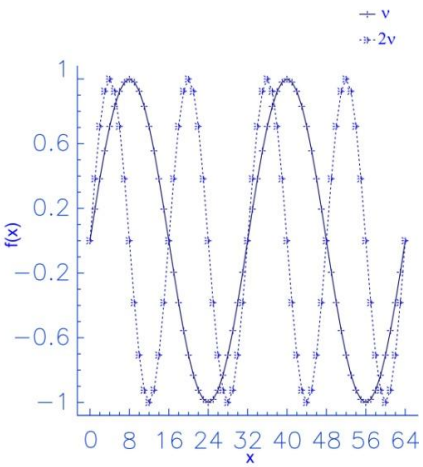

Fig. 3.3.1 (c): change of frequency.

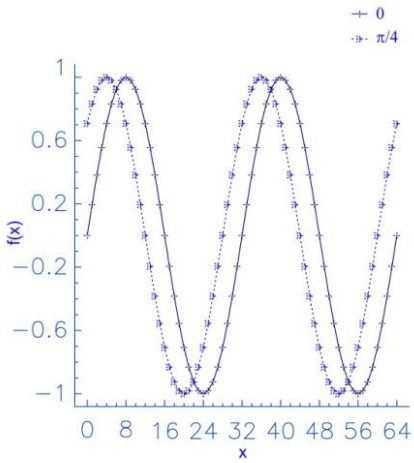

Fig. 3.3.1 (d): change of phase.

Once the concepts of spatial frequency and phase have been introduced and have remembered the sine functions, we are in a position to address the concepts of analysis and frequency representation.

3.4 Frequency analysis in one dimension

Let us first consider a curve like the one in Figure 3.4.1.

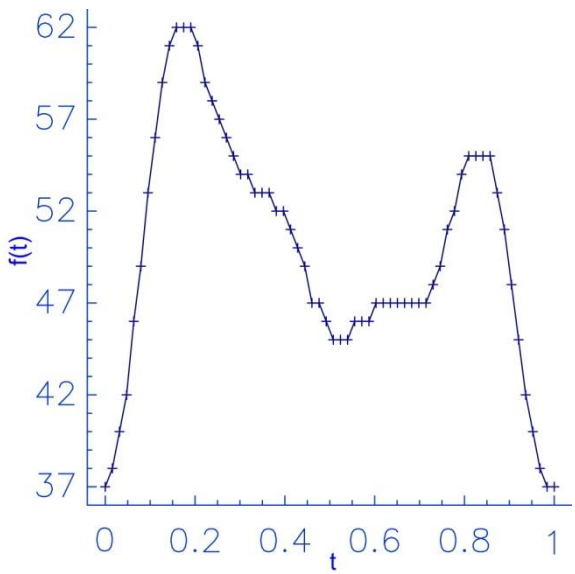

Fig. 3.4.1: activity/time curve.

The shape of this curve is complex and difficult to analyze directly. However, there is a theorem of mathematical analysis (Fourier's theorem) which ensures that simple periodic functions can approximate periodic continuous functions in such a way that the infinite sum (series) of these simple functions reproduces the original function. The sinusoidal functions are the primary functions most commonly used in this type of analysis. All this means that we can break down the original function in Figure 3.4.1 as a sum of sinusoidal functions. Figure 3.4.2 shows how adding four sinusoids of increasingly higher frequencies reproduce the original function correctly. These frequencies are not arbitrary. They are multiples of a fundamental frequency[4]. The underlying idea is to find the mean value of the function (which is a constant value and therefore of zero frequency because it does not change) and to modulate it with sine functions of increasing frequencies (harmonic terms) to bring it closer to the profile of the original function.

[4] For periodic functions, the fundamental frequency is the inverse of its period. For non-periodic functions, to be able to apply the techniques of the periodic functions, it is considered that the period is the duration of the function.

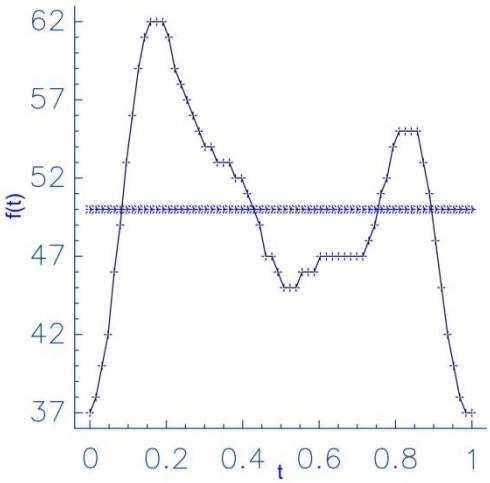

Fig.3.4.2 (a): original and average value.

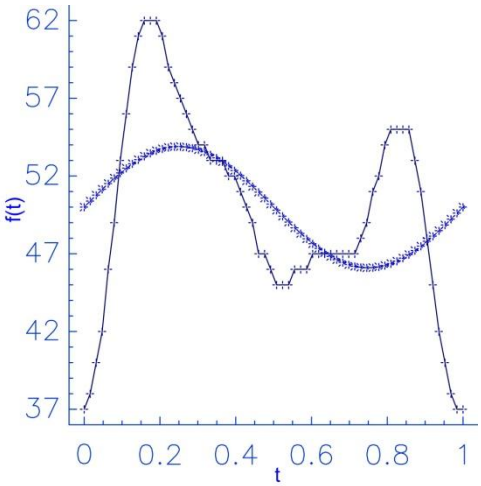

Fig.3.4.2 (b): original, average value and 1 sinusoid.

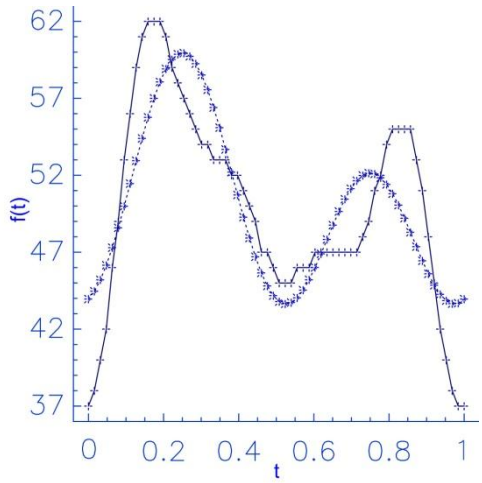

Fig.3.4.2 (c): original, average value and 2 sine functions.

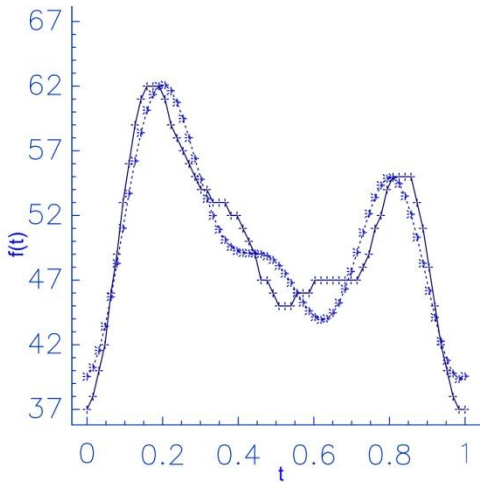

Fig.3.4.2 (d): original, average value and 3 sine functions.

It is important to note that the number of sinusoids, which breaks down the original function is unknown in advance[5]. It is as if it were a "fitting" in which the number of terms depends on the type of function, varying in number according to the different frequencies that are necessary to fit the profile of the function. In this case, four sinusoids are enough to obtain an excellent approximation (Figure.3.4.2 (e)).

[5] If the function is continuous infinite functions are needed. If, as occurs in practice, the curve has a certain number of points N, the maximum number of functions or of frequencies that can be used is N/2.

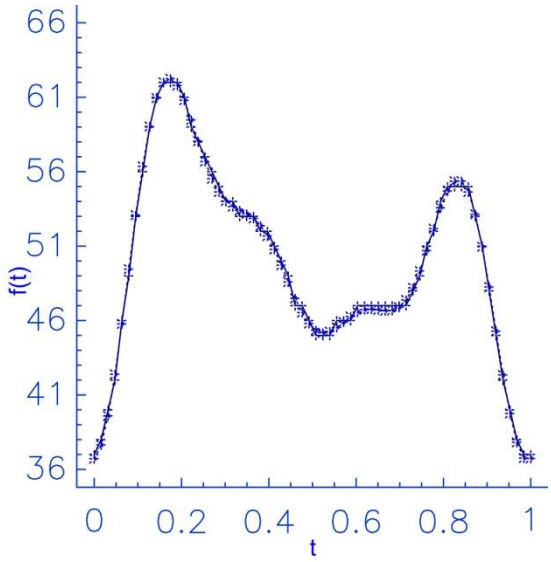

Fig. 3.4.2 (e): original , average value + 4 sine functions.

The concrete way to obtain the coefficients that multiply the basic functions of this type of decomposition exceeds the purpose of this text. They are complex numbers that are represented by two quantities, the amplitude (modulus) and the phase (argument). This type of decomposition of periodic signals is generalized to aperiodic functions using the Fourier Transform. Similarly, the values obtained in this transformation are complex numbers. Their graphic representation has two parts: one that reflects the variations in the amplitude with the frequency called the spectrum of amplitude (classification of the amplitude as a function of frequency) and another part that displays the dependence of the phase with the frequency, which is the spectrum of phase. Figure 3.4.3 and Figure 3.4.4 show the spectra of amplitude and phase of the example. The abscissa indicates the factors (k) used to obtain frequencies as multiples of the fundamental frequency. The magnitude for k=0 corresponds to the average value (zero frequency). Note the significant difference between this value and the amplitudes of the sinusoids to higher frequencies and how these, although decreasing, are virtually identical from k=3 which means that the detail provided by higher frequencies is small. It follows that the soft variations can be reproduced accurately with few low-frequency sinusoids, saying that the smooth changes are of low-frequency content. The phase presents, in this case, two values 0 and π/2 (~1.6).

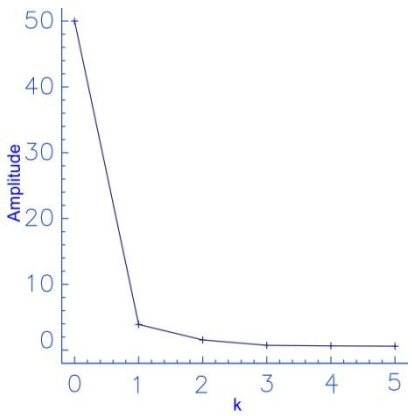

Fig. 3.4.3: spectrum of amplitude.

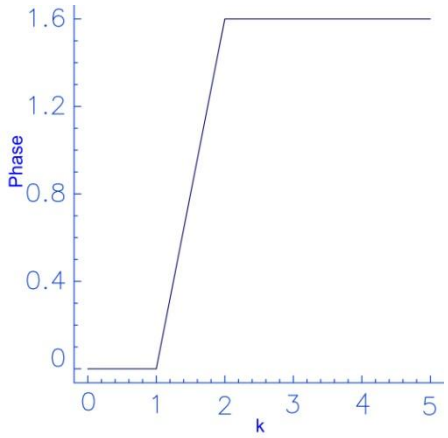

Fig. 3.4.4: spectrum of phase.

Figure 3.4.5 presents the case of a square function, which is a function with sudden changes that suggest a frequency content much higher than in the previous example.

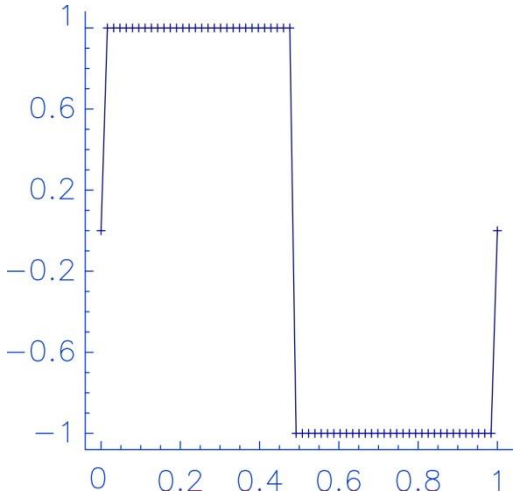

Fig. 3.4.5: square wave.

As can be seen from the succession of graphs in Figure 3.4.6, four terms are inadequate to reproduce this profile. Accordingly, it follows that the abrupt changes require a higher number of frequencies that the soft contours[6].

[6] This case, because it is a discontinuous function, despite an increase in the number of terms it is no possible to reproduce it due to the Gibbs'phenomenon that produces oscillations in the discontinuities.

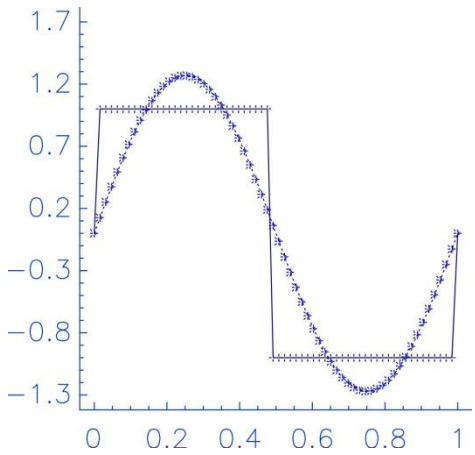

Fig. 3.4.6 (a): original and a sine wave.

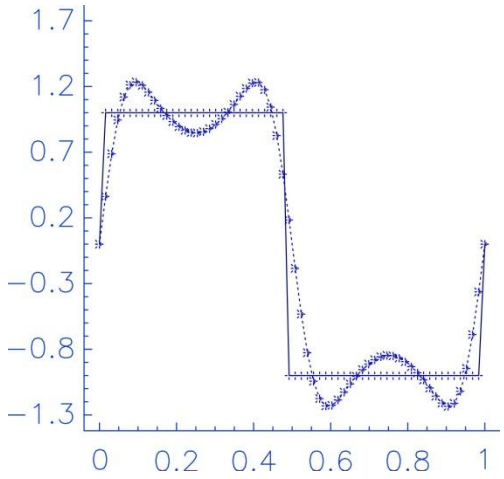

Figure 3.4.6 (b): original and sum of 2 sinusoids.

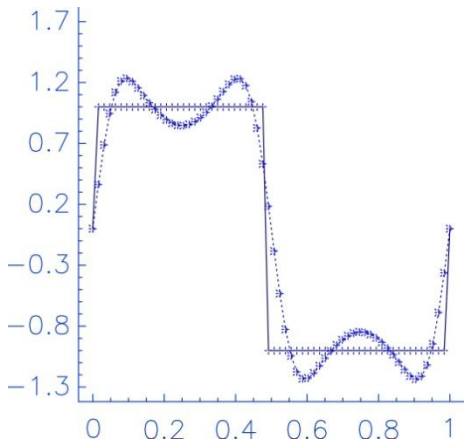

Fig. 3.4.6 (c): original and sums of 3 sinusoids.

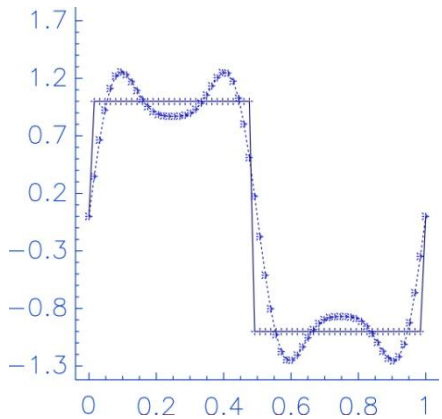

Figure 3.4.6 (d): original and sums of 4 sinusoids.

3.5 Frequency analysis of images

The frequency analysis is not limited to curves. This methodology applies to images in a completely similar way. We have seen that the usual way to represent a distribution of activity is a matrix in which the values correspond to the detected activity.

An alternative way is to have a set of elementary functions that accurately represent the same distribution of activity. The idea behind is fitting the images to as many sinusoids as possible. As we are involved with images, the representation of the amplitudes and phases are also images, in which one axis will correspond to the horizontal frequency (f_x) and a second axis for the vertical frequency (f_y). In these images the origin of frequencies, that is to say, f_x=0,f_y=0 is situated in the center of the image and has central symmetry. In the image of amplitude, the value of each pixel, whose coordinates are (f_x, f_y), corresponds

to the amplitude of the sinusoids for these frequencies. In the phase image, the value of the pixel corresponds to the value of the phase.

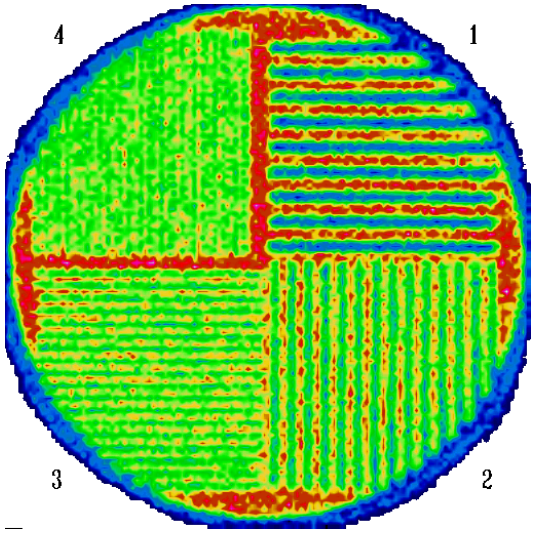

Fig 3.5.1 (a): the original image of the bar-phantom

Figure 3.5.1 shows the image of a bar-phantom (3.5.1(a)), together with its images of amplitude and phase. Each quadrant of the original image has a number according to the decreasing thickness of the bars (1,2,3,4). Note that the thicker bars, because they have a big gap between them, show a lower frequency distribution (fewer bars per unit length) than the other thinner bars.

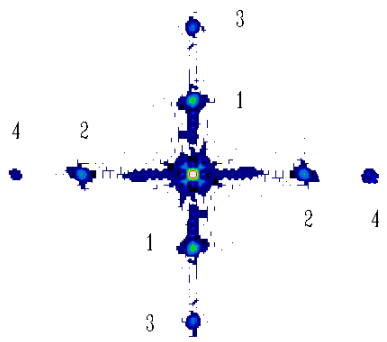

Fig.3.5.1 (b): image of amplitude

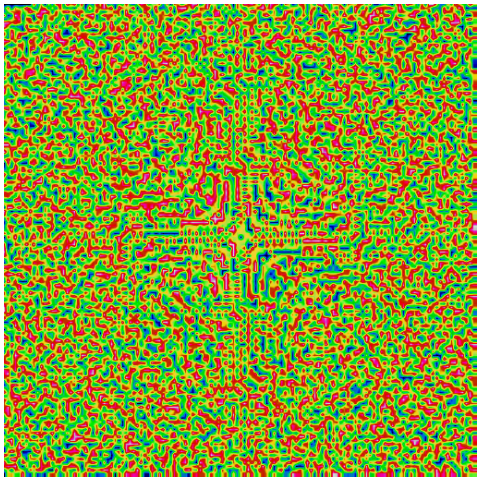

Fig.3.5.1(c): image of phase.

The image of amplitude (Figure 3.5.1.(b)) allows to directly visualize what the frequency characteristics are (which appear as points of high value) as well as

the frequency extension, that is to say, the highest frequency involved significantly in the image. As can be seen, the image or spectrum of amplitude presents symmetry to the center, so that it is sufficient to restrict its study to a quadrant. Note also that in addition to the central bright point (that represents the average value of the image that corresponds to the zero frequencies), in this case, there are two bright dots on each half axis. Each one of them corresponds to each type of bar of the phantom. In this image, the numbering of these points is according to the corresponding quadrant of the original image.

As can be seen, quadrant 1 corresponds to the point closer to the origin of frequencies (which is the center of the image); next is the spot for quadrant 2, followed by quadrant 3 and finally by quadrant 4 which is the one with the highest frequency.

Note that the horizontal bars (quadrants 1 and 3) correspond to vertical frequencies because the sequence of bars is detected when we explore the image in this sense, and therefore we represent them on the vertical axis. Similarly occurs with the vertical bars that we identify when we explore horizontally, and consequently, they will correspond to horizontal frequencies (quadrants 2 and 4).

The phase image, which also is symmetrical to the center, directly does not provide any useful information about the images analyzed in this case[7].

To facilitate the interpretation of the image, we get a profile that summarizes in a curve the frequency content of the image. This profile, which is obtained by averaging over successive rings centered in the center of the image (circular spectrum), although mix frequencies in all directions, indicates the contribution (amplitude) of each frequency to the distribution.

[7] For an in-depth study of the phase, the old work of Oppenheim and Lim: The importance of phase- in signals. Proceedings of the IEEE, Vol 69, no 5.1981, p. 529-541 is an excellent reference.

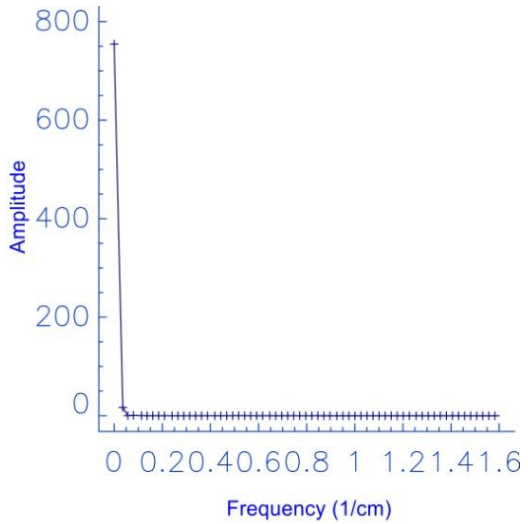

Fig. 3.5.2(a): circular spectrum

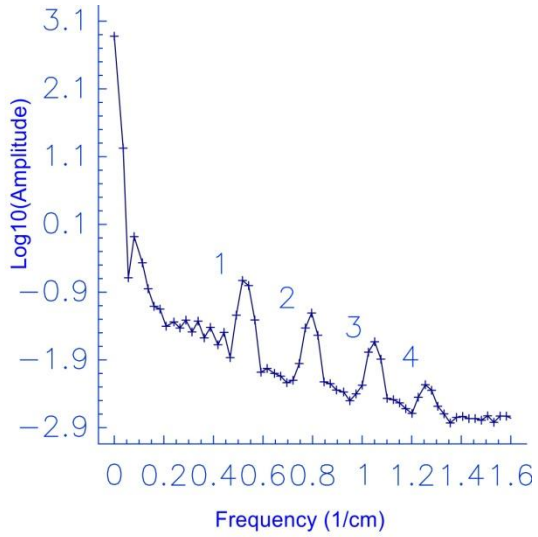

Fig.3.5.2 (b): logarithm of the circular spectrum

To be able to observe the significant differences between the value of the amplitude at zero frequency and the values for the rest of the frequencies (Figure 3.5.2(a)), we usually use the logarithm representation instead of the direct values (Figure 3.5.2(b))[8],[9].

As we can see, the graph expands considerably, making it possible to identify the amplitude for each frequency of the bars. Figure 3.5.2 (b) can be considered as the superimposition of a series of peaks on a curve that decreases as the frequency increases. This fact shows us the nature of the image of the bar-phantom. The continuous component corresponds to the "uniform" activity of the cobalt plate used to acquire the image, and the peaks are due to the layout of the bars according to we observe in the image of amplitude (Figure 3.5.1 (b)). Also, we note that the height of these "spikes" on the continuous curve, decreases with increasing frequency, which corresponds to the fact that the broad bars (lower frequency) are better observed than the thin bars (higher frequency). Logarithms can also be taken directly in the image of amplitude

[8] In addition to the usual spectra, the power spectrum indicates the energy associated with each frequency.

[9] The logarithms are an alternative way to represent a number. Thus, first, it sets a reference value called basis, 10, for example. Second, given a number, it seeks the value to raise the basis to obtain the number. This value is the logarithm of this number. For example, the logarithm of 1000 on basis 10 is 3, since 10^3=1000 and the one of 1000000 is 6. The logarithm allows that a graph represents very different values. Also let convert an exponential relationship in a linear relationship, which greatly simplifies the calculations.

(Figure 3.5.1(b)) obtaining an image in which the maximum corresponding to each sequence of bars is identified easily (Figure 3.5.3).

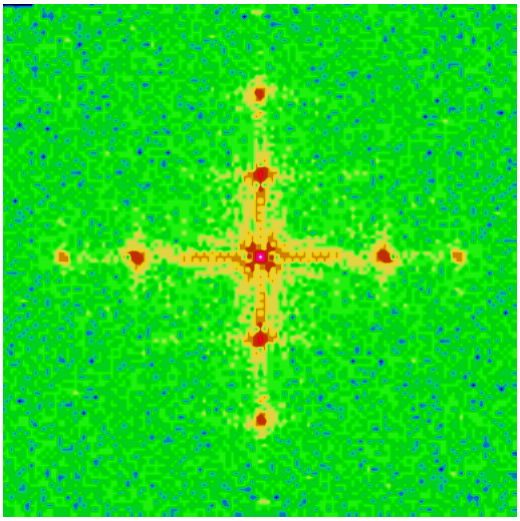

Fig. 3.5.3: logarithm of the image 3.5.1 (b).

The full equivalence between the direct representations (spatial domain) and frequency representations (frequency domain) of the images makes that all transformation in a domain has its translation in the other. Thus, if we rotate the image (e.g., 45°) (Figure 3.5.4(a)), the image of amplitudes will have the maxima of the bars also rotated to the same angle (Figure 3.5.4(b)).

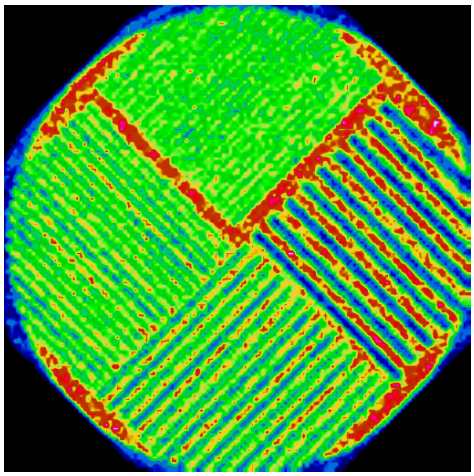

Fig. 3.5.4 (a) bar-phantom turned 45º clockwise.

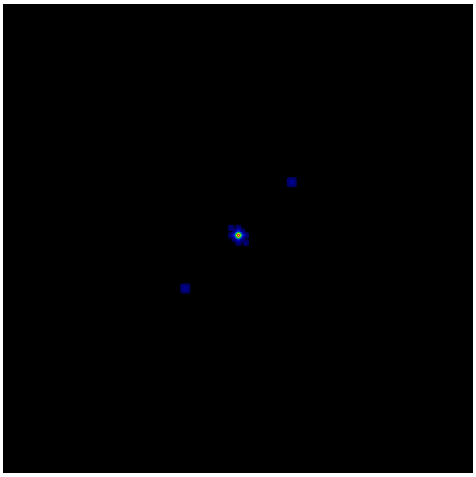

Fig.3.5.4 (b): image of the amplitude of the bar-phantom rotated 45º.

The converse is also true, that is, any modification of the images of magnitude and phase results in a change of the original or direct image; this is the foundation of the application of frequency filters[10].

3.6 Nuclear Medicine Images

Returning to the musical analogy, let's look at how to set new parallelism: the spatial frequencies, which are the ones in what we are involved, are similar to the temporal frequencies. A low-pitched or bass sound, which corresponds to a few oscillations per second, is of low frequency. A high-pitched sound corresponds to many oscillations per unit of time is of high frequency. At the same time, a distribution of activity that gently varies as we move across will be

[10] It is possible to set a similarity with music. The music consists of a succession of sounds generated by the voice or musical instruments with time. These sounds are sets of variations of the air pressure of different frequencies which are represented by a succession of notes on a pentagram that forms a musical score. Depending on the complexity of the score in a short space of time, it can be heard few musical notes or an intricate overlay of them simultaneously. The same is true with the images. These can be "simple," with a small frequency content (few frequencies) or "complex" thinking that an image would correspond to an instant o minimal time interval of a piece of music (as it does not vary in time) which is attempted to illustrate in the following figure:

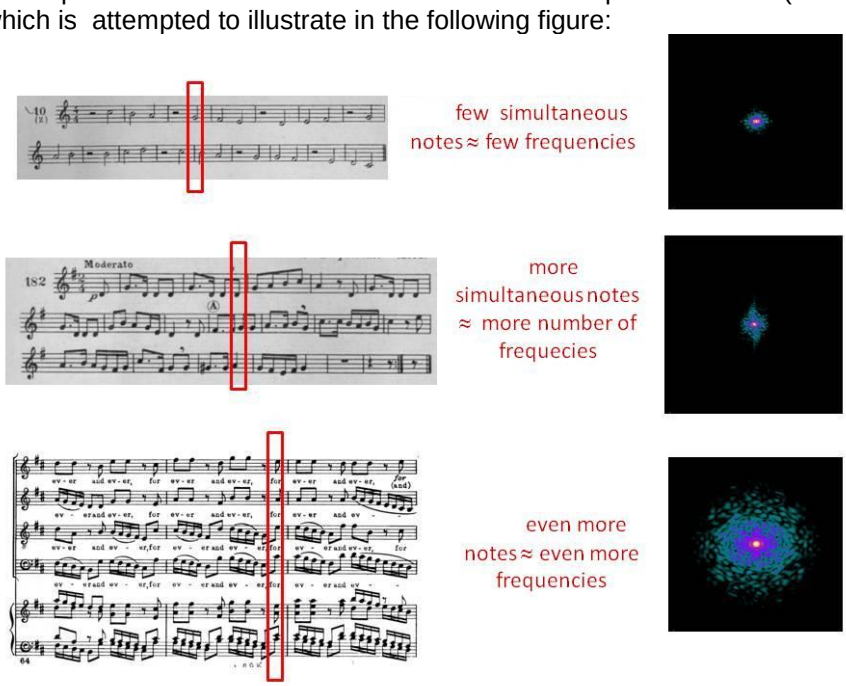

It is well known that any modification of a musical score translates into a change in the sound that represents and that vice-versa- within certain limits - any change in the sound of a piece of music results in a change in its musical score or notes. Through this parallelism between music and images, to alter the phases of an image would be equivalent to alter the time that specific notes are played or that the entry of some instrument is advanced or delayed. To alter the amplitude of specific frequencies would correspond, for example, that some instrument would alter the intensity of its notes from forte to pianissimo.

adequately represented with low-frequency sinusoids while a distribution that differs very much from one point to the next will require high-frequency oscillations. The smoother is the distribution, the smaller the number of different low frequencies needed for reproducing it (the image of amplitude will have a low number of non- zero values near the center). A limit case is a constant distribution that will be entirely defined by a single value which is precisely its amplitude and which corresponds to the case of frequency zero as there are no changes through the image. Another borderline case, opposite to that which we have just seen, is the image of a point. In this case, there is a need for all available frequencies (if it were an "ideal" point it would require an infinite number of frequencies) because it is the most abrupt variation that may exist ("zero-all-zero"). If a radiation source is small ("point size") we will only be able to reproduce if we can use a large number of frequencies. Between the two extremes are the typical images.

From the frequency point of view, we can consider that Nuclear Medicine images are formed by three groups of frequencies (low, medium and high) by varying the relative importance of one or the other depending on the type of images. As discussed earlier (section 2.2), we can consider the "nuclear" images formed by the overlap of the background with the activity of the organ or area of interest (object) and with the statistical fluctuations ("noise") a fact that Figure 3.6.1 reflects and that corresponds to a cross-sectional study obtained from a brain SPECT. Note how the low and mid frequencies define the structure of the object and how the noise "alter" the amplitudes of all frequencies, being this alteration more important as the frequency is higher. The amplitudes of the object decrease with the increasing frequencies and the amplitudes of the noise are approximately independent of the frequency (white noise)[11].

[11] The tomographic reconstruction processes modify the characteristics of the noise by introducing dependencies with the frequency. Figure 3.6.1 is an example to illustrate how the noise masks the images.

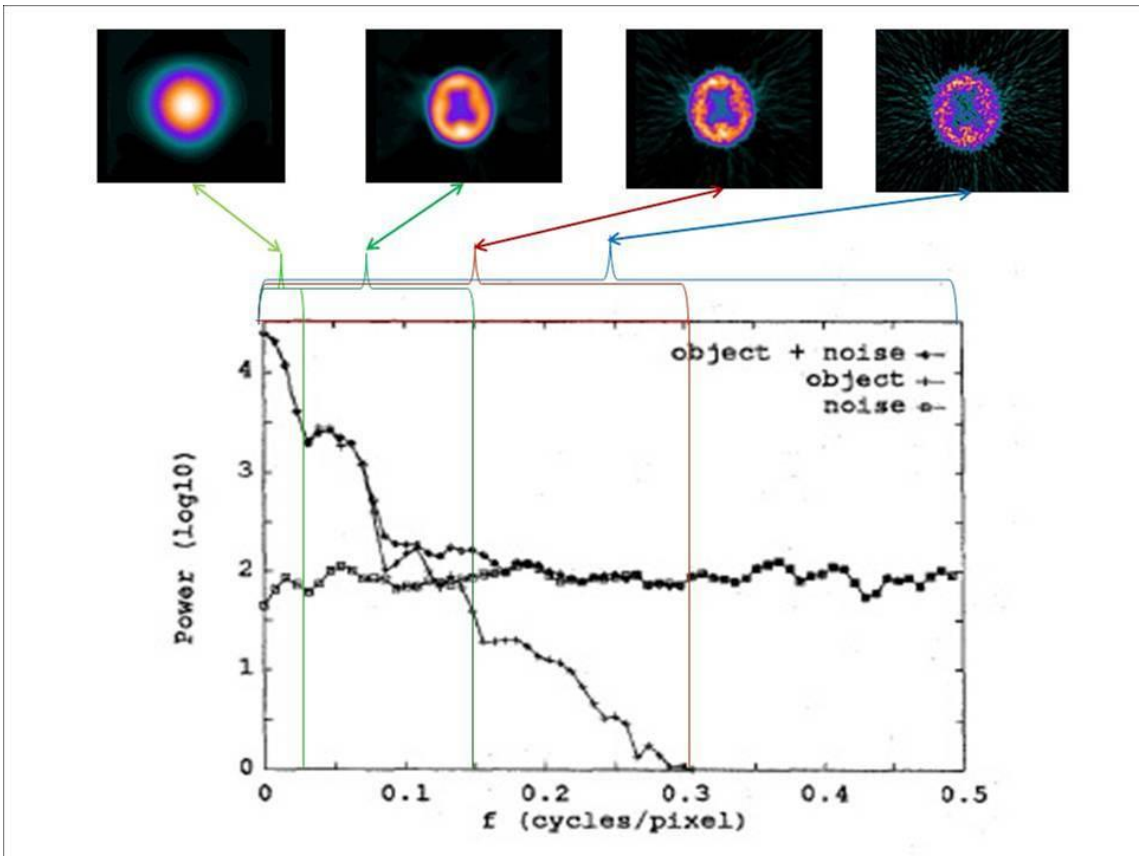

Fig. 3.6.1: the relationship between image and power spectrum (Based on the article by Beis J.S., Celler A., Barney J.S)

An image that is used to describe one of the performances of the gamma cameras is an image of uniformity obtained from a point source. The theoretical spectrum (for an ideal detector) should be a single value at $f_x=f_y=0$ (the mean value). However, the real spectrum depends on several factors and, above all, on the number of counts, that is, the noise level. Figure 3.6.2 shows the spectra for a different number of counts. As the number of counts increases, the relative importance of the amplitudes of the high frequencies in front of the ones of the low-frequency decreases. This behavior allows assuming that the noise in these images has a "flat" spectrum whose relative level with respect to the low frequencies decreases with the increase in the number of counts. From this we infer that the spectrum has two components: one, that decreases as the frequency increases and that explains how the detector changes the amplitude associated with each frequency (independent of the number of accounts), and another , which is approximately constant for all frequencies that corresponds to the noise which in turn, depends on the level of counts. It follows that the noise

level determines the proportion of the spectrum of interest that protrudes above the noise.

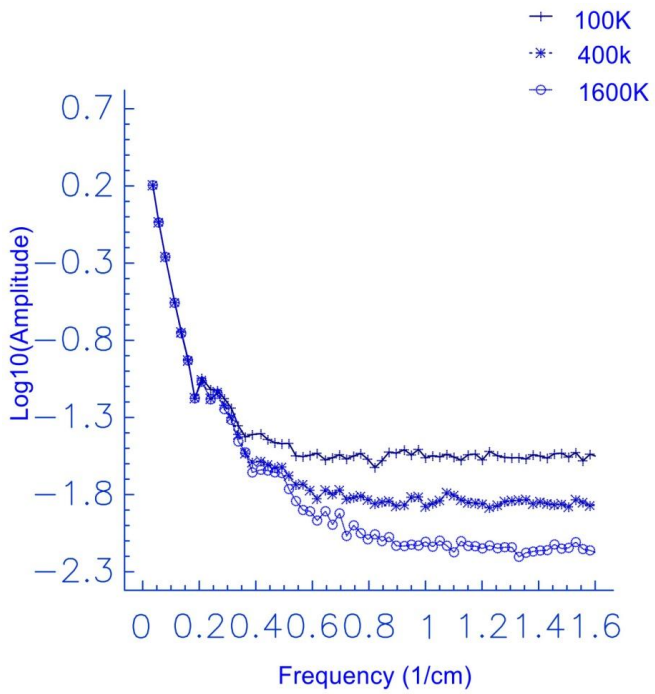

Fig.3.6.2: variation in the spectrum of uniformity with the number of counts.

The frequential behavior of the images of uniformity can be likened to the behavior of the background of the scans since both come from a homogeneous planar source[12].

In the spectra of the bar phantom obtained at a different number of counts (Figure 3.6.3), the same phenomenon occurs. In them, we see how the higher the number of counts (less noise) more frequencies of the phantom are distinguished.

[12] The small bump located at 0.20-0.30 cm^{-1} (Figure 3.6.2) may be caused by the detected relatively smooth contour of the image of the flood phantom because the flood source was smaller than the matrix .

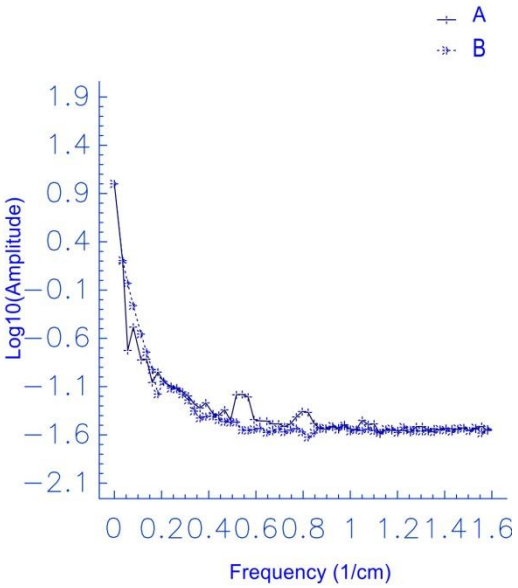

Fig.3.6.3 (a): spectra of: A:the phantom
B: background. Number of counts=100,000.

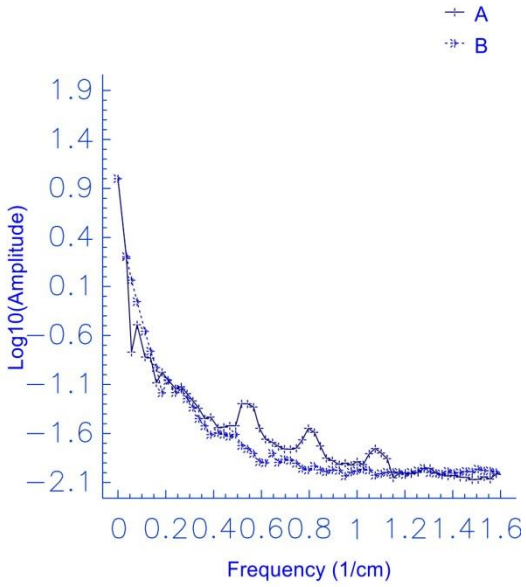

Fig.3.6.3 (b): spectra of :A:phantom
B: background. Number of counts
1000000

As the level of noise decreases, frequencies emerge coming from the object that would otherwise not be distinguishable from the noise. Figures 3.6.3 show the spectrum of the bar-phantom, which contains its "ideal" spectrum (which would be four peaks of equal height) modified by the detector by broadening and flattening the theoretical peaks. It also shows the spectrum of the background (as in Figure 3.6.2) overlaps the spectrum since the image is obtained experimentally by the bar-phantom interposed between a flat source of radiation (as in the determination of the uniformity) and the detector. What you get is a combination of the two spectra in the absence of a clear separation between them.

As the complexity of the image increases, the number of frequencies necessary for reproducing it also increases (the "frequency content" raises).

A typical image of Nuclear Medicine reflects the localized uptake of tracer in a homogeneous organ such as the collection of platelets by the spleen (Figure 3.6.4(a)). In this type of image, there is a specific elevation of intermediate frequencies to account for the localized increase in the activity. Note that although there is a significant elevation of activity in the spleen, the image, on the whole, is "smooth" which translates into an image of amplitude (Figure 3.6.4(b)) concentrated around the origin of frequencies.

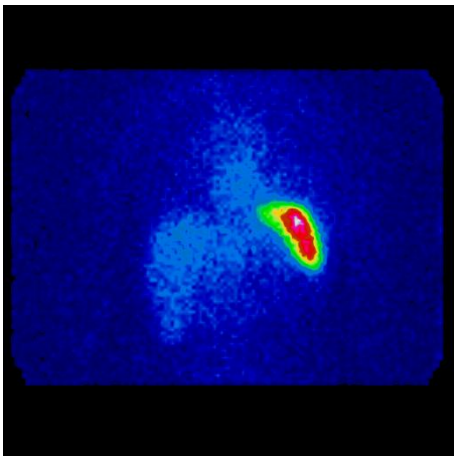

Fig.3.6.4 (a): the collection of platelets the spleen

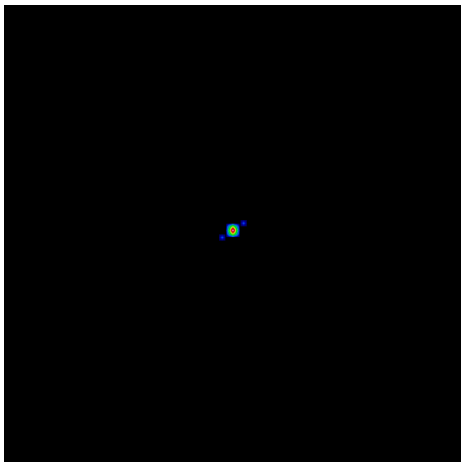

Fig.3.6.4 (b): image of the amplitude of Fig. 3.6.4 (a).

Compare the corresponding spectrum (Figure 3.6.5) with the spectrum of the background with an equivalent number of counts. There has been an increase in the amplitudes in the frequency range of 0.20-0.70 cm^{-1}.

Fig.3.6.6 (a) corresponds to a bone scan, which highlights the contrast between the background and the bone. Note how the amplitude is distributed around the center of a more or less homogeneous extending far more than a collection of platelets in the spleen. Its frequency range is more significant than that in the previous example,

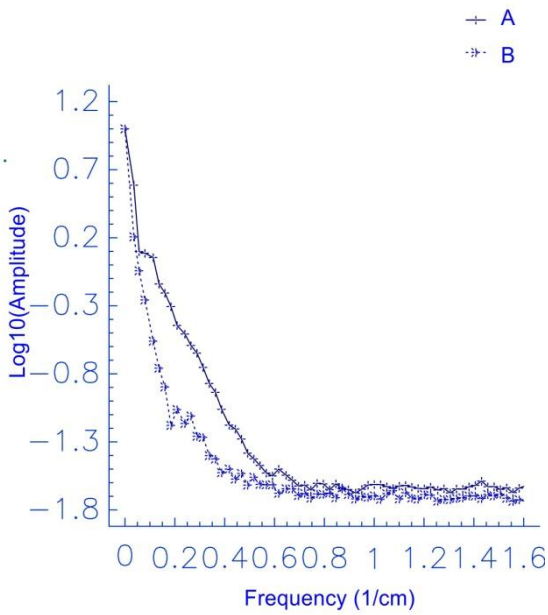

Fig.3.6.5: spectra of A: spleen, B: background.

A bone scan shows a more heterogeneous distribution of activities than splenic scintigraphy with platelets.

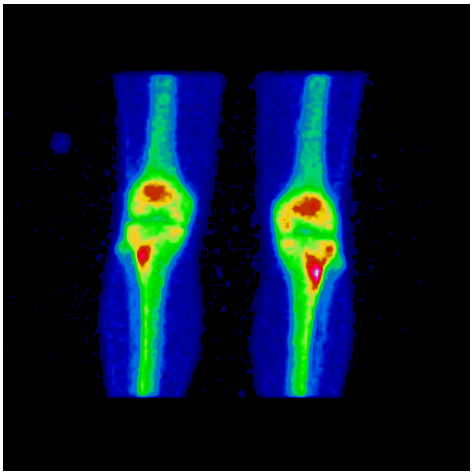

Fig. 3.6.6 (a): bone scan.

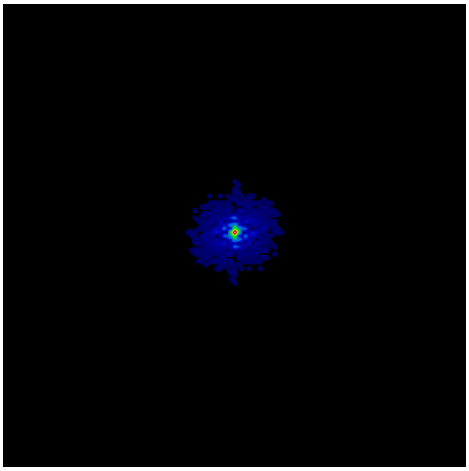

Fig.3.6.6 (b): image of amplitude of Fig.3.6.6 (a).

The overlap in the range of magnitudes of this image and the background (Figure 3.6.6) showed a significant increase in frequencies in the range of 0.10-1.3 cm^{-1}.

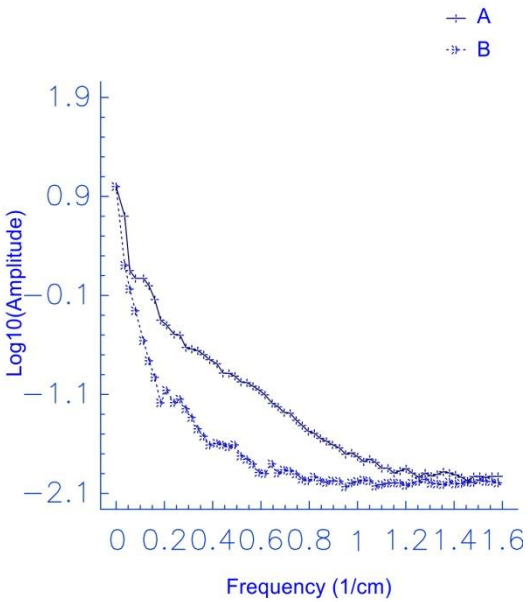

Fig.3.6.7: spectra of A: knees, B: background.

The "frequency content" is higher when the organ to explore has a significant number of different structures, or to be more precise, when the image is more structured ("baroque"), being Fig. 3.6.8 the planar image of a cut of Hoffman's brain phantom a good example.

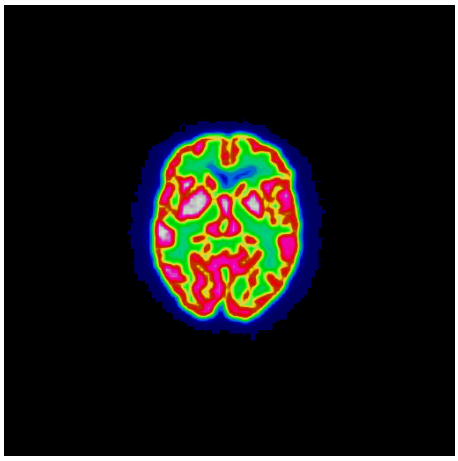

Fig. 3.6.8 (a): phantom of the brain.

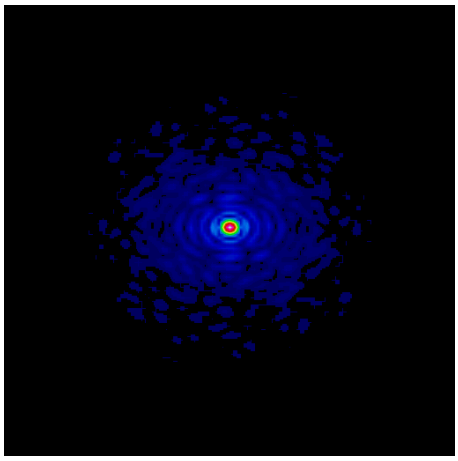

Fig. 3.6.8 (b): image of the amplitude of Fig.3.6.8 (a).

This distribution of activity has homogeneous zones and areas of complex morphology, which translates into an image of amplitude that presents values significantly different from zero to high frequencies (Figure 3.6.9).

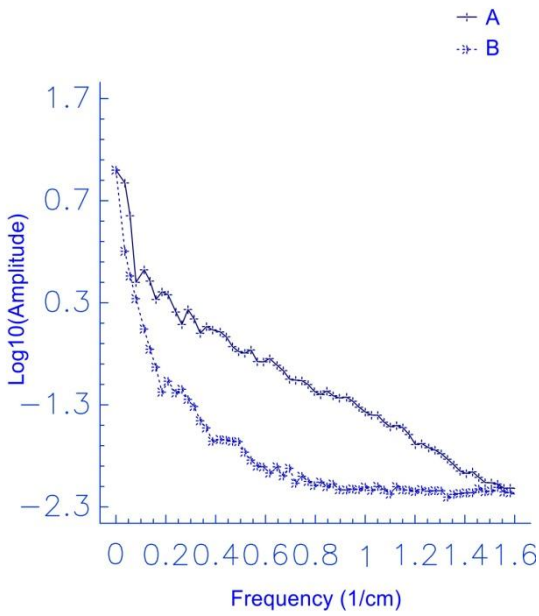

Fig. 3.6.9: spectrum of the phantom of the brain: A: brain, B: background.

3.7 SPECT and PET images

The frequency composition of the SPECT and PET images is more complex than the planar imaging. The complexity comes from the fact that they are obtained by calculation from planar images (in SPECT) or lines of response (in PET) that are recorded from different angles. These calculations can easily introduce artifacts, and the application of filters can substantially modify the original distribution of counts. Nevertheless, and in spite of the manipulations

necessary for their production, the tomographic images, when they are technically correct, provide greater structural information that the planar images by eliminating the overlapping of structures that are inescapably present. An example of the change introduced by SPECT in the spectral composition of the images is the one offered by the image of planar myocardial perfusion obtained in the LAO projection 45º (Figure 3.7.1) and by one of the slices of the tomographic study of the same patient (Figure 3.7.2). The planar image has an artifact by the overlap of extracardiac radiation and by the blurring due to the movement of the heart, while the tomographic slice is only degraded by the heart motion.

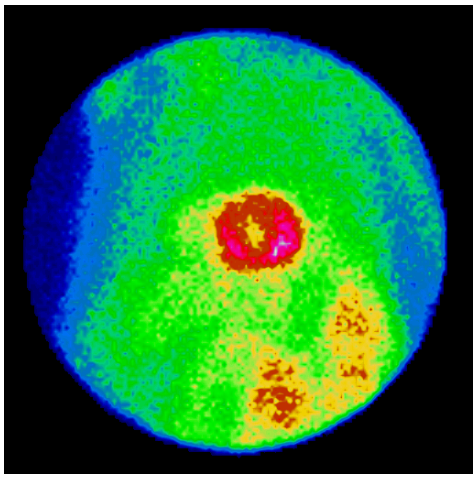

Fig. 3.7.1: planar myocardial perfusion image.

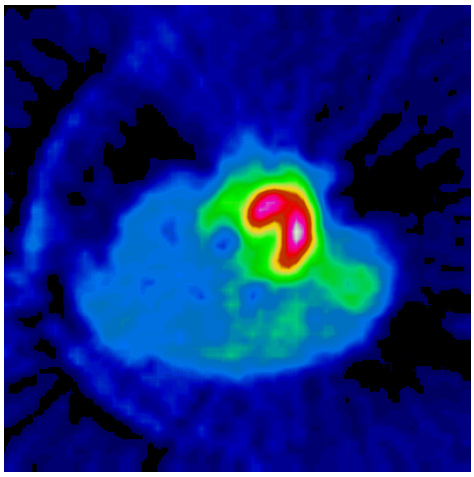

Fig.3.7.2: a cross-sectional study of an SPECT myocardial perfusion

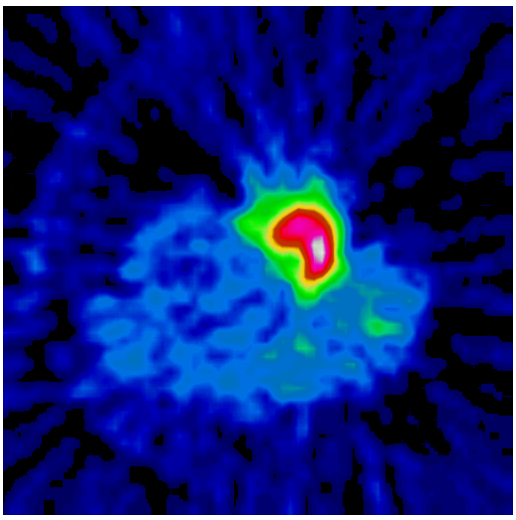

Fig.3.7.3: the image of gated SPECT corresponding to the slice of Figure 3.7.2.

A higher degree of quality is achieved with the tomographic acquisition synchronized (gated-SPECT) with the movement of the heart[13] (Figure 3.7.3) to reduce the blurring due to the motion of the heart while at the expense of a decrease in the number of counts, which makes the statistical noise interference higher than with the other two techniques.

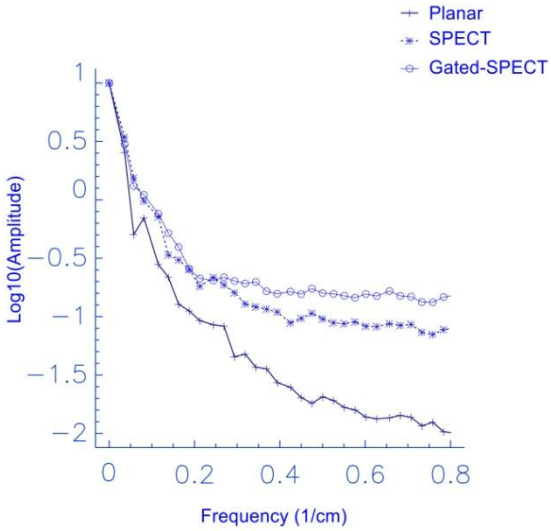

Fig. 3.7.4: spectra of SPECT and planar images GATED-SPECT.

Figure 3.7.4 shows how the spectrum corresponding to the tomographic (SPECT) slice has, in the area of intermediate frequencies (0.2-0.6 cm^{-1}), a much higher amplitude than the record planar. The spectrum of the gated-SPECT image has some intermediate frequency even more significant than that of the conventional SPECT; although it does not represent a gain as spectacular as the planar to SPECT in terms of image quality, it supplies information of the heart movement.

The improvements made by the SPECT are highly dependent on the processing, that is, the reconstruction method employed and the filters used in the reconstruction (chapters 5 and 6). It is interesting to compare, however, the three spectra of the Figure 3.7.4 - obtained with the method of the filtered back-projection without any additional filter - with those of the Figure 3.7.5, in which a smoothing filter is applied and Figure 3.7.6, which is the result of using a restoration filter[14].

[13] The mechanical movement of the heart is related to its electrical activity (ECG) which is used to synchronize the acquisition.

[14] Explained in 5.4.3 these filters try to restore the amplitudes attenuated by the detector.

These graphs show that if you apply a smoothing filter the magnitudes of the middle and high frequencies are significantly reduced, making the image less "noisy" but also less sharp. On the other hand, the implementation of a restoration filter increases the intermediate frequencies, thus achieving an image with more detail and decreases the effect of noise at high frequencies (> 0.6 cm^{-1}).

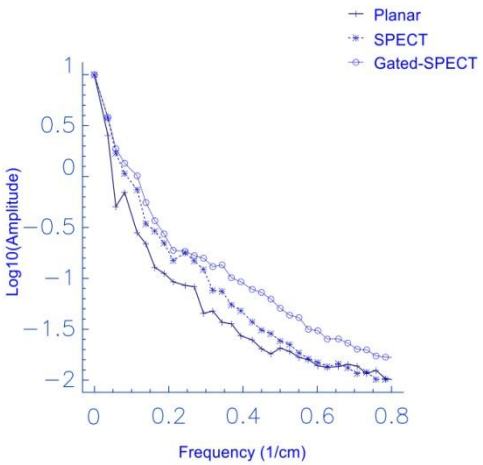

Fig. 3.7.5: spectra after applying a smoothing filter

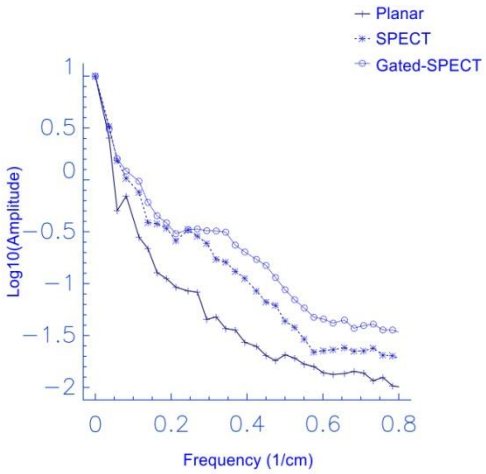

Fig.3.7.6: spectra after applying a restoration filter.

The spectrum reflects the level of detail of the images (scans). Thus, an image of cerebral perfusion (Figure 3.7.7) with a complicated structure, has a high-frequency content, higher than, for example, the myocardial perfusion image seen above (Figure 3.7.2). The spectra of both images (Figure 3.7.8) show this difference.

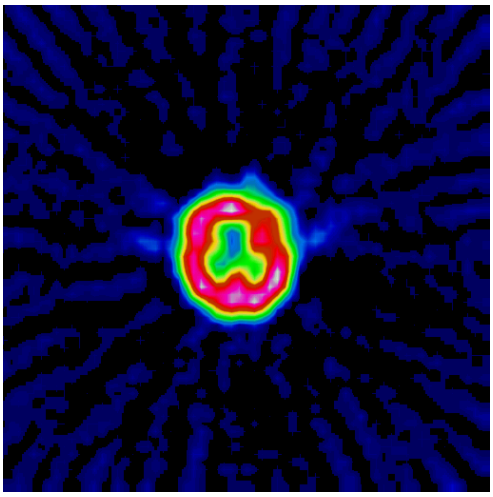

Fig.3.7.7: the image of brain perfusion SPECT

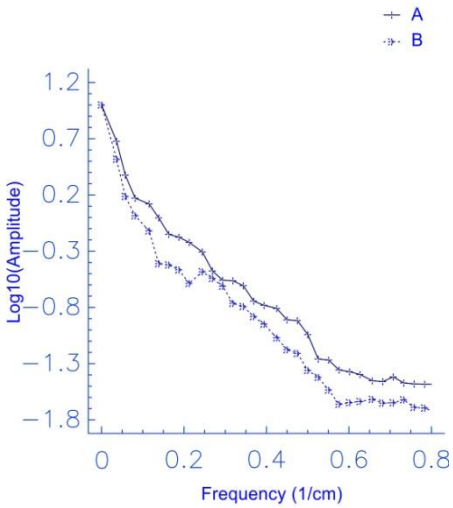

Fig. 3.7.8: spectra of A: brain, B: heart.

Notice how in the spectra of Figure 3.7.8, the line corresponding to the brain (A) presents higher values than the heart, indicating a more extense range at all frequencies, which reflects the fact that the increase in the complexity of an image increases its frequency content.

The dependence of the quality of the results concerning the acquisition parameters and subsequent handling is well known. It is interesting to observe the consequences of some changes in these parameters from the frequency point of view.

3.7.1 Dependence on the number of counts or time by projection.

One of the aspects that more attention has to be paid in the acquisition of studies is the obtainment of an adequate number of counts by projection compatible with the comfort and the immobility of the patient. Figure 3.7.1.1 shows us how the same slice changes with the number of counts/time by projection.

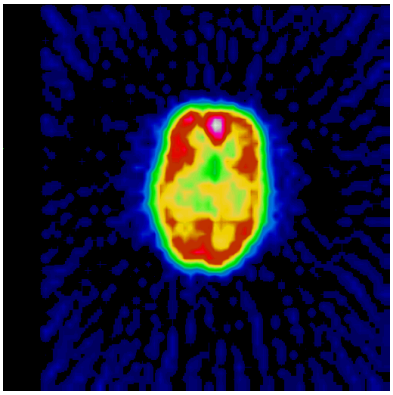

Fig. 3.7.1.1 (a): reconstruction of an acquisition of 20s by projection.

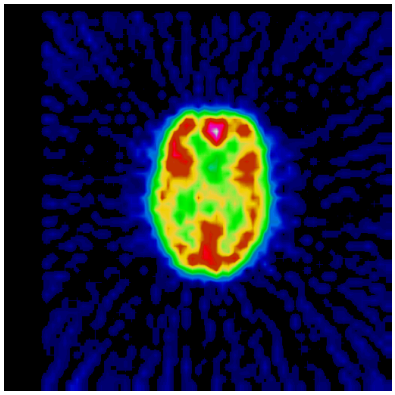

Fig.3.7.1.1 (b): reconstruction of an acquisition 10s by projection

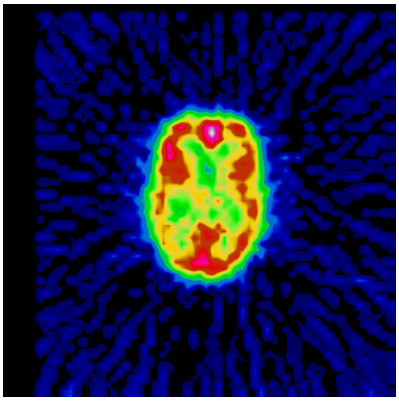

Fig. 3.7.1.1 (c): reconstruction of an acquisition of 5s by projection.

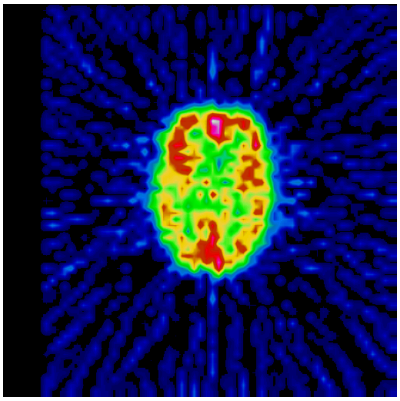

Fig.3.7.1.1 (d): reconstruction of an acquisition 2s by projection

In the spectra of the Figure 3.7.1.2 is seen what happens when the amount of time and therefore the number of counts acquired is low: the noise level "invades" lower frequencies, and consequently, the image becomes less defined, less structured. Or to put it another way, as you increase the number of counts the separation between the signal and the noise increases although, because this is reconstructed images, the relationship between the number of accounts and quality (signal/noise ratio) is not direct as in the planar scans.

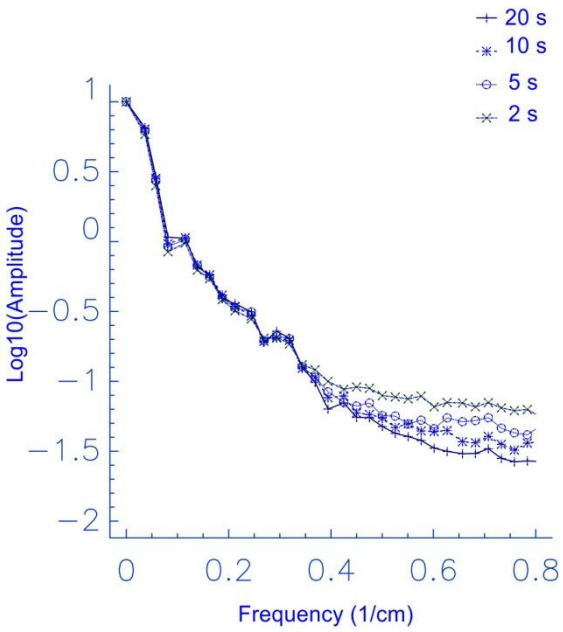

Fig. 3.7.1.2: spectra as a function of time per projection.

3.7.2 Distance between the collimator and patient

Let's take a look at the influence of the distance between the collimator and the patient's body, the distance that is determined by the turning radius in a gamma camera in SPECT. Figure 3.7.2.1 shows two images, one from a study acquired from the normal working distance, approximately 20 cm from the edge of the phantom to simulate the presence of the shoulders, which corresponds to a radius of 30 cm and another obtained by inserting the header to the maximum (12-13 cm that corresponds to a distance of 2-3 cm from the edge of the phantom). Both studies were acquired with the same time-projection (same number of accounts) with 64x64 matrix and 64 projections.

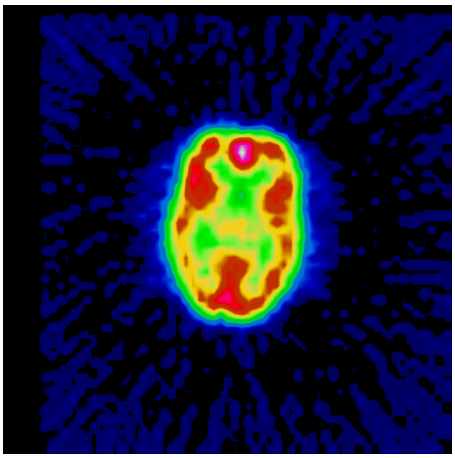

Fig. 3.7.2.1(a): image obtained at a distance of 20 cm

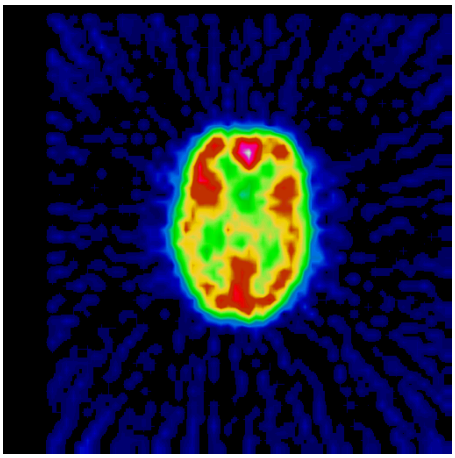

Fig.3.7.2.1(b): image obtained at a distance of 2-3 cm.

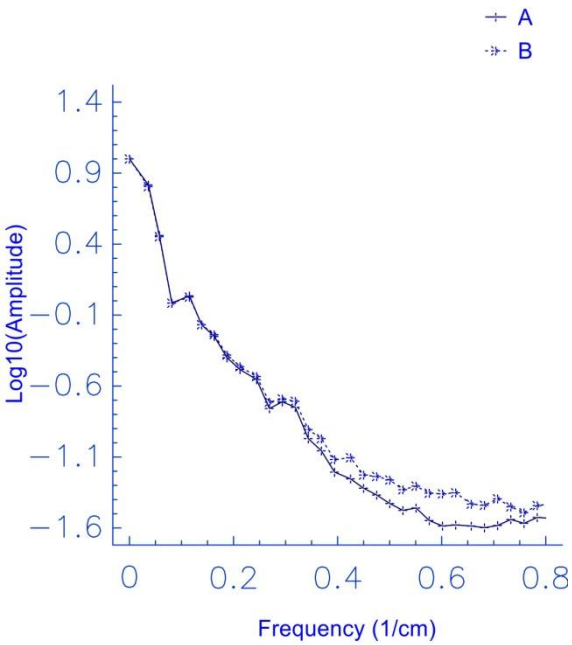

Fig.3.7.2.2: A: spectrum of the image (a).
B: spectrum of the image (b).

Note the slight increase in the amplitudes in the range 0.4-0.8 cm^{-1} in the spectrum at short distance (B) with respect to a greater distance (A) in the Figure 3.7.2.2 which translates into a higher definition of the image to 2-3 cm (Figure 3.7.2.1 (b)) than the one at 20 cm (Figure 3.7.2.2(a)). This improvement in the tomographic resolution is a direct consequence of the increase of the resolution of the original planar projections that depend in turn on the collimator used in the acquisition in SPECT. The well-known worsening of the images with the distance on the planar scan also has an impact on SPECT.

3.7.3 Relationship between distance and matrix size

If we repeat the two previous studies using an array of 128x128 and 128 projections but keeping the same total scan time, and the equivalent tomographic slices (Figure 3.7.3.1), we do not obtain the improvement that would be expected by the fact of using an array of greater dimension. Images are of worse quality due to a decrease in the number of counts per pixel of the original images due both to an increase in the dimension of the matrix (64x64 → 128x128) and the reduction of the time-projection to maintain roughly the same total scan time.

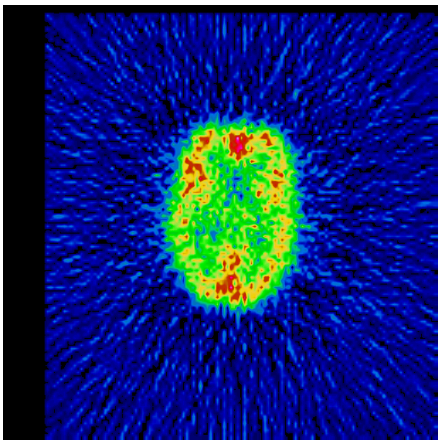

Fig. 3.7.3.1(a): image obtained from the study at 20 cm and matrix of 128x128

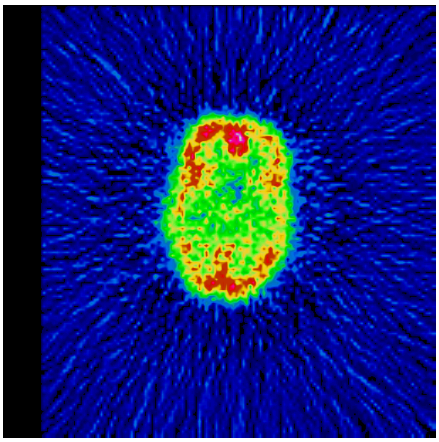

Fig.3.7.3.1(b): image obtained from the 2-3 cm and a matrix of 128x128.

The spectra (Figure 3.7.3.2) indicate that, for the conditions of the acquisition (collimator, distance, etc.), both images are equivalent and that from a frequency of ≈ 0.5 cm^{-1} can be considered that the signal is indistinguishable from noise. Consequently, the use of arrays with higher dimension does not always improve the image as shown in Figure 3.7.3.3, which shows the spectrum obtained with a 64x64 matrix and the one obtained with 128x128 both at the same distance. Note that the spectrum corresponding to 64x64 remains above 128x128 up to about 0.4 cm^{-1} and below at a frequency higher than 0.5 cm^{-1}, indicating in this case that the image of 64x64 has better signal-to-noise ratio than that of 128x128 and with a resolution equivalent to this.

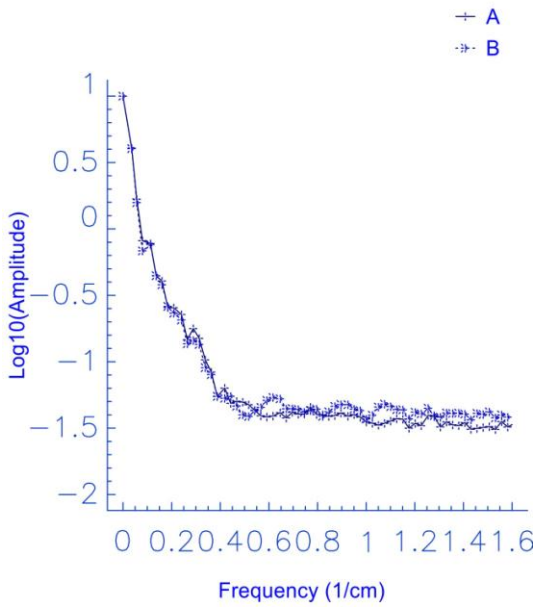

Fig.3.7.3.2: spectra corresponding to A: matrix of 64x64, B: Image of 128x128

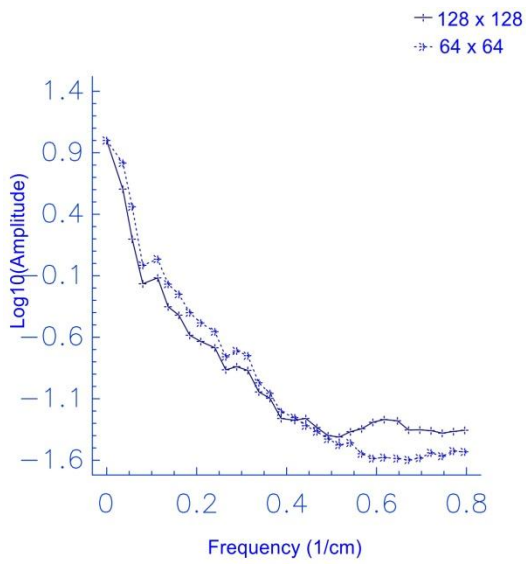

Fig.3.7.3.3: spectra corresponding to the same distance from images of 64x64 and 128x128

3.7.4 Effect of the number of Projections

Within the dependencies of the results with the acquisition parameters, it is interesting to observe how the number of projections affects the results while maintaining the dimension of the matrix. Two studies were obtained, both with a 64x64 matrix, one with 64 projections and another with 128 to decrease the streaks artifact characteristic of filtered backprojection reconstruction[15] . This artifact, which is due to insufficient angular sampling[16], decreases as the number of projections increases. The reconstructed slice with 128 projections (Figure 3.7.4.1 (b)) allows us to appreciate how the density of "bars" around the image has decreased compared to that of 64 Projections (Figure 3.7.4.1 (a)). These alterations of the background in the form of strikes, although only visible outside the organ, also alter the intensities within it. The spectra (Figure 3.7.4.2) show a slight increase in the high frequencies, which indicates both a slight increase in the resolution as a slight deterioration of the signal-to-noise ratio. However, it has greater assurance of the absence of alterations of the intensity within the organ of interest.

[15] See Section 6.3.1 for more details. This method of reconstruction does not require large processing capacity. It is the one that has allowed tomographic studies (CT, SPECT, PET) to be used intensively in clinical routine for many years.

[16] See Huesman 1977, Brian Hutton 1996.

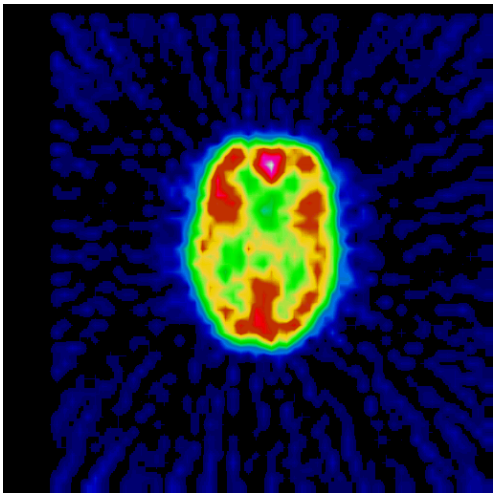

Fig.3.7.4.1 (a): obtained with 64x64 matrix and 64 projections

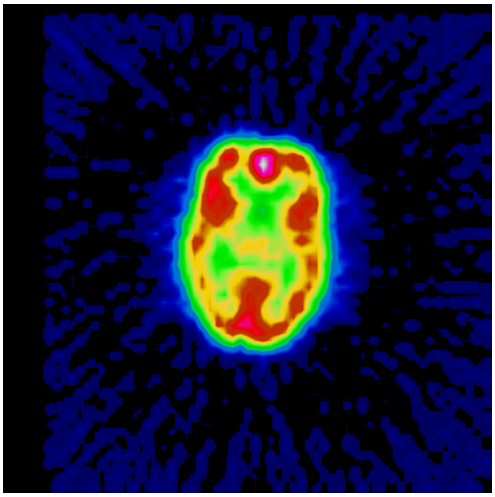

Fig. 3.7.4.1 (b): obtained with 64x64 matrix 128 and projections

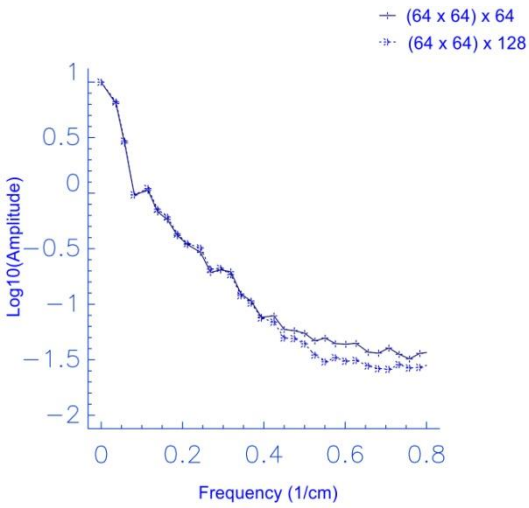

Fig.3.7.4.2: spectra of the same slices with a different number of projections.

3.7.5 Reorientation of images

The reorientation of images is very usual in processing Nuclear Medicine. It serves to reposition the organ studied to standardize the presentation of images and also helps to correct defects in the position of the patient at the time of acquisition or to obviate anatomical differences between patients. The reorientation consists of calculating the intensity of each pixel in their new position. Except if you rotate the images in multiples of 90º (90º, 180º, 270º) in

all other cases the new values are obtained by interpolation, introducing an "extra" smoothing of the image.

The Figure 3.7.5.1 shows two images: an original (a) and (b) slightly reoriented that presents a slight smoothing due to the new values are obtained by a weighted average of the originals. The spectra of both images reflect how the rotated image shows a decrease of the amplitudes in the area of high frequencies (Figure 3.7.5.2) due to this smoothing.

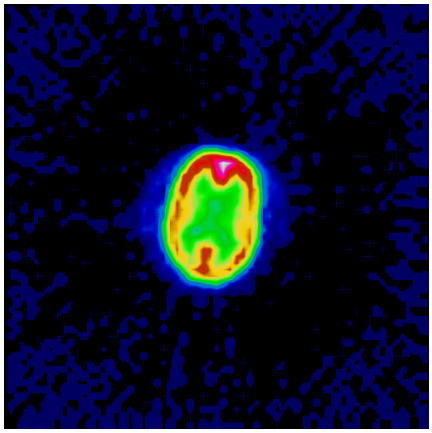

Fig.3.7.5.1 (a): original image.

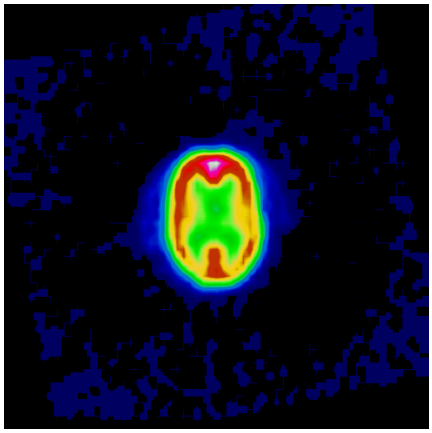

Fig.3.7.5.1 (b): Image reoriented.

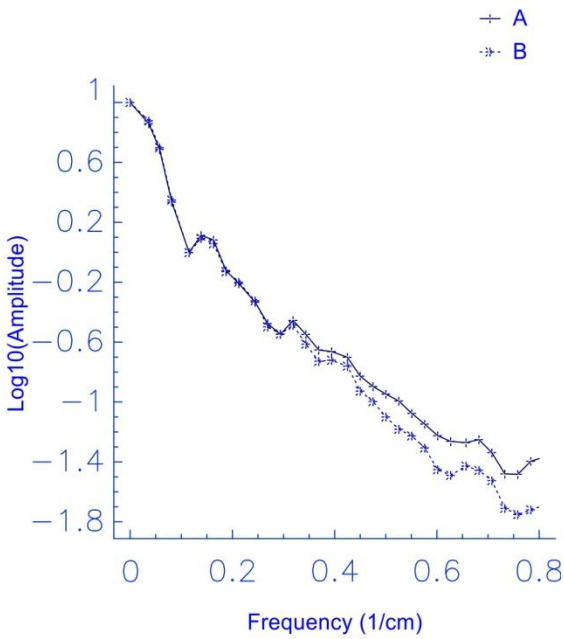

Fig. 3.7.5.2: Spectrum of the original image (A) and reoriented(B).

The conceptual baggage and terminology to analyze the images from the frequency point of view has been presented. However, before entering into the subject of frequency filters, to know the limitations imposed by the detector and by the matrices used in the acquisition of the images is also needed.

4 Imaging in Nuclear Medicine

4.1 Introduction

The frequency content of a Nuclear Medicine image depends on the distribution of radioactivity in the object explored, on the assumption that the imaging system does not impose any limitation on the images. This assumption is not accurate. The collimators impose restrictions on the resolution and sensitivity of the gamma cameras and also how the dimension of the matrices affect the final image are very well known. The size of the crystals and the distance from the axis in PET scanners also restrict their performances. Of course, the spectral representation reflects these effects. These limitations must be coordinated to optimize resources and avoid the final degradation as much as possible.

4.2 Limitations of the detection equipment

Let's consider a detector as a piece of equipment that transforms and transmits information of an object (distribution of radioactivity in the patient) in intelligible information (activity). If the imaging system is not able to detect subtle variations in the object, then these variations will be lost, will not be present in the image. Since the distribution of activity has associated a frequency distribution (spectrum), an ideal detection system would be one that does not change the content of this spectrum. The detectors have limitations, one of which is the attenuation of the amplitude of specific frequencies (usually the highest that correspond to the details). The spatial resolution is one of the parameters to quantify the quality of the transmission of the "details."

The spatial resolution of a detector is the minimum distance that may exist between two points to be detected as separate. This minimum distance is the consequence of that the image of a point is not precise, but a roughly circular spot called the Point Spread Function (PSF)[17]. This minimum distance is the width at half-maximum (FWHM) of the activity profile of the PSF[18]. Figure 4.2.1 shows the application of this criterion through 2 separate identical PSF exactly a

[17] A count profile is a curve showing the activity of the cells according to their position in any direction. It can also be obtained as the sum of adjacent rows or columns.

[18] This criterion is equivalent to the Rayleight'resolving power for optical devices.

distance equal to their width at half maximum. Figure 4.2.1(a) shows how to detect each one separately, and Figure 4.1.1(b) shows the profile when they are detected simultaneously (the sum of them).

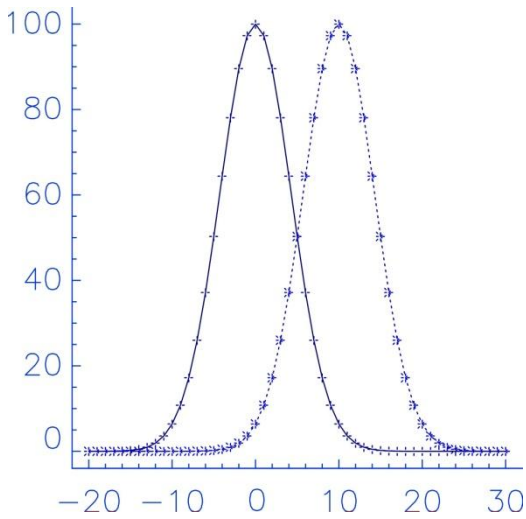

Fig.4.2.1 (a): 2 PSF profiles FWHM=10 separated a distance equal to their FWHM.

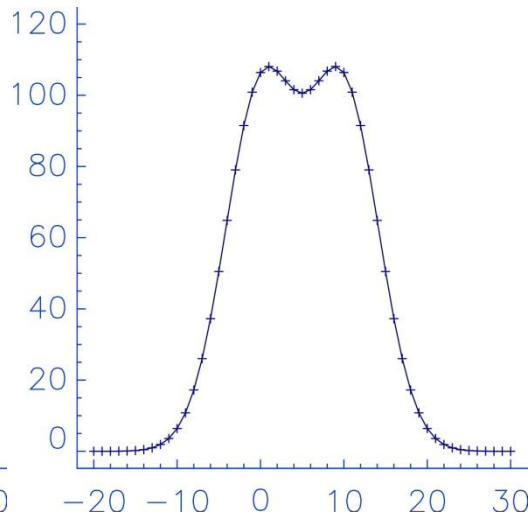

Fig.4.2.1(b): profile sum of 2 PSF

The superposition of the PSFs means that the detector only distinguishes, as different, areas separated by a distance equal to or greater than the FWHM (losing all differences that may exist within a circle of diameter FWHM centered at each point). In turn, this is equivalent to say that the smaller interval with which makes sense to sample (scan) is precisely equal to the FWHM as smaller samples (smaller cells) do not provide more detail as the PSF blurs them.

If the minimum distance of sampling is FWHM, then the maximum frequency (νmax) that a detector can transmit is 1/FWHM. The spectral characterization of a detector is called modulation transfer function (MTF) and reports of how the imager reproduces frequencies of the object. Therefore, the more resolution has the imaging device (lower FWHM), the higher the maximum detectable frequency. It follows, therefore, that as the FWHM (Figure 4.2.2(a)) increases, the frequency at which the MTF becomes zero, decreases (Figure 4.2.2(b)) and that effectively to 1/FWHM the frequency responses are practically zero[19].

[19] Using the analogy with the sound, the quality of music systems can be appreciated for their ability to reproduce frequencies and subtle changes of intensity. Think about the difference of nuances in the music between HiFi equipment and a cheap portable radio! The first has a much more wide-ranging frequency response or "MTF" than the second.

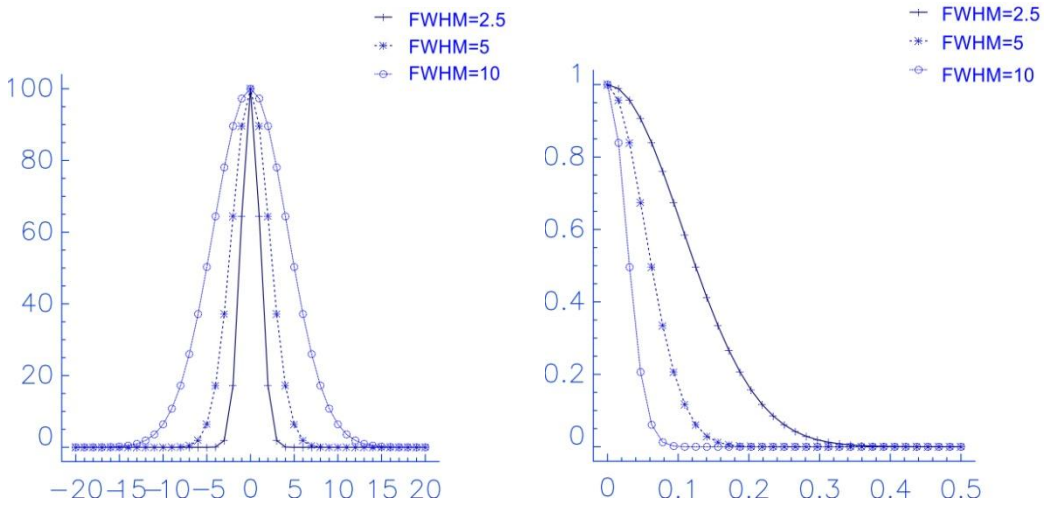

Fig.4.2.2 (a): activity profile of PSFs. Fig.4.2.2 (b): frequency response of 4.2.2(a):"MTFs"

4.3 Planar gamma camera

As is well known, the spatial resolution of a gamma camera depends on the detector, the collimator, and the distance between the collimator and the source of radiation. Consequently, the maximum frequency that the imaging system can reproduce manifests the same behavior. Experimentally we obtained these values for three collimators and four distances with the same gamma camera:

Distance [cm]	0	5	10	20
FWHM [cm]	0.57	0.71	0.83	1.23
ν_{max}[cm^{-1}]	1.75	1.41	1.20	0.81

Table 4.3.1 High Resolution (HR) collimator

Distance [cm]	0	5	10	20
FWHM [cm]	0.63	0.76	1.06	1.54
ν_{max}[cm^{-1}]	1.59	1.32	0.94	0.65

Table 4.3.2 All purpose (AP) collimator

Distance [cm]	0	5	10	20
FWHM [cm]	0.64	0.85	1.25	1.97
ν_{max}[cm^{-1}]	1.56	1.18	0.80	0.51

Table 4.3.3 High Sensitivity (HS) collimator

In these tables is seen as, for the same collimator, by increasing the distance, the maximum frequency that can transmit the gamma camera decreases and how this frequency decreases with increasing the sensitivity of the collimators. These facts are well known because decreasing the maximum frequency is the same as losing spatial resolution. Figures 4.3.1.1, 4.3.1.2 and 4.3.1.3 show images of a bar-phantom obtained under the conditions set out in the tables above to see how these performances of the detector have an impact on real images. Below are detailed the features of the bar-phantom.

4.3.1 Bar-phantom

The bar-phantom consists of a succession of bars of lead spaced a distance equal to their width inside of a plastic block. If we call "d" to this width, we will have a bar each 2d cm, or equivalently, the bars have a frequency equal to 1/2d cm^{-1}. The most common model consists of four widths of bars arranged in quadrants. The phantom used in these examples has the following characteristics (widths and frequencies):

3/8"=0.952 cm ⇒ 1 bar each 2x 0.952 cm = 1.904 cm ⇒ 1/1.904≈0.5 cm^{-1}

1/4"=0.635 cm ⇒ 1 bar each 2x 0.635 cm = 1,270 cm ⇒ 1/1.270≈0.8 cm^{-1}

3/16=0.476 cm ⇒ 1 bar each 2x 0.476 cm =0.952 cm ⇒ 1/0.952≈1.0 cm^{-1}

5/32=0.397 cm ⇒ 1 bar each 2x 0.397 cm = 0,794 cm ⇒ 1/0.794≈1.3 cm^{-1}

A bar can be detected if its frequency is significantly lower than the maximum frequency that can be detected. Thus, in the Figures (4.3.1.1, 4.3.1.2 and 4.3.1.3), the bars are "disappearing" as the distance increases from the detector. We observe this disappearance when analyzing the spectra of

amplitudes[20]. The fact that the bar-phantom had four characteristic frequencies makes its spectral representation easily interpretable because we know that each quadrant has its frequency. Consequently, if one of these frequencies does not appear in the spectrum, it means that the corresponding bars do not differ from the background. Consider (Figure 4.3.1.1) the bar-phantom image acquired with the high-resolution collimator (HR) and the bar-phantom directly supported on it (distance=0 cm). The bars of the four quadrants are completely distinguishable. In the spectrum, we will observe four peaks superimposed on a curve of smooth variation. Each peak corresponds to one of the frequencies of the bars, and the continuous curve to the image background. The position of the maximum of the peaks matches the values of the frequencies of the bars. With increasing the distance detector-phantom, the peaks representing the bars cease to be viewed, being confused with the background. Figure 4.3.1.2 presents a similar behavior for the all-purposes collimator (AP).

Looking at the image of HS20 -High Sensitivity collimator at 20 cm- (Figure 4.3.1.3), we see that the only bars that can be distinguished are the gaps between quadrants. Its spectrum shows a small peak located about 0.1 cm^{-1}, which corresponds to the limits of each of the quadrants and borders because they are separated about 20 cm (1/20=0.1). This little peak appears in all the spectra of all the images of the bar-phantom.

[20] The following spectra Figures (4.3.1.1,4.3.1.2,4.3.1.3) are Log10(Amplitude) vs frequency

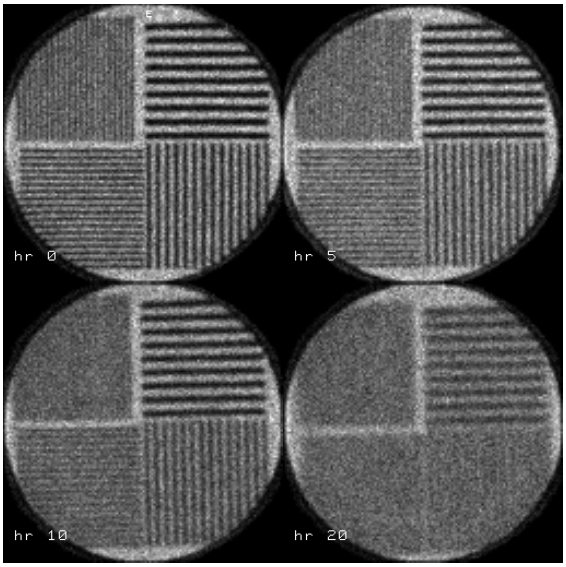

Fig. 4.3.1.1: images of the phantom with collimator HR (High Resolution) 0, 5, 10, and 20 cm away. Corresponding spectra.

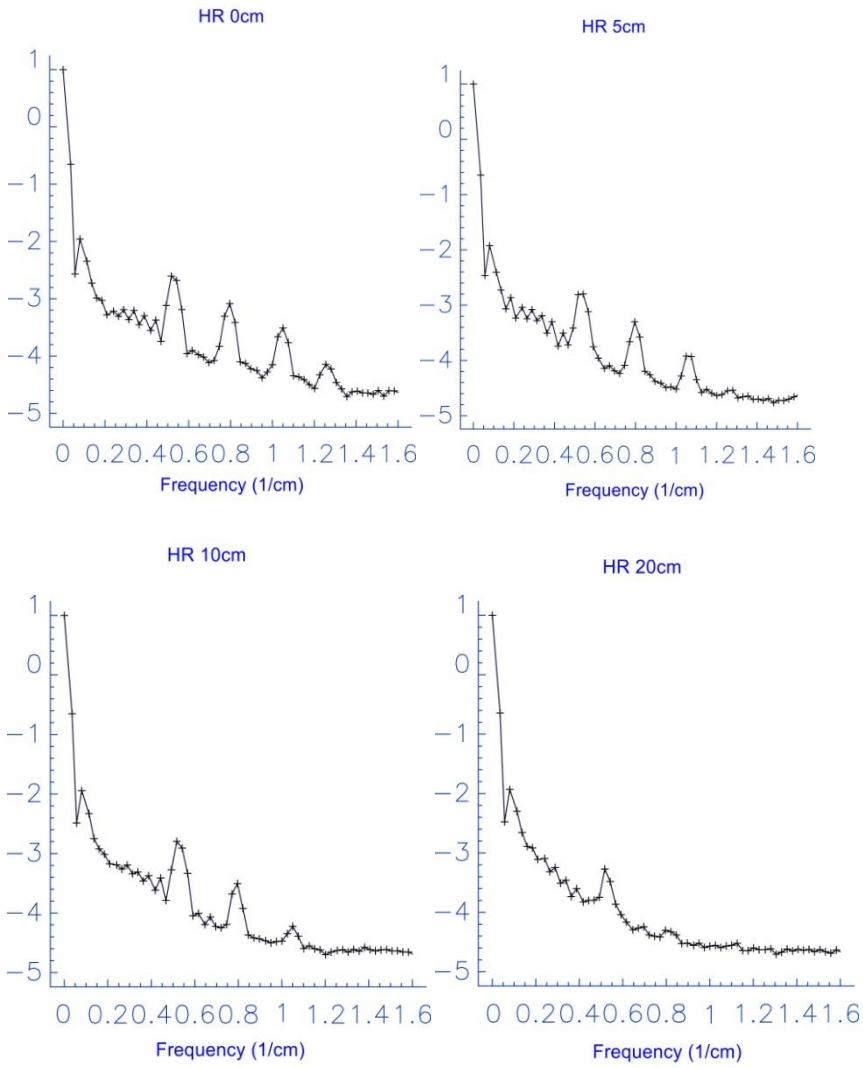

.

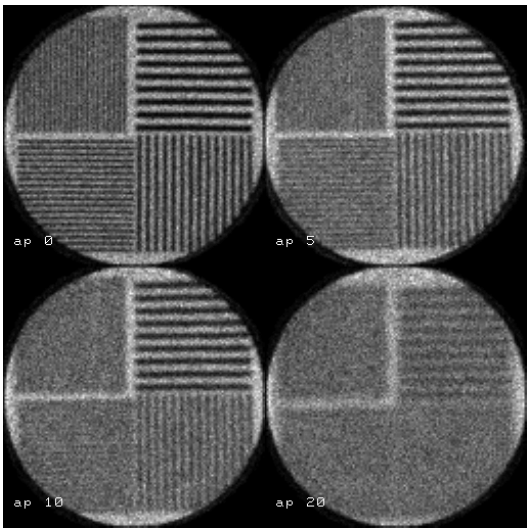

Fig. 4.3.1.2: images of the phantom with collimator AP (General Purpose) 0, 5, 10, and 20 cm away. Corresponding spectra

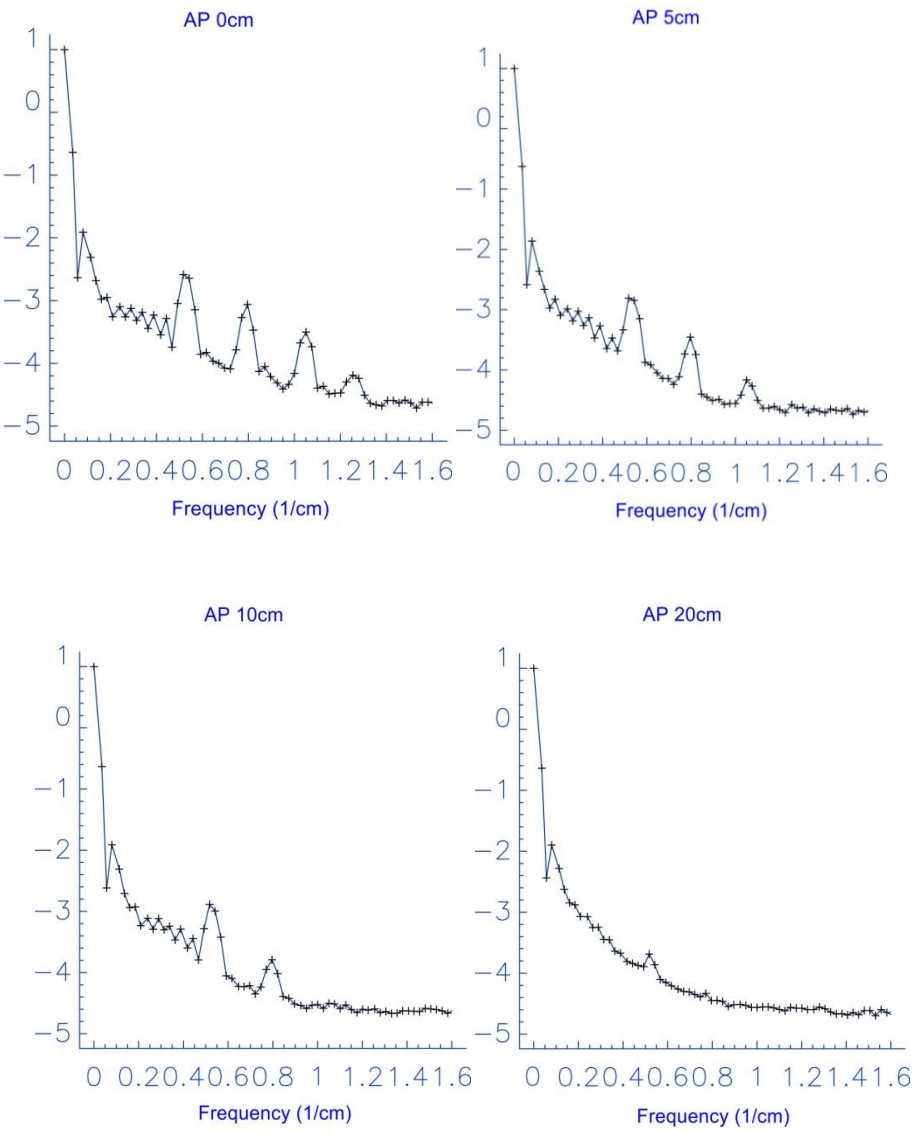

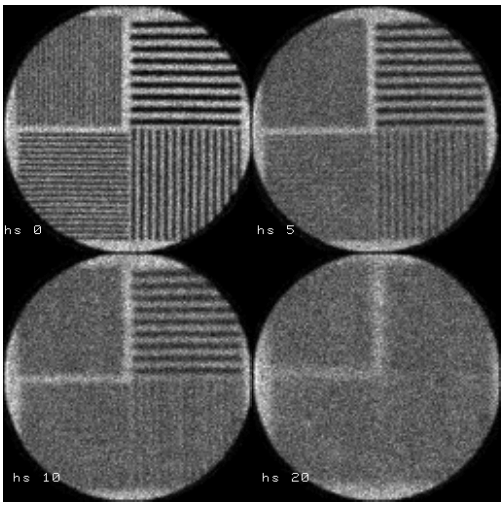

Fig. 4.3.1.3: images of the phantom with collimator HS (High Sensitivity) 0, 5, 10, and 20 cm away. Corresponding spectra.

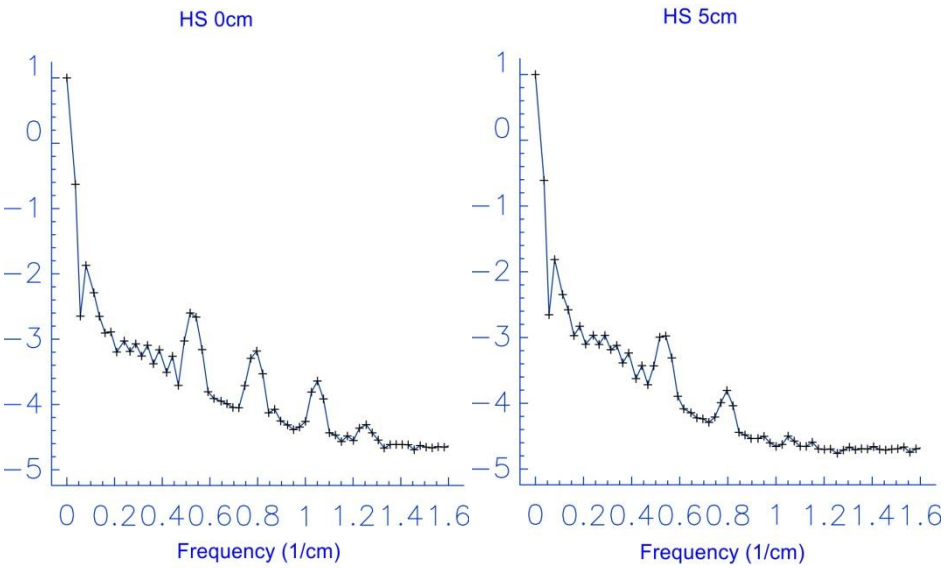

.

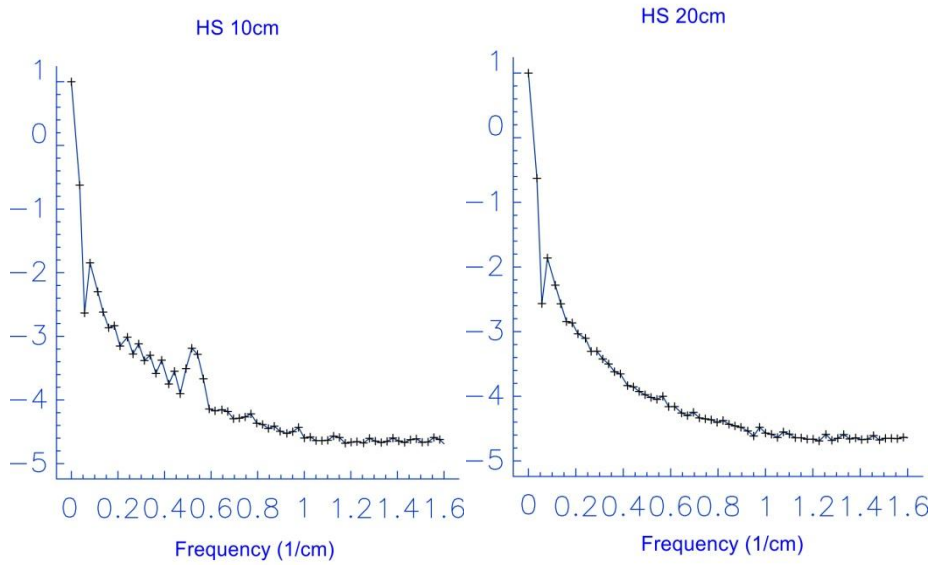

4.3.2 Interference of collimators.

The collimators affect the spatial resolution and the sensitivity of a gamma camera, and may directly interfere with the quality of the images. The use of medium and high energy photons oblige to use collimators with septa sufficiently thick to attenuate the gamma rays that enter obliquely to the collimator, which, in turn, determines the minimum gap that may exist between the holes in the collimator. If these holes do not match with the squared grid of the cells of the matrix, an artifact of a hexagonal structure appears which is due to the hexagonal distribution of the holes. Figure 4.3.2.1 shows the original image (a) and the amplitude image of its Fourier Transform(b) where appears a hexagonal distribution of maxima. This hexagonal pattern disappears from the original image (c) removing these maxima.

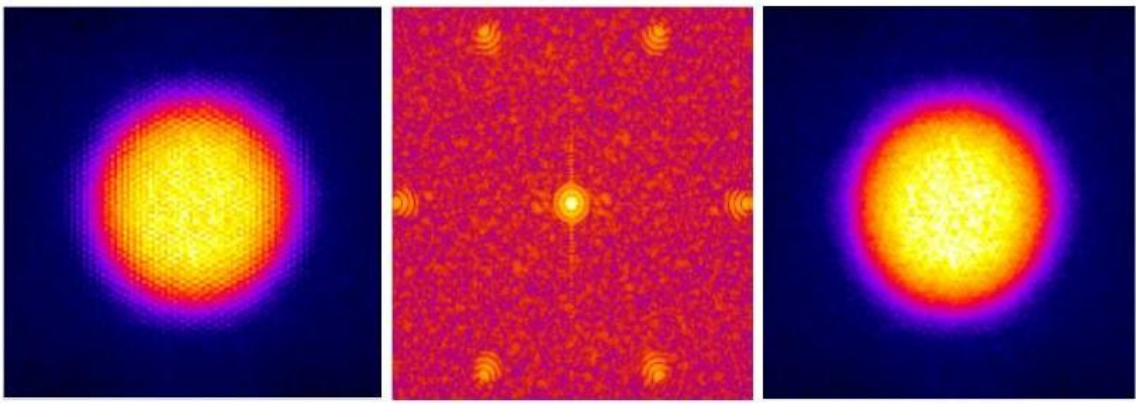

Fig. 4.3.2.1: original image (a), amplitude (b) and filtered (c)
(Image obtained from Perez-Garcia H., Boatman R. Rev Esp Med Nucl Imagen Mol 2017;36:27-36)

If we compare these images (a) and (b) with the corresponding to the phantom (Figure 3.5.1 a and b) we see once again that the two representations contain the same information. The frequency image allows detecting easily variations that follow the regular pattern of the bars, in one case, and the collimator holes on the other.

4.4 Tomograph of positrons

The detection of the photons resulting from the annihilation of positrons is carried out using solid scintillation detectors arranged in a circle that delimits the field of view of the tomograph. The two photons coming from the annihilation are emitted simultaneously in opposite directions in the same direction, as a straight line between the two detectors that have detected them (line of

response or LOR). Based on the simultaneity of the emission only are considered valid, those photons detected in a narrow time window (detection by coincidence). Figure 4.4.1 shows the simulation of the generation of LORs in a Cardiological exploration.

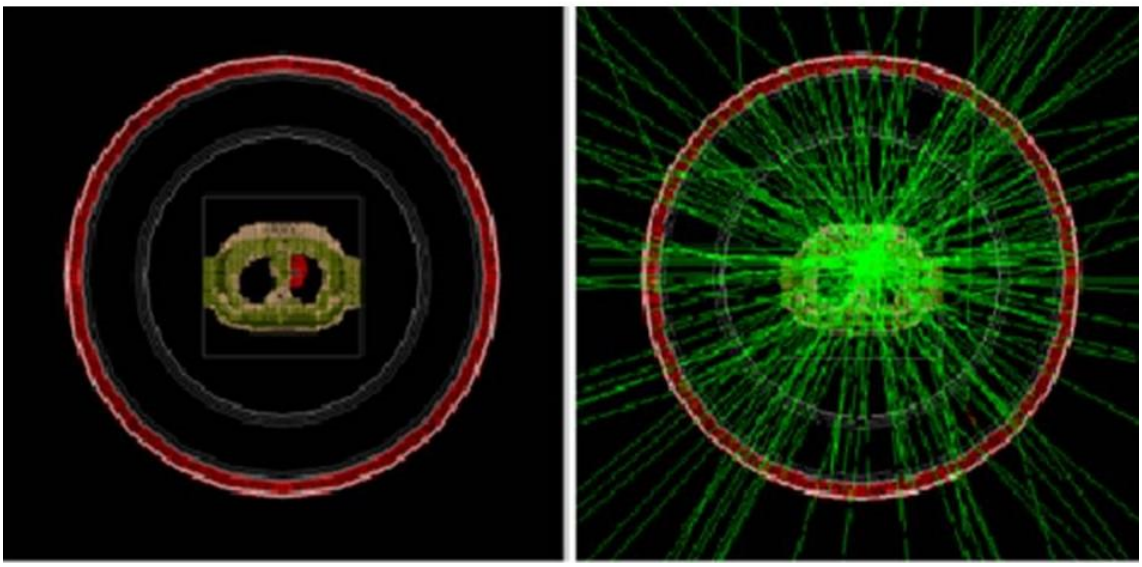

Fig. 4.4.1: Model of the torso with the myocardium emitting positrons and LORs generated (extracted from Florez Pacheco and Furuie Shigemi, S. Computing in Cardiology 2014; 41:949-952)

The lines of response are virtual lines that inform that at some point in them the annihilation has been produced not knowing its exact position. Without more information, all locations of the LOR have the same probability of being the focus of the emission, which is the basis of the conventional PET. The difference in time that the photons need to reach the two detectors, which is the basis of the coincidence technique, can also be used to restrict the segment of the LOR where most likely the annihilation of the positron had taken place. This restriction allows for increasing the signal-to-noise ratio by eliminating much information that did not contribute to the calculus of the location (Figure 4.4.2). If the tomographs where faster enough it would be possible to determine the point of annihilation at the pixel level and there would no need to reconstruct the image; a cross-sectional study directly would result.

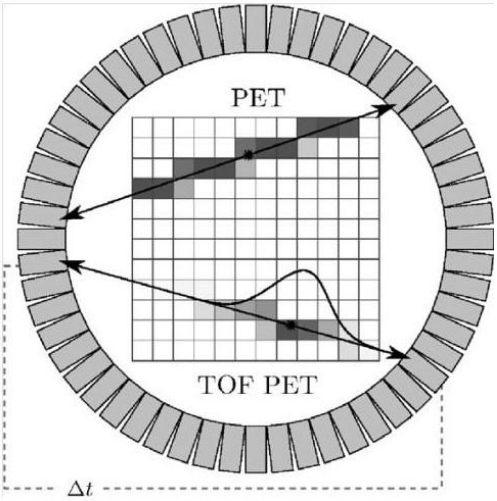

Fig.4.4.2: LORs with and without time of flight (TOF-PET). Δt symbolizes the difference in time of arrival to the detectors. (Obtained from PET: Physics, instrumentation, and scanners, Simon R. Cherry and Magnus Dahlbom PET Molecular Imaging and its biological applications. Phelps M.)

The circular arrangement of the detectors and the small size of the crystals produces two types of deviations from what would be ideal. One is that according to the direction in which gamma photons interact with the scintillation crystals, the interaction can occur in different contiguous crystals. That is, they can penetrate one but do not end up being completely absorbed until the second or third, as illustrated in Figure 4.4.3; more than one detector element detects the light photons produced in the scintillations by which makes the PSF not symmetrical and broader.

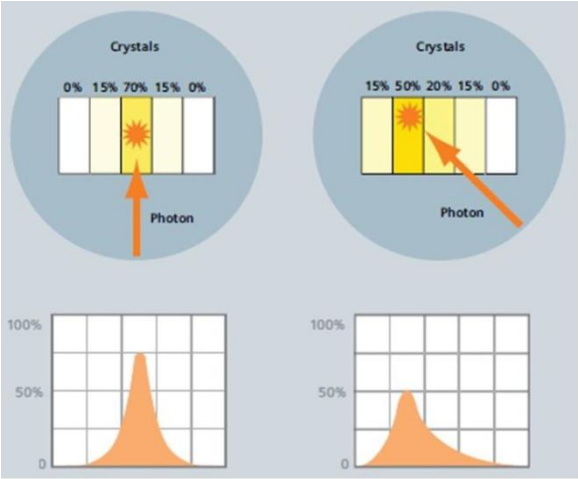

Fig.4.3.3: variation of the PSF as a function of the angle of incidence
(Extracted from Siemens Brochure: Are you HD ready?)

On the other hand, the interaction is not always at the same depth. Because of that, the width of the PSF varies with the depth of interaction (DOI: Δd), making

the spatial resolution not constant. The FWHM varies with the distance from the center and with the depth of the interaction (Δd) (Figure4.4.4).

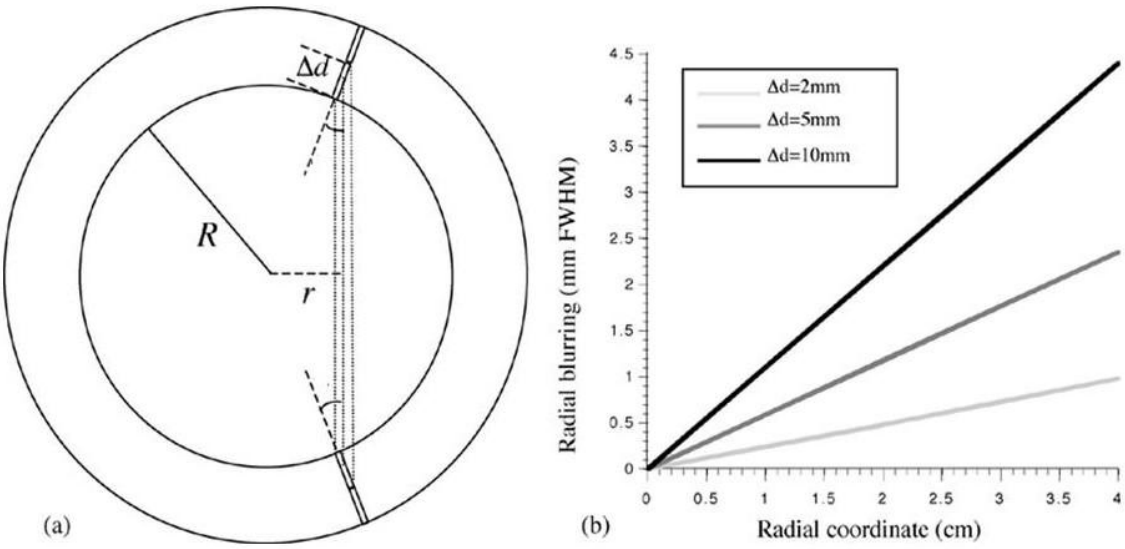

Fig. 4.4.4: variation of the FWHM with the distance to the center of the field (r) for different depths of interaction (Δd). R is the radius of the field of view. (Extracted from C.Levin Proceedings of the IEEE | Vol. 96, No. 3, March 2008)

This dependence results in that the lines of response are not correctly determined because there is an essential difference between the point of entry (which would be the right point) with the one calculated from the response of the crystals involved (Figure 4.4.5). This error is called parallax.

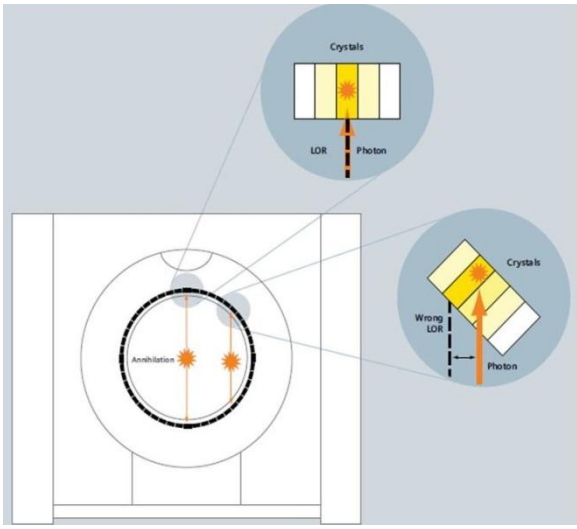

Fig. 4.4.5: misallocation of LOR by the tilt of the detectors.
(Extracted from Siemens Brochure: Are you HD ready?)

The circular arrangement of the detectors causes a geometric distortion. The angle between the rays and the detectors decreases from 90º to 0º as parallel rays move from center to the border. The effective area of the crystals goes

from a maximum, which is the width of the scintillation crystal, to zero. This fact makes the lines of response to be not equally spaced, reducing the distance between them with increasing distance to the center (Figure 4.4.6). The result is that the sampling is not constant in the direction of the radius.

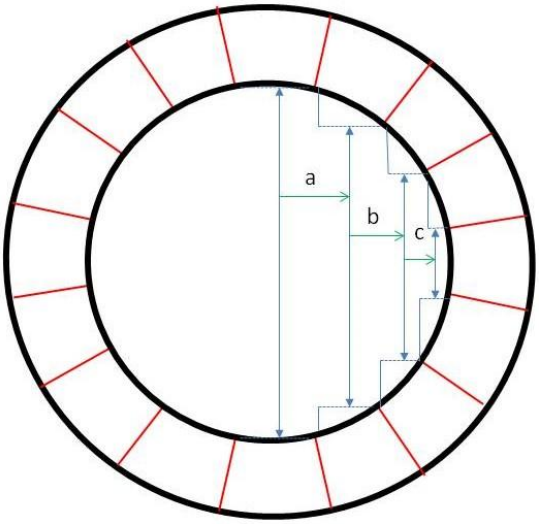

Fig. 4.4.6: the LORs are unequally spaced along the radius (a>b>c).

Also, the size of the crystals affects the spatial resolution. A point source located at the center of the field of view generates a PSF with an FWHM equal to half of the width of the crystal. As the source approaches the detectors, the FWHM increases up to the thickness of the crystal (Figure 4.4.7). Consequently, the intrinsic spatial resolution depends on the position of the point source within the line of response.

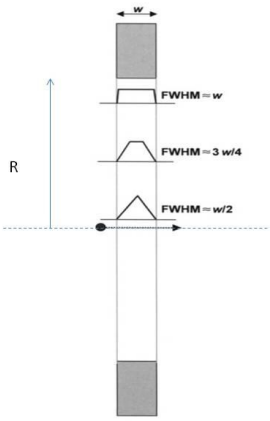

Fig.4.4.7: variation of the intrinsic spatial resolution with the distance to the center of the field. W is the thickness of the crystals, and R is the radius of the field of view. (Obtained from PET: Physics, instrumentation, and scanners. Simon R. Cherry and Magnus Dahlbom PET Molecular Imaging and its biological applications. Phelps M.)

All the exposed limitations of the detection equipment currently are corrected in the acquisition or during reconstruction.

It is important to note that the final resolution, i.e., the ability to obtain the position of the emission of a positron correctly, is limited by physics involved in their detection. On the one hand, the annihilation of the positron only takes place when it is practically at rest. If it stops completely, the two gamma rays are emitted exactly at 180º to each other. If there is small residual energy ("almost stopped"), then a deviation occurs between one and the other up to 0.35º which is the so-called error of colinearity and is not very important for practical purposes. What is important is the range of positrons inside the patient's body. This value is the average maximum distance between the point of emission and the point where the positron has released all its energy. This maximum distance depends on the positron's energy. Thus, for positrons of ^{18}F of 630 keV (Figure 4.4.8) this distance is about 2.3 mm, but for ^{15}O is 8.0 mm. This range means that a perfect tomograph will never be able to specify at which point of the sphere of radius the range the positron emission has occurred and, therefore, where is located the radiopharmaceutical emitter. It is the uncertainty inherent to PET.

From the instrumentation point of view, the great advantage of PET to SPECT is its high sensitivity, which means better image quality by having a very high signal-to-noise ratio.

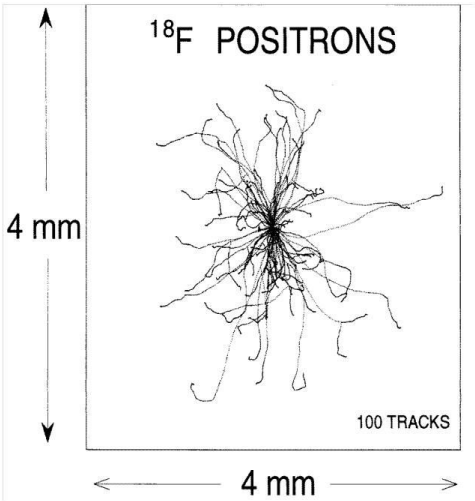

Fig.4.4.8: simulation of the trajectories of the tomography issued by ^{18}F in a similar medium to soft tissue. (Extracted from Levin C.S., Hoffman, E.G., Phys. Med. Biol. 44 (1999)).

4.5 Digitization dependence

Digital imaging is carried out through a matrix that consists of many pixels or cells sorted according to a Cartesian coordinate system. In the gamma cameras, the matrix generally covers all the useful field of view so that each pixel corresponds to a particular area of the scintillation crystal. According to the place of the crystal where the scintillation occurs, it will be assigned to one or another pixel. With a matrix of 64x64, the image has 4096 cells, as the elements of a mosaic. These squared elements have a measure (in X and Y), which is called pixel size (x), and are calculated from the useful field of view of the gamma camera (UFOV), the size of the matrix (DIM) and the magnification factor (ZOOM). The pixel size is given by

$$Px = \frac{UFOV[cm]}{ZOOM \cdot DIM}\ [cm]$$

Note that the extent of the pixels is another factor that limits, once more, the spatial resolution of the image. If two pulses corresponding to slightly different positions are assigned to the same pixel, they will have the same coordinates in the image, so that they can not be differentiated. Since the matrix recovers the entire field of view, there is no space between pixels, the distance between pixels is equal to its size. This fact originates the spatial sampling frequency (ν) to be exactly the inverse of the pixel size.

$$\nu = 1/Px\ [cm^{-1}]$$

Each stage of the process of detection imposes its limitations. However, there are some conditions which, if met, ensure that the digitations does not degrade the signal, or conversely, that is possible to reproduce the original signal[21] from the digitized signal. These conditions (fixed by the sampling theorem or Shannon theorem) set how the pixel size (which is the sampling period) has to be in order not to lose information. In this context, this theorem states that for an object whose maximum frequency is ν_{max}, the minimum sampling has to be

[21] The original signal is the distribution of activity detected through the imaging system (crystal, collimator,...) not the activity emitted by the patient!

done at least twice of this maximum frequency so that you have at least two samples per period to be able to reproduce each frequency. The maximum frequency of the object determines the minimum sampling period, which is given by:

$$T_{min} = \frac{1}{2 \cdot \nu_{max}} \; [cm]$$

Conversely, if the object is sampled each Px [cm], the maximum frequency of the object that can be recovered is given by ν'_{max}, which is the inverse of twice the pixel size.

$$\nu'_{max} = \frac{1}{2 \cdot Px} \; [cm^{-1}]$$

This maximum frequency is called the Nyquist frequency (Nyq). For the user of Nuclear Medicine, this theorem states the limits of the resolution to which it can aspire according to the pixel size. It is important to note, therefore, that if you do not want to lose resolution in the digitalization, the pixel size has to be such that the maximum frequency that can rebuild was higher than or equal to the maximum frequency given by the detector which is the inverse of the FWHM:

$$\frac{1}{(2 \cdot Px)} \geq \frac{1}{FWHM}$$

or, in an equivalent form[22],

$$Px \leq \frac{FWHM}{2}$$

Suppose a UFOV of 40 cm, depending on the dimension of the matrix and the zoom will obtain different frequencies of Nyquist (Table 4.5.1):

[22] Some texts, as a practical rule, establish Px=FWHM/3

Dimension of the matrix	Magnification Factor	Pixel size [cm]	Nyquist f. [cm^{-1}]
64	1	0,626	0.80
64	1.5	0,417	1.20
64	2	0,313	1.60
128	1	0,313	1.60
128	1.5	0,209	2.39
128	2	0,157	3.18

Table 4.5.1 Table of Nyquist frequency for different matrices

By comparing the Nyquist frequencies of this table with the maximum frequency tables 4.3.1,4.3.2 and 4.3.3, it is seen that to not sacrifice the best resolution (the highest maximum frequency =1.75 cm^{-1}) a matrix of 128x128 with a zoom of 1.5 which has a maximum frequency of 2.39 cm^{-1} should be used. This comparison also indicates that it is not always better to work with the smallest pixel size (e.g., 256x256 or 512x512) as it implies an increase in the number of pixels without achieving higher resolution. Also, doubling the dimension of the matrix quadruples the number of pixels, which decreases the statistical quality (the relationship between signal and noise) by dividing by four the number of counts per pixel.

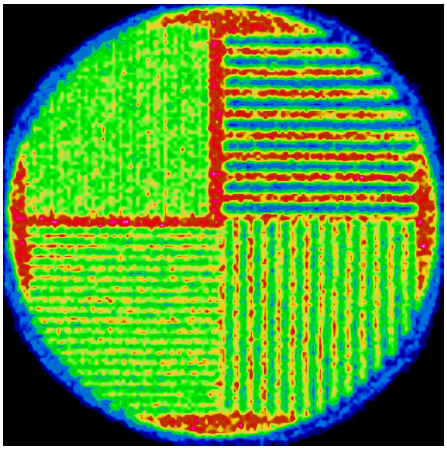

Fig.4.5.1: image with a matrix of 128x128.

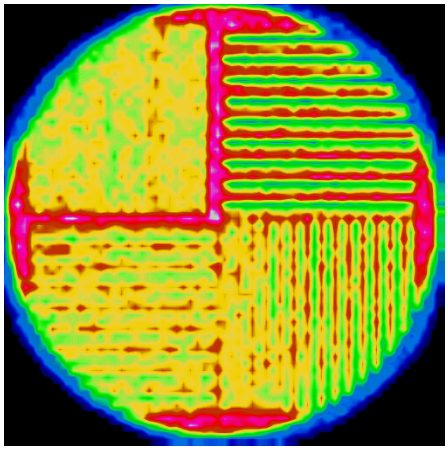

Fig.4.5.2: image with a 64x64 matrix.

Figures 4.5.1 and 4.5.2 show us the images of the bar-phantom acquired with a matrix of 128x128 and with one of 64x64. In the 128x128 matrix, we observe the bars correctly since the Nyquist frequency for 128x128 (1.60 cm^{-1}) is higher than that of the thinnest bars (1.3 cm^{-1}) as evidenced in the corresponding spectrum (Figure 4.5.3). If you are using a matrix of 64x64, then you can only discern the two quadrants with thicker bars (0.5 and 0.8 cm^{-1}) since they are the only ones whose frequency characteristics are lower than the Nyquist (0.80 cm^{-1}) for this matrix (see Figure 4.5.4). This last figure shows clearly how with arrays of 64x64 the range of frequencies is half the size of the ones with 128x128 and that therefore the resolution also will be the half.

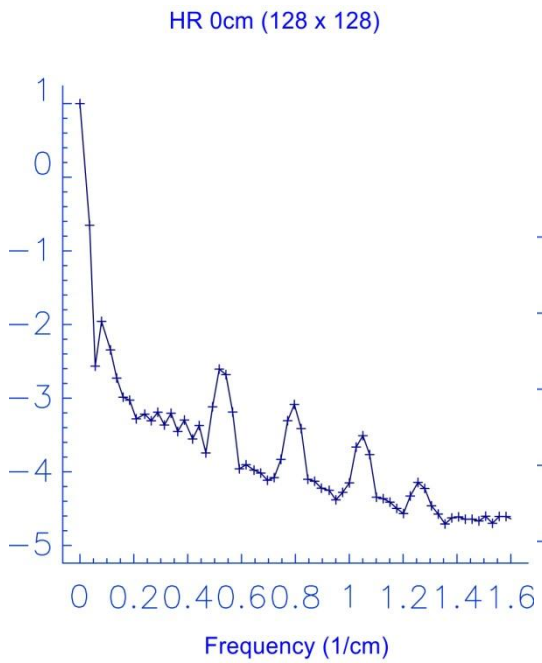

Fig.4.5.3: spectrum of the image with 128x128 matrix (log10(amplitude)).

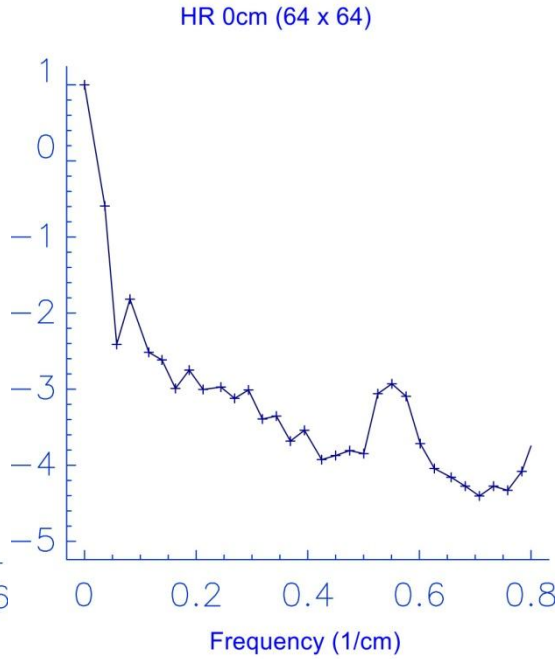

Figure 4.5.4: spectrum of the image with 64x64 matrix (log10(amplitude)).

Although less apparent, the same effect occurs in any image, as is the case of a phantom of a tomographic brain. The two following images (Figures 4.5.5, 4.5.6) show how can be affected by the change of dimension of the matrix, the first derived from 128x128 is sharper than the second obtained with a 64x64 matrix.

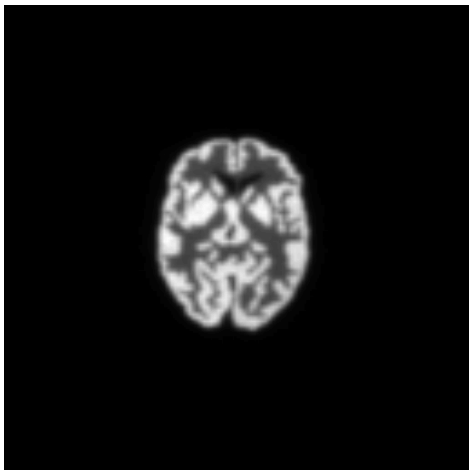

Fig. 4.5.5: Phantom of the brain with a matrix 128x128.

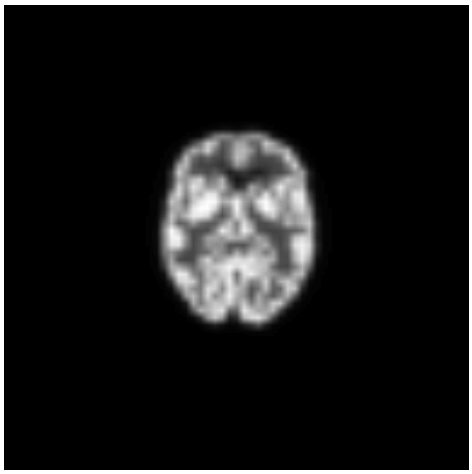

Fig. 4.5.6: Phantom of the brain with a matrix of 64x64.

4.6 Distance patient-collimator dependence

Figure 4.6.1 shows the loss of definition due to the increase in object distance-collimator. Figure 4.6.2 reflects the changes in the spectra. In this case, with the collimator (HR) and the matrix of 128x128, at 10 cm, the spectrum is flat for frequencies above 1.2 cm^{-1}. This frequency coincides with that obtained from the FWHM for this collimator and distance (table 4.1). The same is true for the distance of 20 cm, being the maximum frequency in this case of 0.8 cm^{-1}.

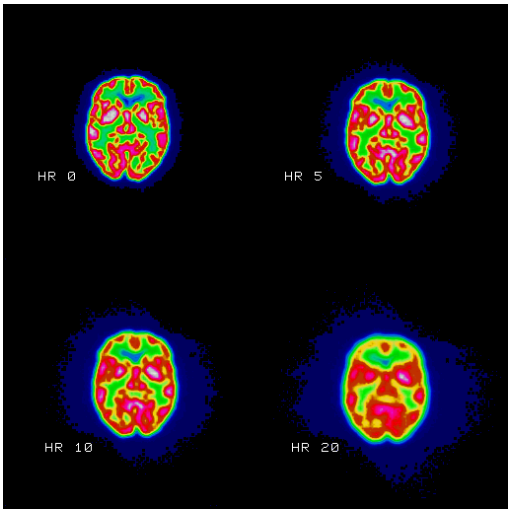

Fig. 4.6.1: Phantom of the brain obtained at 0,5, 10 and 20 cm away from a collimator HR 0,5,10 and a 128x128 matrix

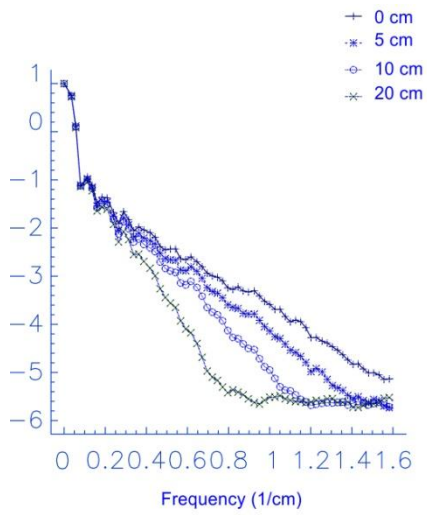

Fig.4.6.2: Spectra of the brain phantom at 0,5,10 and 20 cm.(Log10(amplitude))

It follows that the collimator, distance, and dimension of the matrix have to be coordinated. For example, with the high-resolution collimator at a distance of 20

cm, it is sufficient to use a matrix of 64x64 as the maximum frequency transmitted by the system detector (0.8 cm-1) is equal to the maximum that you can register with this equipment. The use of a 128x128 only brings a decrease in the signal-to-noise ratio.

Conversely, at a distance less than 10 cm, for which the gamma camera transmits a frequency higher than 0.8 cm^{-1}, it is appropriate to use a matrix that can reproduce frequencies higher than this.

From the values in Tables 4.3.1,4.3.2 and 4.3.3 and 4.5.1, we can establish a relationship between the collimator, distance, and matrix (table 4.6.1), which indicates the optimal matrix size.

Distance [cm]	0	5	10	20
Collimator HR	256	128	128	64
Collimator AP	128	128	128	64
Collimator HS	128	128	64	64

Table 4.6.1 Example of optimal combinations collimator-distance-matrix

4.7 Signal-to-noise dependence

The last factor to take into account is the signal-to-noise ratio. Figure 4.7.1 shows that when the number of counts (100000, 500000, 1000000, and 5000000) increases, the frequencies of the phantom appear more markedly. Note that the position of these picks is constant (does not change with the number of counts). The frequency of the signal does not depend on the number of counts, but it does its amplitude and, consequently, its detectability.

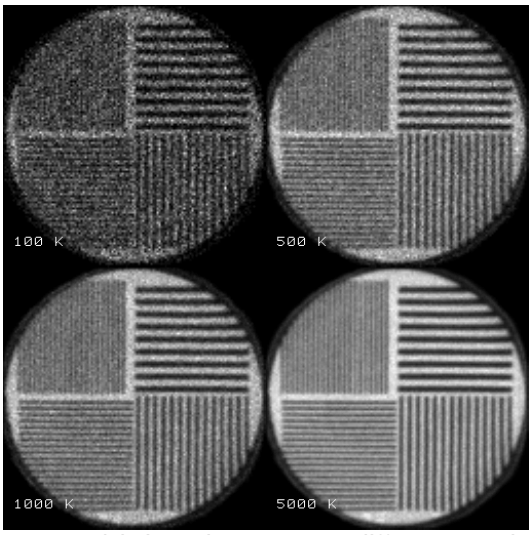

Fig. 4.7.1 (a): bar phantom at a different number of counts.

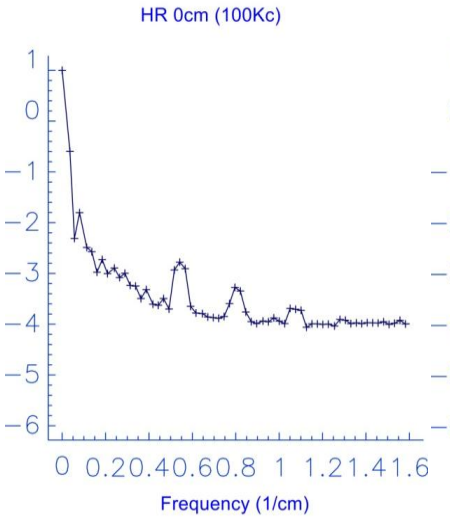

Fig. 4.7.1 (b): 100,000 counts Log10 spectrum

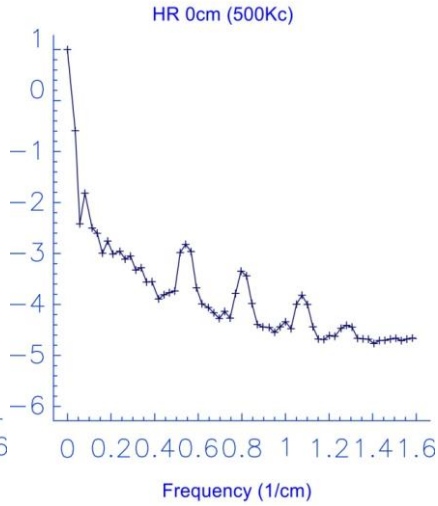

Fig.4.7.1 (c): 500,000 counts Log10 spectrum

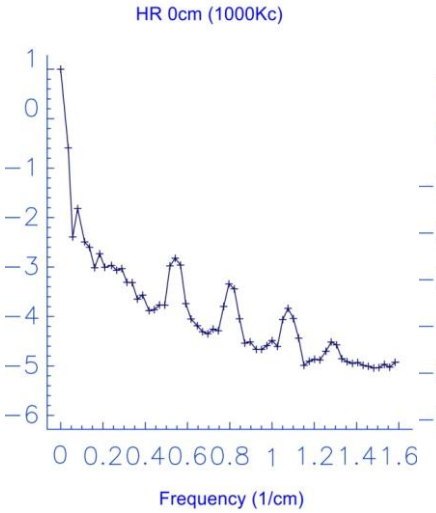

Fig.4.7.1(d): 1,000,000 counts Log10 spectrum

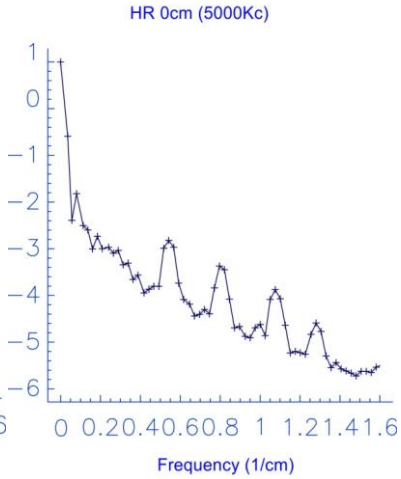

Fig.4.7.1 (e): 5,000,000 counts Log10 spectrum

Of the latter, it appears that the number of counts per pixel is essential to obtain the best possible resolution. For equal resolution, we should always look for the combination of detector and collimator that possesses the highest sensitivity for the noise "muddies" as little as possible the amplitudes of the frequencies that the detector system has been able to recover from the patient.

5. Frequency Filters

5.1 Introduction

After a lengthy introduction already we have the necessary tools to return to the subject of the filters. As a first approximation, to filter is to transform a signal according to a defined pattern (see Chapter 2). You can now say that to filter a signal is to modify its frequency content. One kind of modification can be done to achieve the desired effect eliminating or changing the amplitude associated with the frequencies on which we wish to act. Another modification is the one due to the process of obtainment of images, such as detection, collimation, digitalization,...that can be also viewed as filters as it has been seen in the preceding chapter.

Given that on the amplitude image the value of each pixel corresponds to the amplitude for each pair of frequencies (f_x, f_y), filtering consists in simply to multiply the value of the pixels corresponding to the frequencies on which we wish to act by an appropriate gain factor: 0 to erase, between 0 and 1 to attenuate, greater than 1 to amplify.

A filter is, therefore, a matrix of factors, equal to the dimension of the image that we want to filter (64x64, 128x128,...), and that acts by multiplying pixel by pixel the images of amplitude and phase of the original image. From these two new images (filtered amplitude and phase), using the inverse Fourier transform, we get the filtered image (if the direct Fourier Transform decomposed an image in sinusoids, the inverse Fourier Transform reconstructs an image from sinusoids).

5.2 Representation of frequency filters

Although the frequency filters are matrices, this type of representation in Nuclear Medicine is seldom used. Instead, a much more easy and intelligible form, consisting of a curve that shows the variation of the gain factors as a function of the frequency is used (Figure 5.2.1). These diagrams show how to modify the contribution of each frequency of the original image to form the filtered image. A null value indicates that that frequency is not transmitted, that is to say, it does not appear in the filtered image. A unit value means that it is no modified. To decrease the effect of noise, we reduce the amplitude of the high frequencies as it is in this range of frequencies where it is more noticed. On the contrary, to detect contours should enhance the mid and high frequencies. The

filter in Figure 5.2.1, is a filter that practically does not modify the amplitudes of the frequencies of less than 35% of the Nyquist frequency and then decreases gently up to 0 for the 100% of this frequency. This means that applied to the bar-phantom, the thicker bars that are located on the 30% of Nyquist remain "unchanged" and that the amplitude of the sinusoids with frequencies involved in the representation of the thinner bars (1/4") is decreased by a factor of approximately 0.7 for being situated around 50% of Nyquist. The following bars, which roughly correspond to the 62.5 %, have had sharply reduced its contrast (≈0.3) and the corresponding to 81.25% of Nyquist become indistinguishable as the amplitude of the frequencies that they involve have been practically annulled (0.07). The rotation of this curve around the Y-axis generates a matrix (Figure 5.2.2), which is used to multiply the images of magnitude and phase.

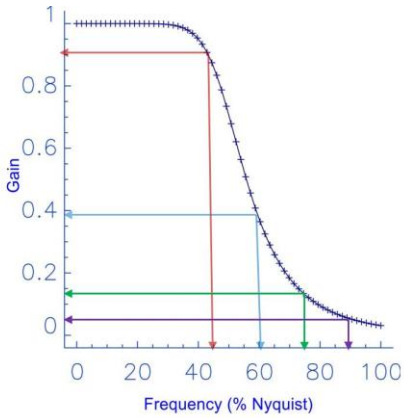

Fig.5.2.1: one-dimensional filter.

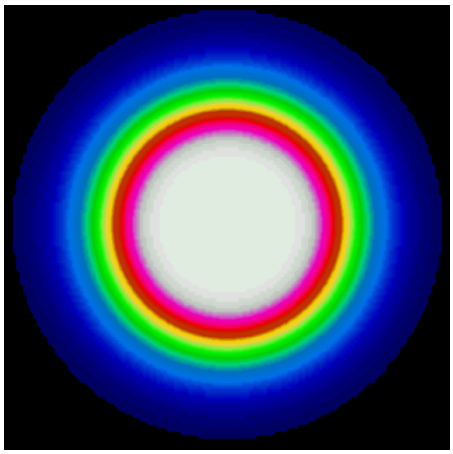

Fig.5.2.2: Two-dimensional filter obtained by rotation of the one-dimensional filter.

The effect of this filter is observed directly on the image of the amplitude of the "filtered" (Figure 5.2.4) obtained by multiplying the original amplitude image (Figure 5.2.3) by the matrix obtained from the filter (Figure 5.2.2). In the amplitude of the filtered image (Figure 5.2.4), the most distant points to the center of Figure 5.2.3 have disappeared. This disappearance means that the more "fine" vertical bars are not distinguishable from the background, as documented in Figure 5.2.5(b). This image has been obtained by applying the inverse Fourier transform to the filtered image representation (Figure 5.2.4).

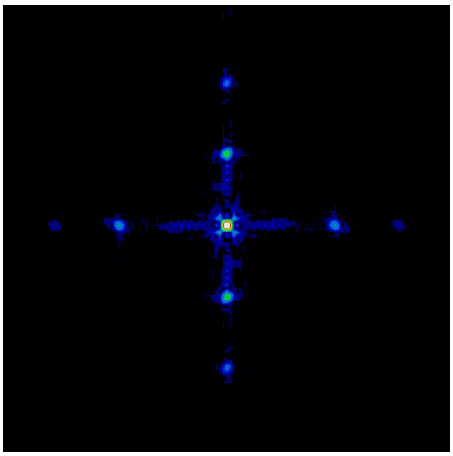

Fig. 5.2.3: the image of the amplitude.

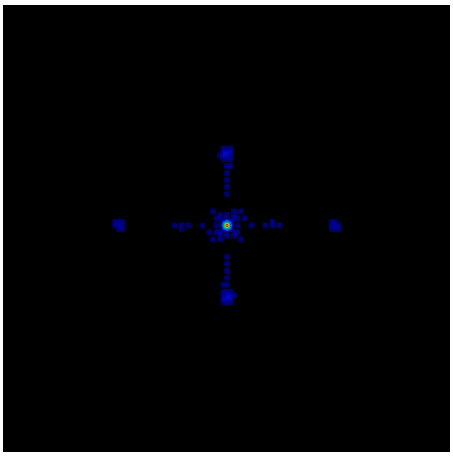

Fig. 5.2.4: the image of filtered amplitude.

The comparison of the two figures 5.2.5 serves to clarify the effect of the applied filter. On the one hand, there has been a decrease in the mottled or irregularities in the counts in the whole image (noise), being more clear this effect in the first quadrant and somewhat less in the second. On the other hand, we also note that the bars in the third quadrant almost do not differ from the background and that those of the fourth quadrant have disappeared. This example shows again how the smoothing filters reduce noise and also reduce details of the images that may be of diagnostic value.

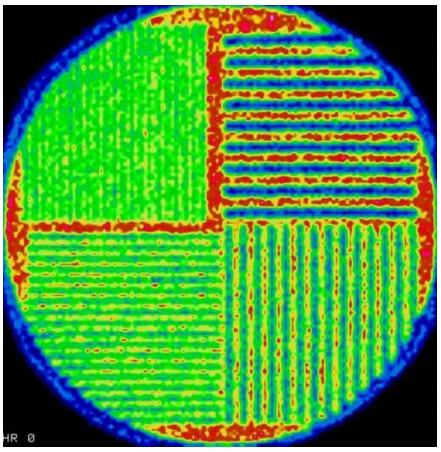

Fig. 5.2.5(a): original image

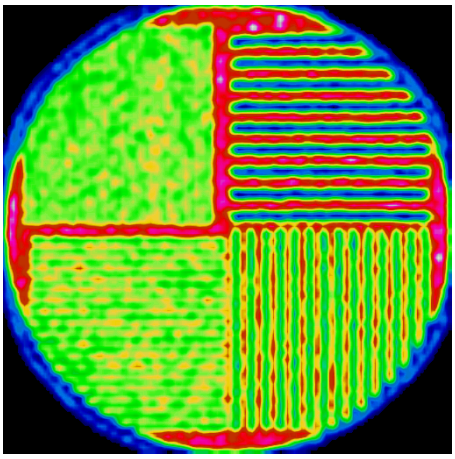

Fig. 5.2.5 (b): filtered image

Figure 5.2.6 shows the frequency spectra of the original and filtered images to show how the magnitudes of the frequencies that correspond to the bars that are no longer visible (in blue) and almost indistinguishable (green) using the same color coding as that shown in Figure 5.2.1.

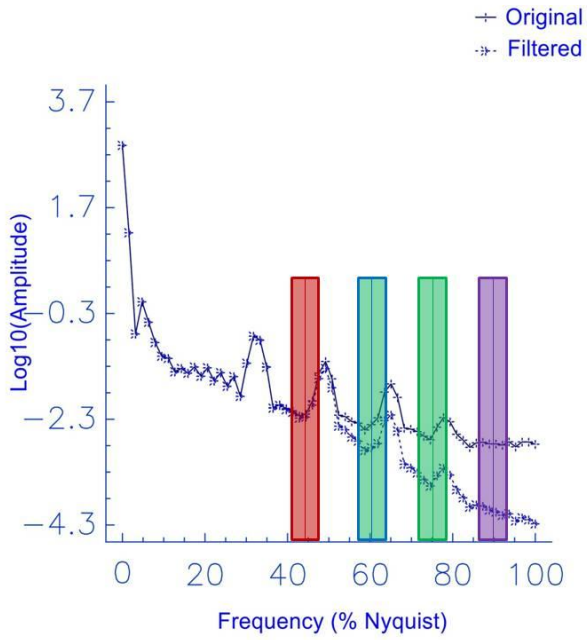

Fig.5.2.6: Spectra pre and post-filtering.

The entire process of filtering in the frequency space consists of:

1) Apply the direct Fourier transform to an image to "pass it on" to the frequency domain.

2) Multiply the images of amplitude and phase by the filter.

3) Apply the inverse Fourier Transform to "get back" into the spatial domain.

5.3 Equivalence of filter representations

It is interesting to note that the filtering processes described, the one in the real space (chapter 2), the other in the frequency space, are equivalent. This means the absolute concordance of results by both methods provided that they use the same filters: As well as the filters used in the convolution (masks) have their spectral representation (obtained by the Fourier Transform), the filters defined in the frequency space have their equivalent in the form of a mask of factors. Figure 5.3.1 corresponds to the frequency profile of the smoothing filter that was seen in chapter 2.

Some Nuclear Medicine computers work exclusively in the spatial domain, although the users define the filters in the frequency space. Others act only in the frequency domain both in the definition and implementation. The diagram (Figure 5.3.2) summarizes the equivalence and the underlying processes of filtering.

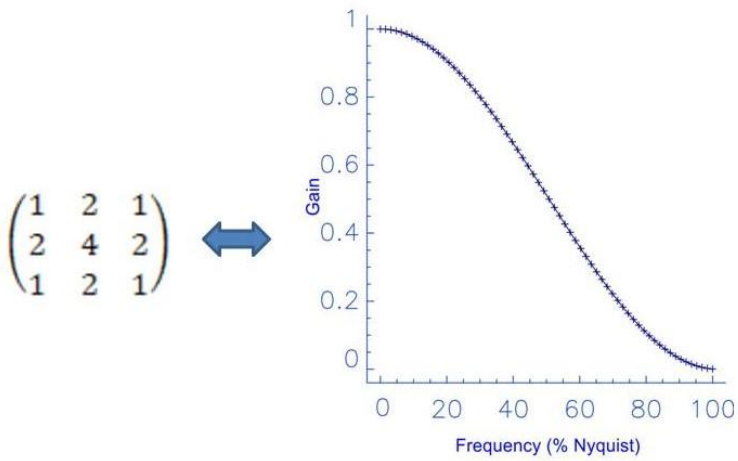

Fig. 5.3.1: Mask of factors (filter) and the equivalent frequency representation.

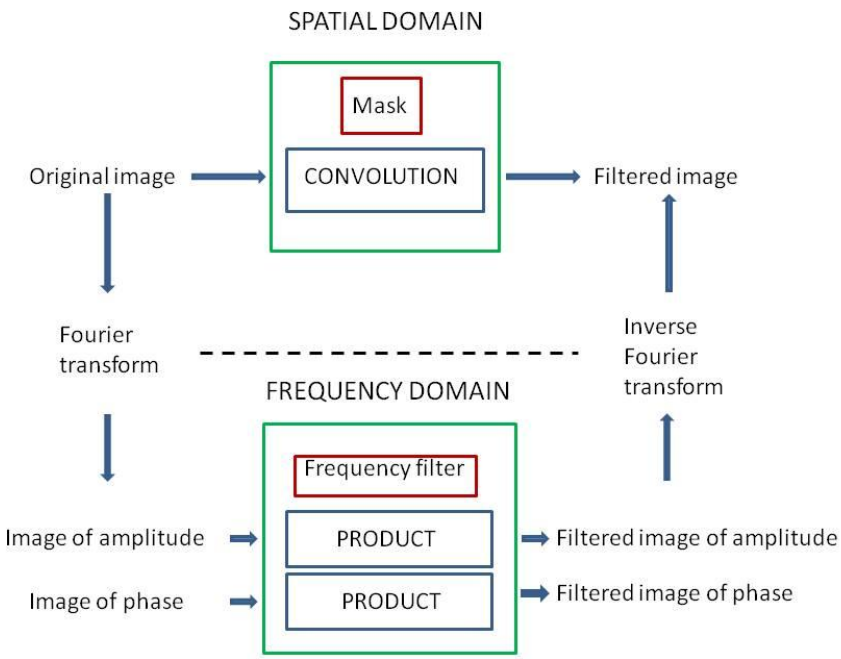

Fig. 5.3.2: schematic of the equivalence of filtration methods.

5.4 Types of filters

Frequency filters are defined by mathematical functions more or less complicated. However, for its ordinary use, it is enough to know how to interpret its graphical representation, which indicates reasonably the effect that produces. According to the area of the spectrum in which they operate, the filters are classified as:

Pass all: let pass all frequencies while modifying them.

Highpass: only let pass the high frequencies, eliminating the lowest.

Lowpass: only let pass the low frequencies, eliminating the highest.

Bandpass: only let pass frequencies between two limits.

5.4.1 Ideal filters

An ideal lowpass filter is equal to 1 for all frequencies that let pass and equal to 0 from a default frequency called cutoff frequency. Figure 5.4.1.1 represents a filter of this type with cutoff frequency of 50% Nyquist, which corresponds to 0.8 cm^{-1} and Figure 5.4.1.2 represents the result of applying it to the image of the bar-phantom. We note three phenomena in the image. First, with the disappearance of the upper half of the frequencies, we have lost the bars of the bar-phantom of higher frequency (1.05 and 1.26 cm^{-1}). Second, the typical mottled background has disappeared because of the filter have wiped out part of the frequencies that belong to the noise and third, that have appeared a few artifacts (enlargement of the bars out of the picture) and that mask the entire image that due to the filter used (Figure 5.4.1.1) cut off abruptly the spectrum of frequencies. All the filters applied in practice have a soft profile to avoid this effect.

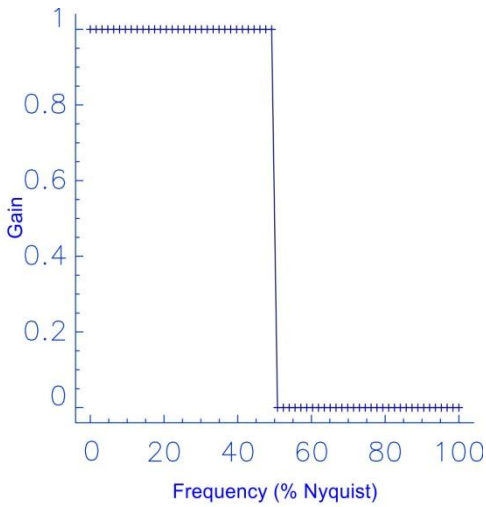

Fig. 5.4.1.1: lowpass filter with a cutoff frequency of 50% of the Nyquist

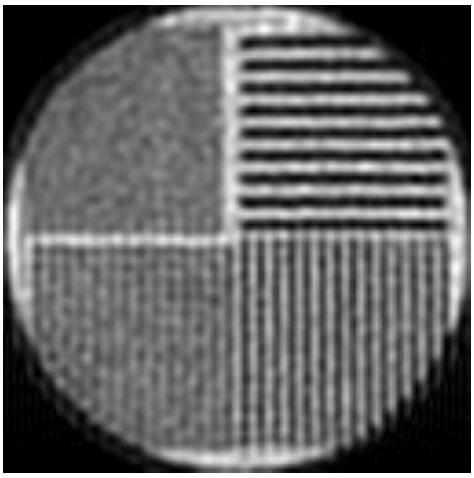

Fig.5.4.1.2: filtered image.

As an example of a highpass filter, we use a filter (Figure 5.4.1.3) whose cutoff frequency is also the 50 % of the Nyquist frequency.

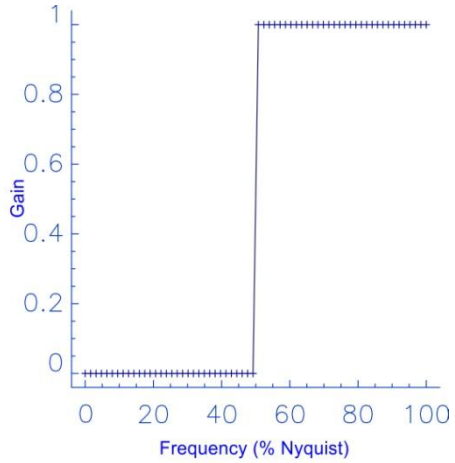

Fig. 5.4.1.3: Highpass filter with cutoff 50%

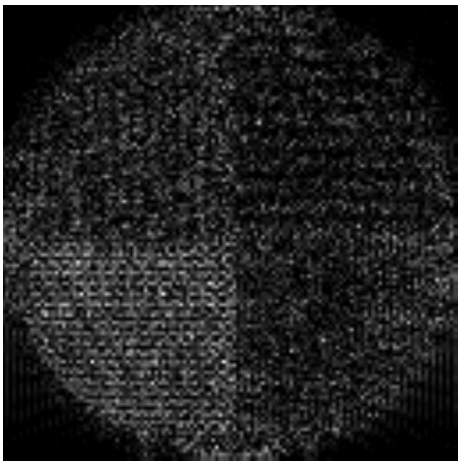

Fig.5.4.1.4: the result of applying the highpass filter

We see how in this case that the background of the image (Figure 5.4.1.4) has disappeared (because it corresponds to the low frequencies) and that we only observe the areas of change of activity, which correspond to the edges of the bars of the phantom. In the second and third quadrants also appears the artifact generated by the abrupt cutoff frequencies.

An ideal bandpass filter, as shown in Figure 5.4.1.5, which allows only frequencies between 25% and 75% of the Nyquist frequency, suppresses on one hand the background (since it is located in the area of low frequencies) and reduces the noise on the other hand, preserving three of the four quadrants since the finest lines are located at ~1.3 cm^{-1} that corresponds to 81% of Nyquist) as shown in Figure 5.4.1.6.

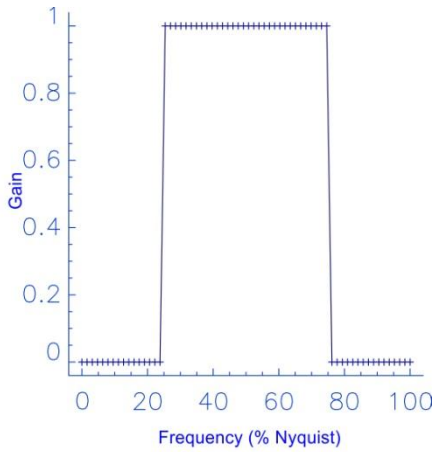

Fig. 5.4.1.5: bandpass filter frequency with 25% and 75 % cutoff of Nyq.

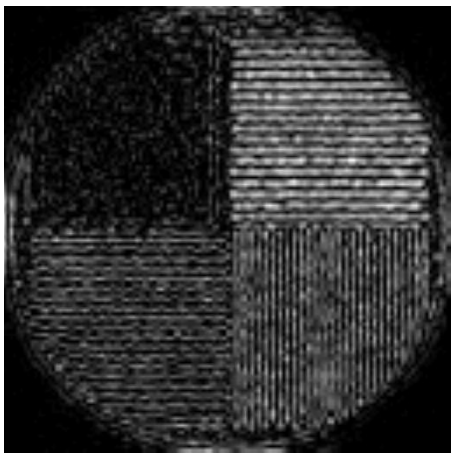

Fig. 5.4.1.6: the result of applying the bandpass filter.

Filters are also classified by the type of effects, such as smoothing and restoration.

5.4.2. Smoothing filters

The smoothing filters have been designed to decrease, in the extreme case to reduce to zero, the amplitudes of the range of the high frequencies. They are, therefore, lowpass filters designed primarily to reduce noise. The specific form depends on the mathematical expression used to define your profile. However, in all of them there are to be considered 2 fundamental parameters: one, which gives the frequency threshold from which amplitudes are not transmitted (cutoff frequency) and another parameter, although in many cases it is determined by the mathematical formula, which regulates the speed with which the filter tends to cancel the amplitudes. In addition to reducing noise, these filters reduce the spatial definition ("Sharpness") of all the contours, producing a smooth image.
Examples of these are the filters Butterworth, Parzen, Shepp-Logan, as described in chapter 6 (Figure 5.4.2.1).

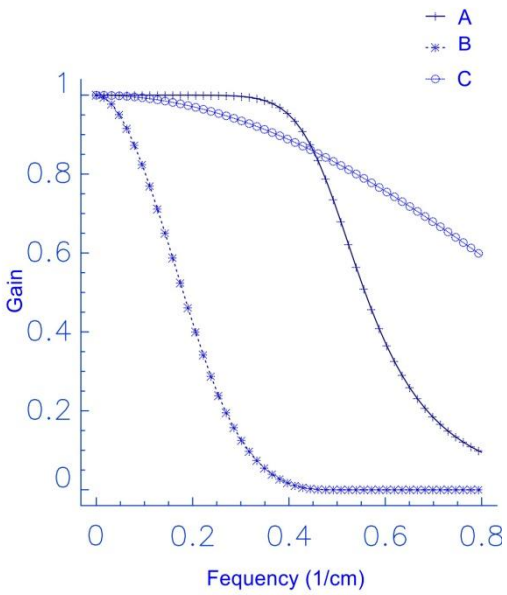

Fig. 5.4.2.1: Smoothing filters. A: Butterworth,
B: Parzen, C: Shepp-Logan.

Note that by its very definition, the values of the gain of the smoothing filters are always equal to or less than the unit to attenuate the amplitudes associated with medium and or high frequencies.

5.4.3 Restoration filters

The primary purpose of the restoration filters is to compensate for the degradation that the detector produces in the image. As we have seen above (4.1 and 4.2) the resolution of the images depends on the detector, the distance, and the matrix used. In the spatial domain, the way to characterize this response is through the Point Spread Function (PSF), and in the frequency domain, with its Fourier transform, which is the Modulation Transfer Function (MTF)[23].

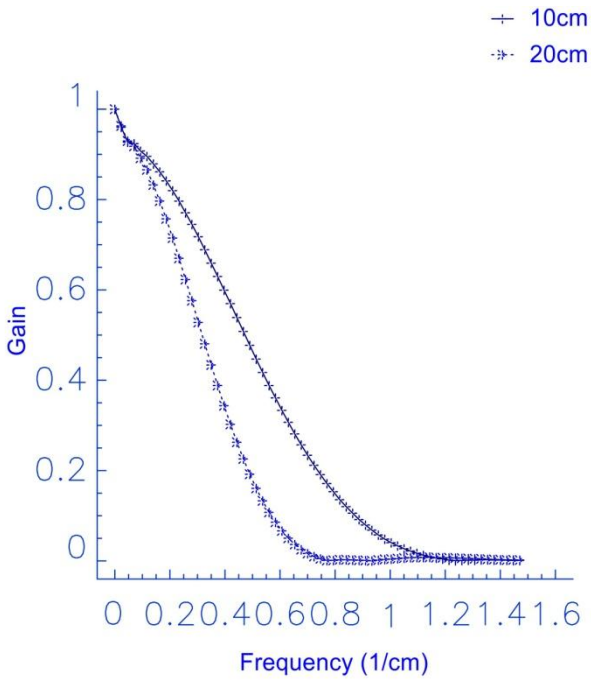

Fig.5.4.3.1:Modulation transfer functions (MTF) for high-resolution collimator at 10 and 20 cm away.

Fig. 5.4.3.1 shows the MTF for a gamma camera with a high-resolution collimator, at 10 and 20 cm distance using a matrix of 128x128 pixels.

Based on the fact that an image is a collection of points and that the response of the detector to a point is the (PSF), the images are generated by convolution of the original distribution of points (object) with the detector response for each point (PSF).

The restoration consists of inverting, to the possible extent, the degradation ("blurring") introduced by the detector. It is, therefore, necessary to deconvolve the image generated by the detector with the characteristic function (PSF) in the

[23] The MTF is a lowpass filter, a smoothing filter.

spatial domain[24] or apply the inverse of the MTF in the frequency domain to obtain an estimate of the original distribution of activity (object).

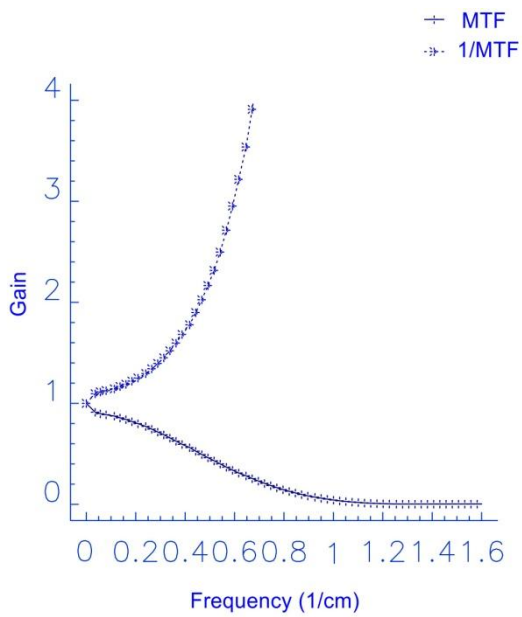

Fig.5.4.3.2: MTF and the inverse.

In the frequency space, the estimate of the actual distribution of the radioactivity in the object can be obtained, in principle, by applying a filter that is the inverse of what produces the blur, that is, the inverse of the MTF (1/MTF). Unfortunately, the MTF takes values very close to zero, which makes that from specific frequencies, its inverse disproportionately grows, as shown in Figure 5.4.3.2. Here the MTF and part of its inverse which presents these very high values from 0.8 cm^{-1} is shown. The direct application of this method is not viable, since, among other problems, it amplifies disproportionately the values corresponding to frequencies that are only due to noise. This amplification results in need to modify the function 1 /MTF to include a term of smoothing that acts in the upper range of the spectrum, achieving in this way to implement this type of filter (Figure 5.4.3.3).

[24] The restoration in the spatial domain allows applying methods of calculation to take into account the variation of the response of the gamma cameras and PET scanners with the position of the detection allowing the correction, for example, of the variation of the PSF with distance from the central axis in the PET scanners.

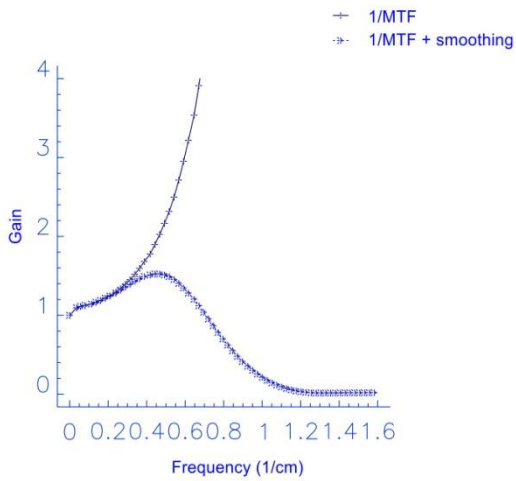

Fig. 5.4.3.3: 1/MTF directly and with smoothing

Fig. 5.4.3.4 shows a transfer function and a restoration filter obtained from it. The frequency characterization of the detectors (MTF) for specific conditions of measurement (collimator and distance) is obtained experimentally or by theoretical modeling. Gamma cameras come characterized by the factory so that for each collimator and distance interval they already have the PSF or MTF. The user only needs to adjust the amplification and degree of smoothing.

Note that there is a range of frequencies in which the filter has values greater than 1 (amplification) and another range in which the values are lower than the unit (attenuation or smoothing).

The restoration filter more extended and flexible in Nuclear Medicine is the Metz filter. Figure 2 shows 5.4.3.5 Metz filters generated from the characteristics of a high-resolution collimator at 10 and 20 cm.

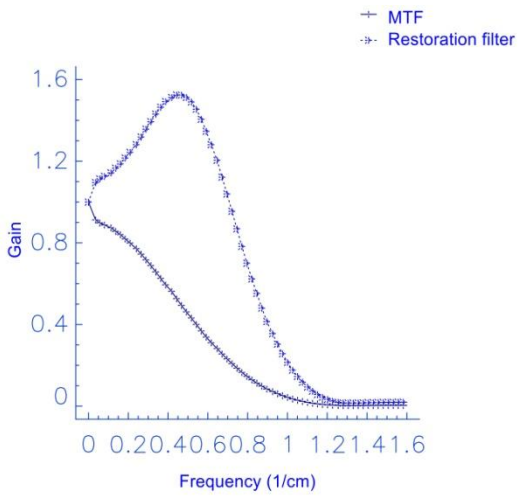

Fig.5.4.3.4: MTF and restoration filter.

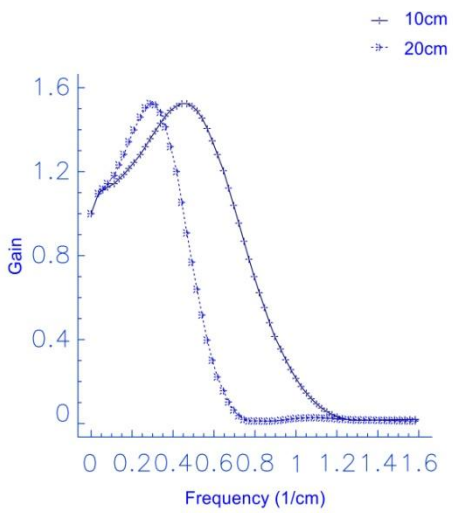

Fig.5.4.3.5: filters of Metz for collimator HR. At 10 and 20 cm.

It is essential to take into account that the dependence of the response of the gamma cameras with the distance means that, in general, the restorations applied to the tomographic reconstruction in the frequency domain are approximate, not being implemented the possibility of varying the filter according to the distance from the center of rotation. However, using the spatial domain representation, it is possible to restore planar, and SPECT studies, considering that the point spread function (PSF) varies both with the distance between object and collimator and with its position in the scintillation crystal of the detector. The most recent PET scanners incorporate from the factory the PSFs for all points of the field of view to correct almost all "imperfections" described above (section 4.3).

6. Tomographic reconstruction and filters

6.1 Introduction

Planar scintigraphy and tomography apply filters. They are used to smooth planar images and, in tomography, they have had and still have an essential role in the reconstruction. Consequently, it is convenient to make a schematic overview of the procedures for the acquisition of studies and the usual methods of tomographic reconstruction in Nuclear Medicine.

In SPECT and PET, obtaining the distribution of the radiopharmaceutical inside the patient's body is carried out in two phases. The first phase is the detection of the radiation emitted by the patient (acquisition), and the second phase, is the mathematical processing to obtain an estimate of the distribution of the radiopharmaceutical (reconstruction).

6.2 Acquisition of tomographic studies

The technology used in the acquisition depends on the type of radiation of the radiopharmaceutical. If it is emitting gamma radiation, gamma cameras are used whose detector or detectors rotate around the patient (SPECT) obtaining images sequentially at a series of angles along the orbit. These scans, called projections, are the result of accumulating in every pixel the activity detected according to each angle. The projections are subject to the limitations imposed mainly by the collimators. The main constraints are the variation of the spatial resolution with the distance and, above all, the low number of accounts due to their low sensitivity, making the noise level very important.

The following figure (Figure 6.2.1) shows how the information is ordered in a study of SPECT for later reconstruction. This arrangement, called sinogram, represents the variation of the activity of one row (counts profile) according to the angle of the projection to which belongs. There is a sinogram for each slice that we want to reconstruct. A sinogram is an image made by the superposition of the rows ordered by their angle. In this way, this matrix condenses the information needed to reconstruct a slice. The reconstruction is carried out one slice to slice, and each sinogram is the starting point of the reconstruction the slice (Figure 6.2.2).

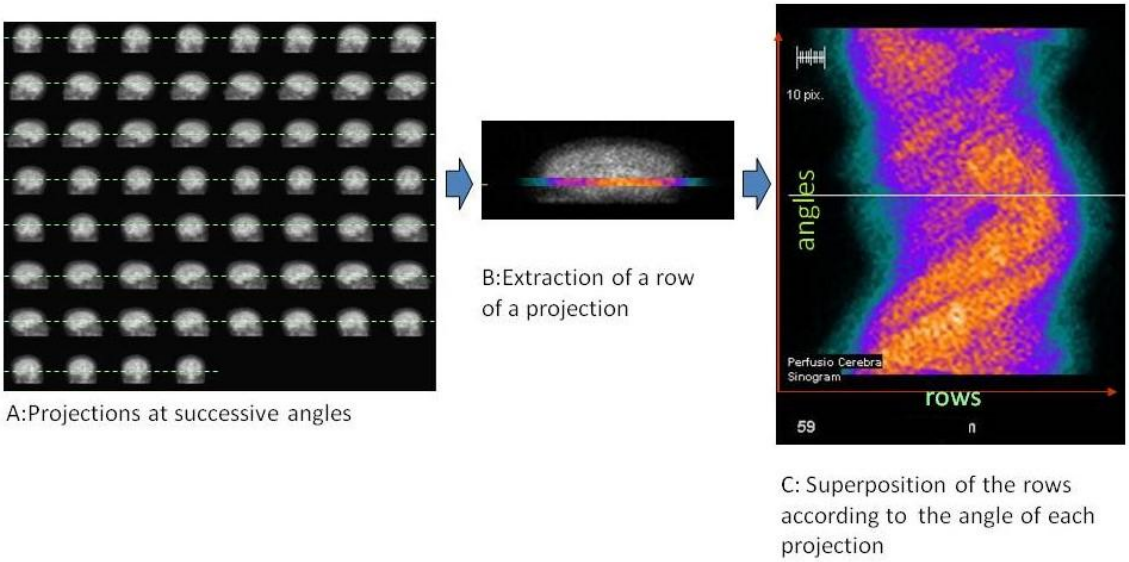

Fig. 6.2.1: scheme of the construction of the sinograms in SPECT

If it is a positron's emitter (PET), the tomographs detect the photons created by the annihilation of the positron inside the patient. The tomographs are constituted basically by several rings of static detectors arranged around the patient. Since the way to locate the annihilation of the positrons is based on the generation of lines of response by two different detectors[25] (of the same ring in 2DPET). A LOR represents that the annihilation occurred at some point in this "virtual line." LORs are classified by their distance from the center of the field of view and by its angle. For each slice, a sinogram is generated as in SPECT. The values of each cell represent the number of lines of response that had a certain angle and distance to the center of the field-of-view (Figure 6.2.2). The "counts" in PET do not directly correspond to photons but lines of response!

[25] See section 4.4.1

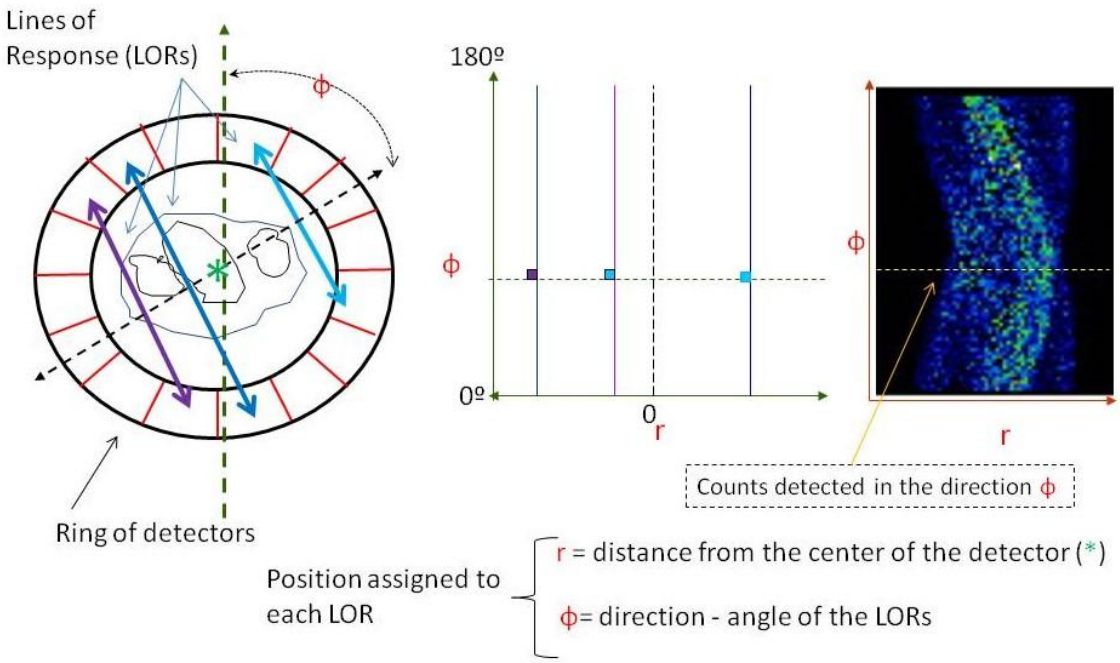

Fig. 6.2.2: scheme of the formation of the sinograms in PET

In both SPECT and PET, the starting point of the reconstruction is the sinogram. In both techniques, sinograms indicate the same thing, that is, the ordered "counts" from which the studies are reconstructed (Figure 6.2.3).

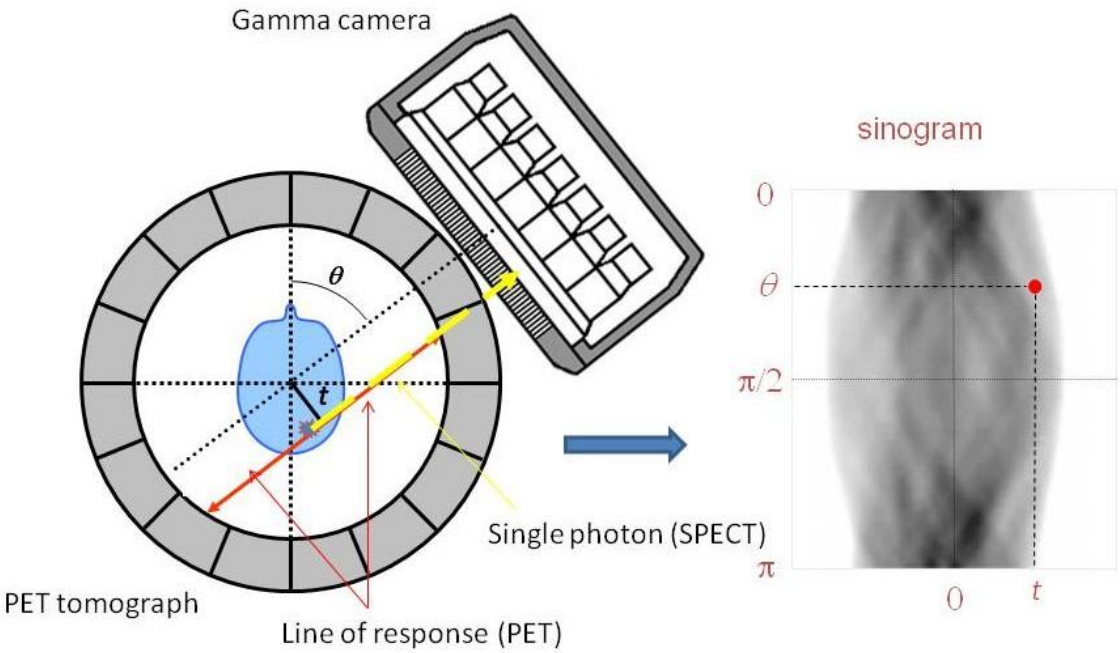

Fig 6.2.3: equivalence between SPECT and PET. Single Photon (yellow), Line of response (red). (Sinogram extracted from Principles of PET: reconstruction/simulations of Irène Buvat)

Currently, the most common form of PET acquisition is 3D. It consists in admitting oblique lines of response whose origin and end do not necessarily

occur in the same ring of detectors. This acquisition and reconstruction requires an enormous amount of computation to treat the data directly in 3D, but if they are recombined ("re-binning") to rebuild them as if they were acquired in 2D a standard 2D-reconstruction can be applied . This method significantly increases the quality of the studies with respect to 2D and makes it feasible to use 3D routinely in clinical practice.

6.3 Reconstruction of tomographic studies

Despite the various corrections in one and another modality to correct defects or limitations of the equipment[26], SPECT and PET use the same basic reconstruction methods. The reconstructions are slice-by-slice (2D). The basic idea underlying in 2D is to consider the volume to rebuild broken down into sections or slices corresponding to the transverse sections. Each slice is reconstructed separately, and in the end, all of them are stacked to reconstruct the entire volume. From this volume, it is easy to obtain the sagittal and coronal slices, as shown in the diagram in Figure.6.3.1.

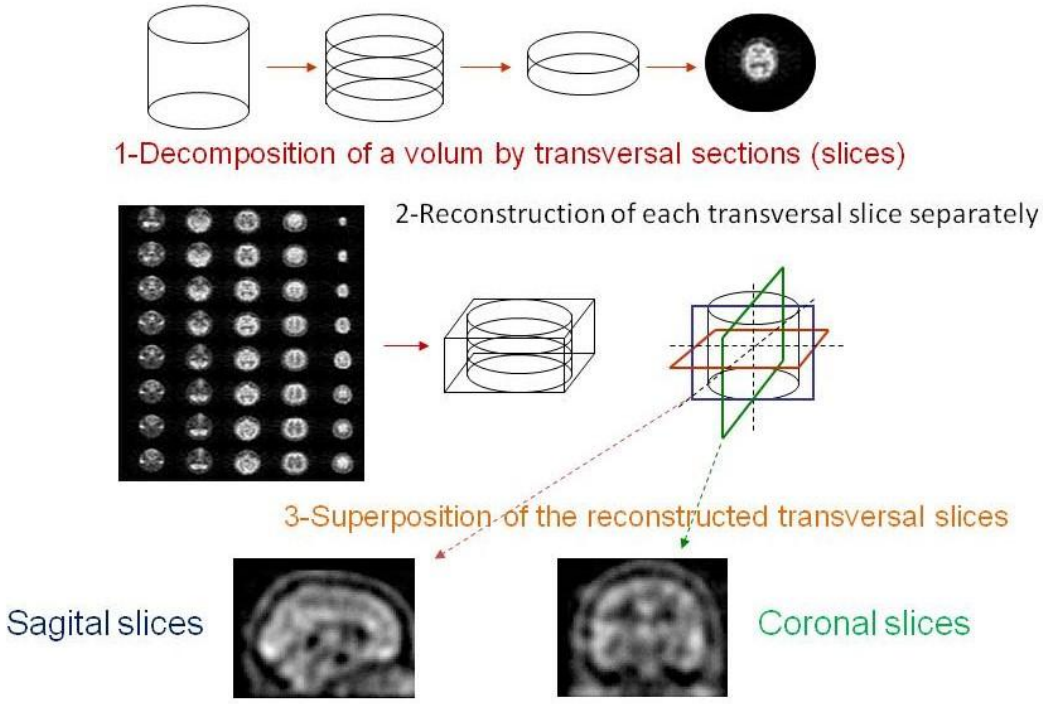

Fig. 6.3.1: diagram of the standard 2D reconstruction

[26] The corrections prior to and during reconstruction, especially in PET (correction of attenuation, random coincidences, "scatter", spatial resolution,...) make the statistics governing the values not to be strictly Poisson (remember that it is the one that allows you to assign as uncertainty of a number of count its square root).

The reconstruction methods currently available in the market are of two types. The first, which is the filtered backprojection ("FBP") and which belongs to the analytical methods, has been and continues to be implemented in Nuclear Medicine. It was the first method clinically usable by the reduced capacity that requires and PET, SPECT, as well as X-ray computed tomography (CT), extensively used it. The second type is the set of iterative methods, the most common being the "Maximum Likelihood Expectation Maximization" (MLEM) accelerated through the ordered subsets method that is known as Ordered Subsets Expectation Maximization (OSEM).

6.3.1 Filtered backprojection

This method consists of considering that if the projections are the profiles of the unknown internal activity obtained at different angles, this "unknown" activity is estimated by overlaying these profiles on a matrix taking into account their angle (hence the name of backprojection).

This algorithm, by the very system of calculation, produces a blurring of the images. This blurring, in the frequency space, is as if the filter defined by the inverse of the frequency ($F(\nu)= 1/\nu$, being ν the frequency) was applied. Fig. 6.3.1.1 shows its graph.

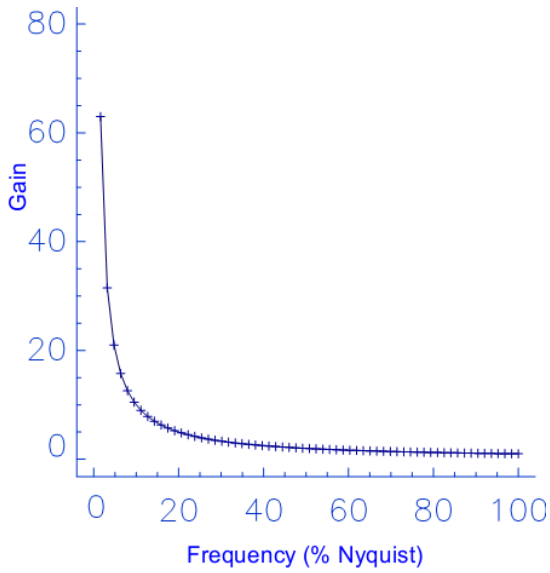

Fig. 6.3.1.1: Filter " 1/v" induced by the method of backprojection

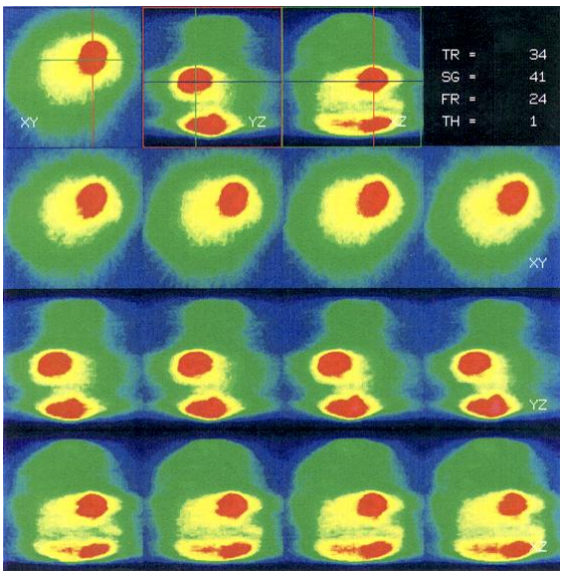

Fig.6.3.1.2: "raw" transverse, sagittal, and coronal views from backprojection.

.

Fig. 6.3.1.2 shows the result of having applied, the backprojection procedure to a myocardial perfusion study: the area corresponding to the myocardium is like a "stain" and all the slices have a look blurry.

This blurring is corrected by multiplying the amplitude image by " ν " to compensate for the effect of the "1/ν".

The graphical representation of the correcting filter ($F(\nu)= \nu$) as a function of frequency is a straight line to 45º by what is called the ramp filter (Figure 6.3.1.3).

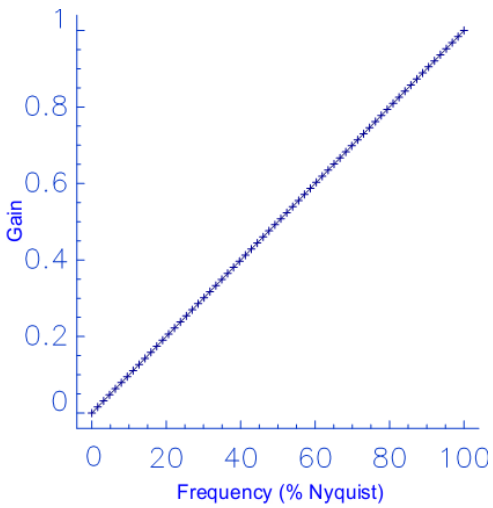

Fig. 6.3.1.3: ramp filter.

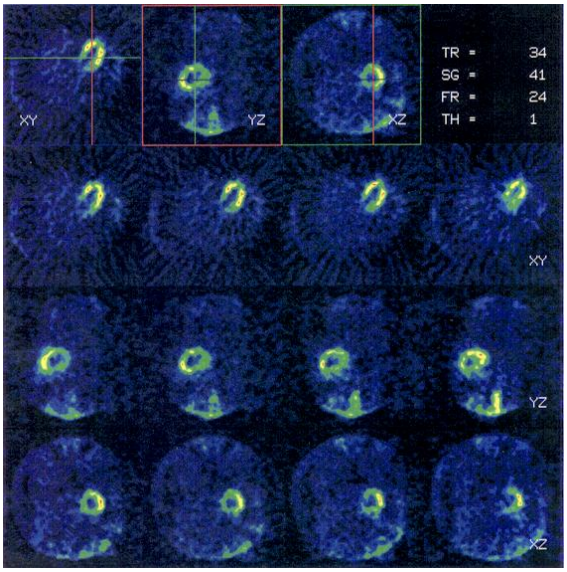

Fig.6.3.1.4: transverse, sagittal and coronal after applying the ramp filter.

For this reason, the tomographic reconstruction algorithm implemented in the computers of nuclear medicine is commonly referred to as filtered backprojection ("FBP"): backprojection by the method of calculation and filtered by applying inescapably the ramp filter. Figure 6.3.1.4 shows the result of applying the ramp filter to the study of Figure 6.3.1.2.

The ramp filter acts on the entire range of frequencies, by multiplying the amplitudes of all the frequencies in a progressive form (linearly), which means that the higher the frequency, the greater is the factor by which multiplies its amplitude (Figure 6.3.1.5).

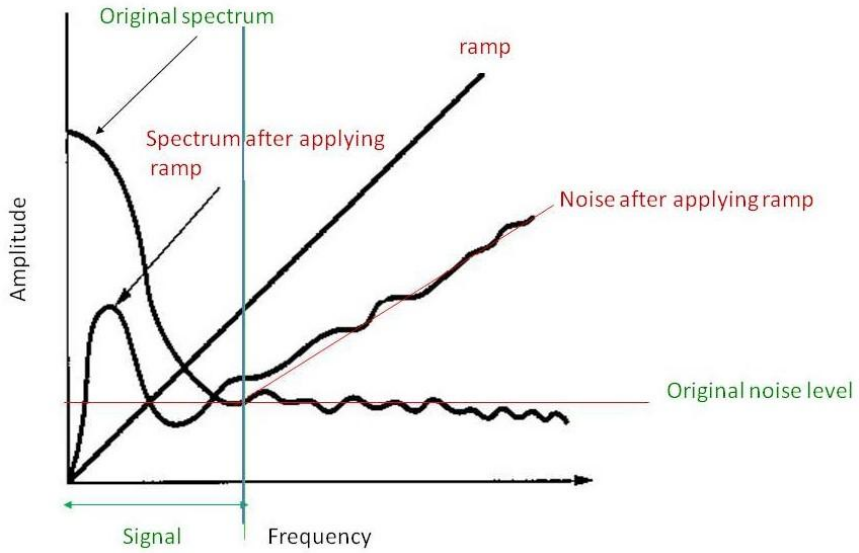

Fig.6.3.1.5: The effect of applying the ramp filter on a spectrum.

On the other hand, the effect of the noise is much more important in the range of the high frequencies, as these are the weak point of the equipment (remember the shape of the MTFs in Figure 4.2.2(b)).

The Figure 6.3.1.6 shows the normalized spectra before and after applying the ramp filter to the already know spectrum of the bar-phantom. As you can see, the relationship between the signal level and noise is lower after applying the ramp, or, to put it another way, the noise has increased compared to the original. The final effect of this increase in the picture depends on the quality of statistics (signal-to-noise ratio). If this relationship is high, that is, if the structures of interest (signal) are well distinguished, the quality of the images is not affected significantly, but, on the other hand, if the signal is weak (low number of counts), then it is severely damaged.

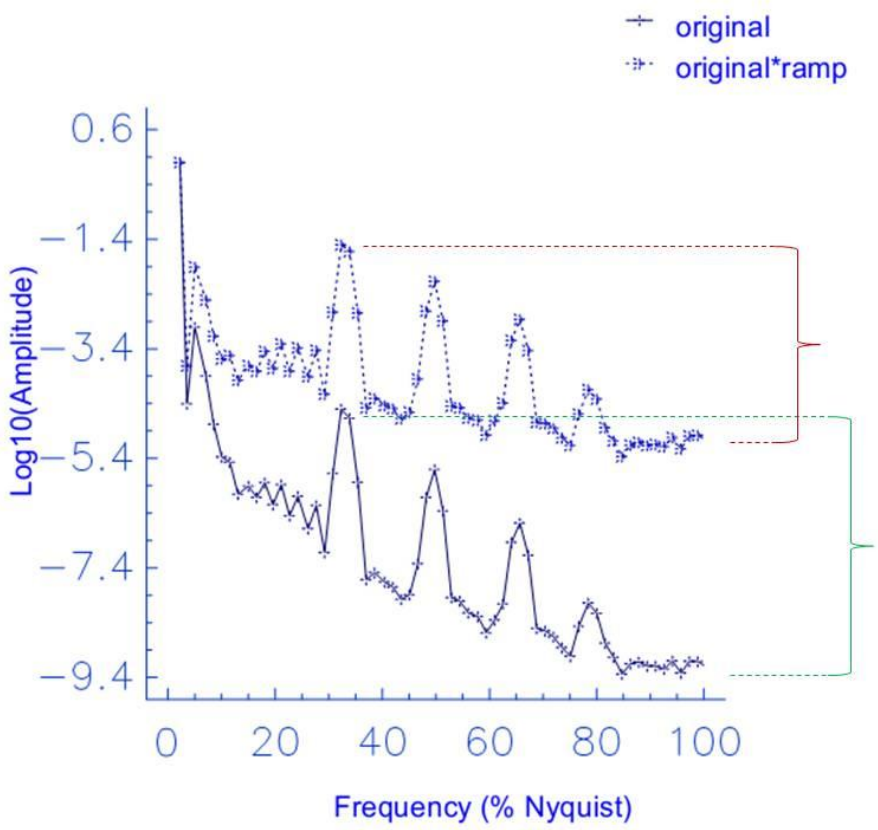

Fig.6.3.1.6: spectra of the phantom of bars before and after applying the ramp filter. The ramp decreases the SNR.

In PET the number of counts in the acquisition and the reconstructed image is far higher than that of the SPECT and consequently is not as sensitive to noise. If the signal-to-noise ratio is low as in SPECT, a relative increase of noise in the signal can be inadmissible, which forces to reduce the noise where its effect is more significant (medium-high frequencies), even at the cost of losing resolution. This reduction is made using a second filter, which leads to paying particular attention to its selection. This filter must be considered and optimized in each type of study and imaging equipment.

The implementation of a "second" filter is equivalent to apply a single filter that is the combination of both (Figure 6.3.1.7).

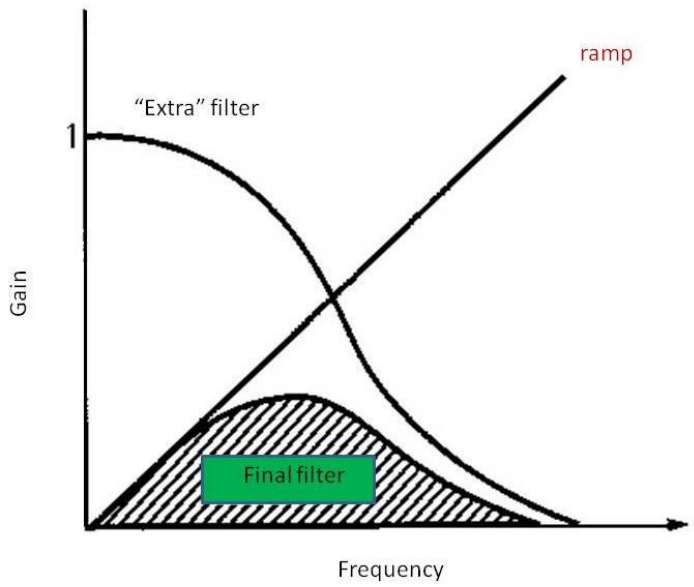

Fig.6.3.1.7: composition of the ramp filter with a second filter.

The heavy reliance of the final images with the "second" filter is what has given rise, especially in SPECT, to a certain degree of caution in their use, caution caused most of the times, by ignorance of its foundation (which is what it sought to remedy this book).

6.3.2 Iterative Reconstruction

The basis of the iterative reconstruction is entirely different from that of the filtered backprojection. The idea is to create a mathematical model of the obtainment of the images. This model includes detection and degrading effects. These effects are the attenuation in the patient[27], the variation of the spatial resolution with the distance, the radiation scattered by Compton effect,...

The more corrections are included, the more complex is the model and more extended computation time is necessary for the reconstruction of the studies, but more accurate is the result. The model has the mathematical form of an algebraic matrix, where each element ("m_{ij}") represents the probability of detecting one photon in the pixel "j" of a projection (p_j) which comes from an emission located in position "i" in the patient (x_i). The method consists of solving a system of linear equations (Figure 6.3.2.1).

[27] Attenuation correction is usually performed using CT scan as they provide directly the attenuation coefficients of the patient. PET needs to use special impulse sequences if MRI is used instead.

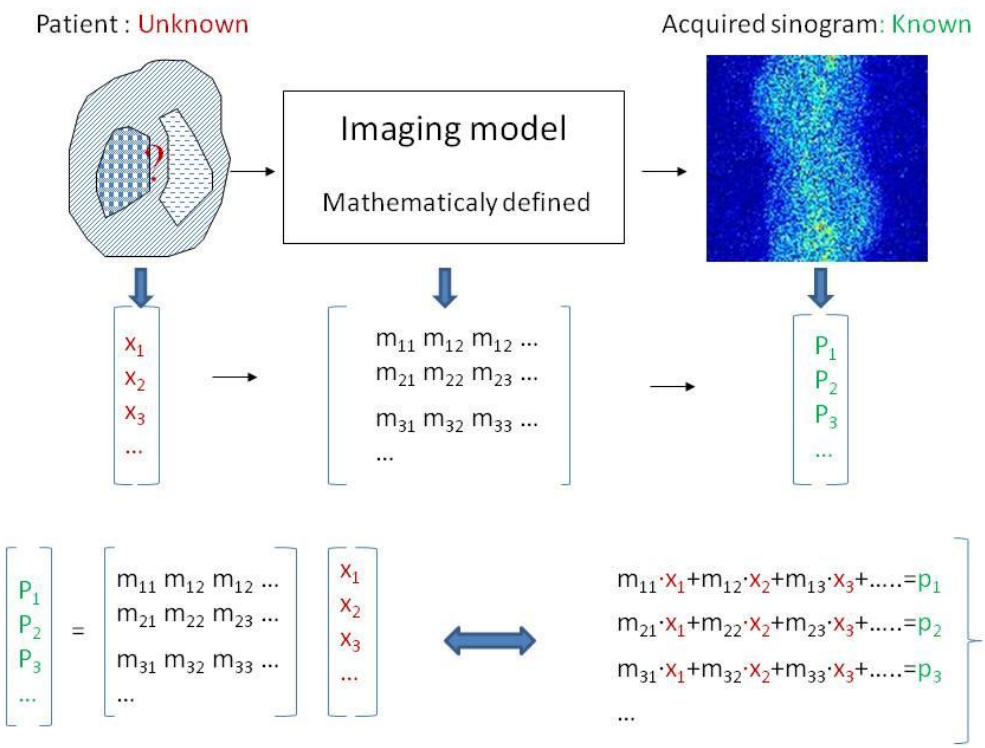

Fig. 6.3.2.1: Modeling of the imaging acquisition

The enormous number of unknows and equations oblige to use iterative methods which take into account the radioactive character of the emission.

Once established the model - which, according to each manufacturer, can include different corrections (attenuation, PSFs, Compton,...)- an initial estimate of the detected projection or sinogram is generated from an initial guess which usually is a uniform image (for example with all its values equal to 1). The model is applied to this first image to simulate the projections that represent what the imaging system would obtain if the data in the patient were all of them equal to 1. Then, this image is compared with the projections obtained experimentally. From this comparison, the method calculates values to modify the initial estimate resulting in a new simulated estimate. The model is then applied to the latest estimate, and the result is again compared with the experimental data. From this comparison, the method calculates further corrections that modify the previous estimate again. The process repeats until the acquired data, and the simulated projections fulfill a criterion of equivalence, or a prefixed number of iterations is reached (Figure 6.3.2.2).

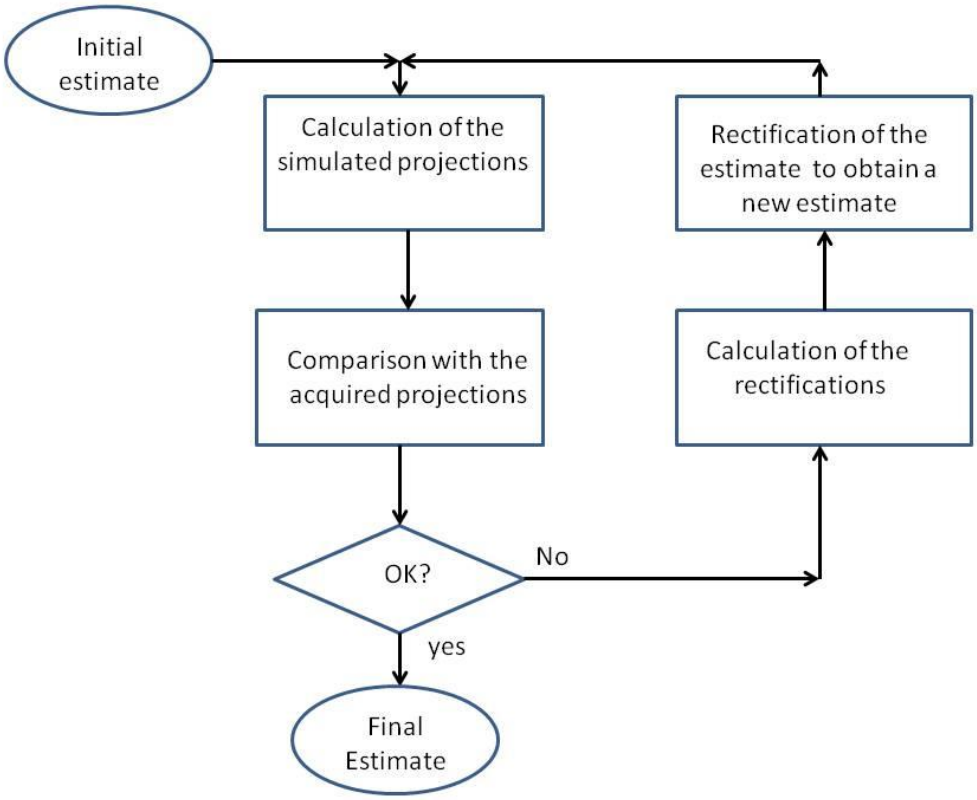

Fig. 6.3.2.2: procedure of the iterative methods

The sequence of images of the Figure 6.3.2.3 allows us to observe how it is shaping up the solution as the iterations increase. At the first iteration the area of interest is already located and the detail increases in the following iterations. It is important to note that there are, for each type of study, an optimum number of iterations that reconstructs the object correctly because if you continue iterating the method attempts to reproduce the noise since it is also part of the acquired studies. In the case shown in Figure 6.3.2.3, this range is 5 to 7 iterations. Subsequent iterations only increase the noise as it is well observed.

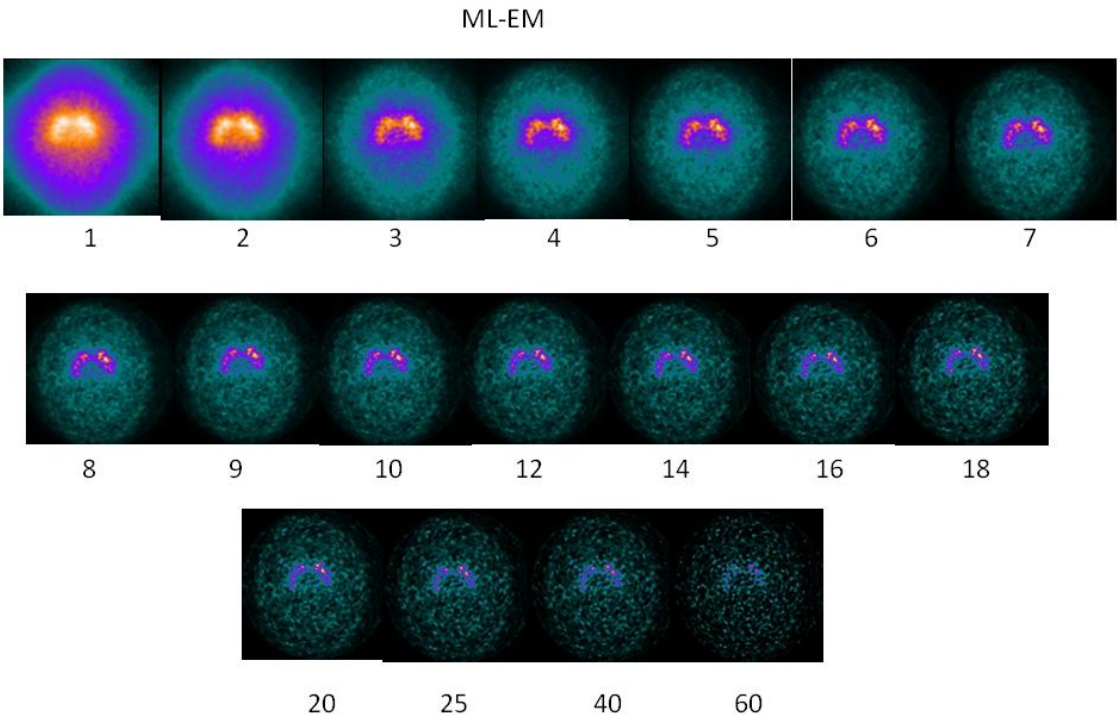

Fig. 6.3.2.3: the successive images in iterative reconstruction. The numbers indicate the number of iterations of the corresponding image

In some cases, it is iterate over a little and then is applied a smoothing filter to the final solution (post-filtering). This filter can be applied to each transverse slice or perpendicularly to "harmonize" each slice with its neighboring slices.

6.3.3 Iterations and frequency spectra

The sequence of images of the example of iterative reconstruction can be observed from the frequency point of view. That is, the initial estimate (iteration number 0) is a uniform image and therefore described by a single value which is the average value, and that corresponds to the frequency 0 since there is no change for being a uniform image. This initial estimate is corrected in the first iteration, obtaining a first location of the focus of radiation, which corresponds to the low frequencies. Figure 6.3.3.1 (a) shows us the first estimate, a profile of counts of this image and the one-dimensional spectrum of the latter. Note that the frequency content of this first estimate is scarce and limited to the low frequencies. The next iteration outlines the nuclei of the base of the brain, and therefore, new frequencies appear (Figure 6.3.3.1 (b)), but the image still has a "rounded" shape. The next iteration (Figure 6.3.3.1 (c)) outlines perfectly both nuclei appearing a new frequency at some distance (0.16 mm^{-1}). The last figure

(Figure 6.3.3.1 (d)) shows the result of more advanced iterations that retrieve the noise that distorts what previous iterations achieved. Note how new frequencies have "appeared" and how some of the previous ones have had increased their amplitude. The basic form remains but completely disfigured by the overlap of the noise.

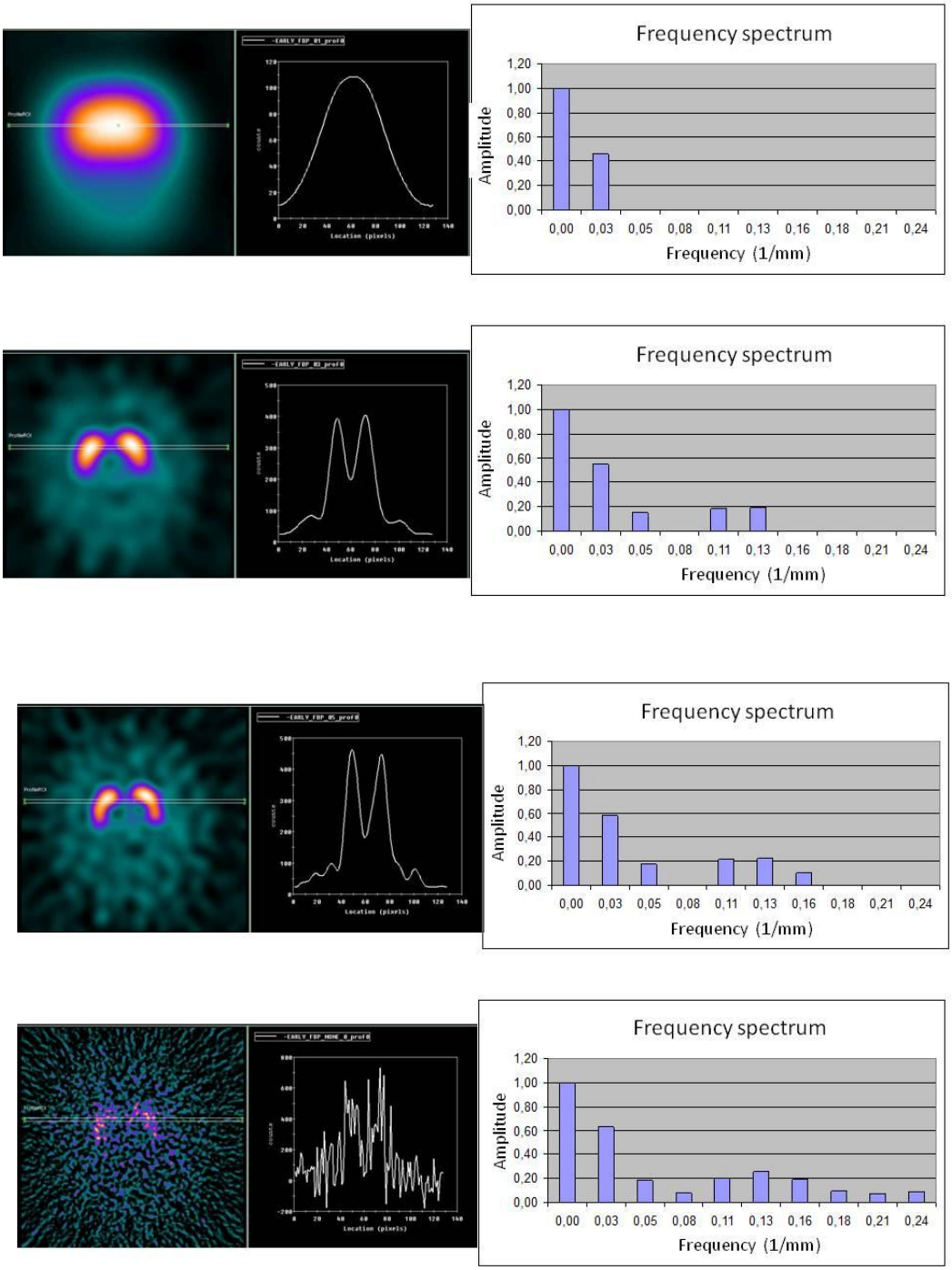

Fig. 6.3.3.1 (a,b,c,d): frequency content in successive iterations

The evolution of the images with the iterations can be analyzed, obtaining the spectrum of the amplitude in each iteration. Figure 6.3.3.2 shows the logarithm of the circular spectrum for the iterations (between 1 and 100) using OSEM with one subset and without any correction (which is equivalent to apply MLEM directly). The study was another brain SPECT but similar behavior was observed on other kind of studies..

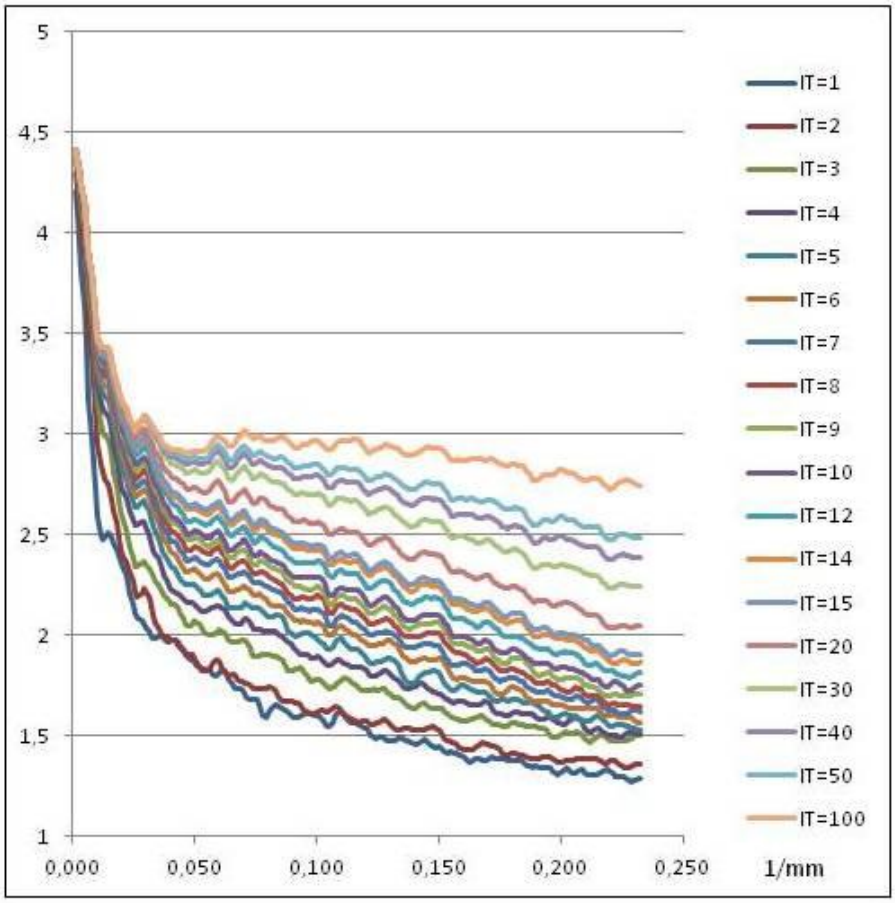

Fig. 6.3.3.2: variation of the amplitude (Log10) with the number of iterations.

In this graph, we can observe several things:

1) The spectrum for IT=1 is almost identical to Figure 3.6.2, which comes from an image of uniformity with 1600 kcounts. This similarity means that the frequencies that compose the image of the study are not yet present. These frequencies are for SPECT[28] in the range 0-0.05 mm^{-1} which agrees with the

[28] The tomographic spatial resolution in a dispersing medium such as water parameterized by the FWHM is about 16.5 mm at a distance (radius) of 20 cm and 18.5 mm at 25 cm according to Yokey et al. The maximum frequency that can transmit an imaging system (in this case a SPECT is 1/FWHM which translates into a maximum frequency of 0.06 mm^{-1} at 20 cm and

values obtained experimentally in the Nuclear Medicine Department of the Hospital Universitari de Bellvitge from where the SPECT study comes.

2) In the range of interest (0.01- 0.06 mm^{-1}) which corresponds to the "true" structure of the images, the spectra are very close to each other (almost indistinguishable), mainly from IT=5 to 100 which means that each new iteration does not provide substantial changes to the image but is the noise that increases.

3) The high frequencies are more amplified than the low ones making that the SNR decreases with increasing iterations. For example, A(0.06)/A(0.230)=3.55 for IT=1 and the same relation for IT=100 equals 1.78.

4) The amplitudes for frequencies > 0.06 mm^{-1} increase faster than the ones that "belong" to the object. For example, A(0.03) varies from 2.125 to 3.2 which means an amplification factor of 11.8 in 100 iterations, while A(0.1) has a factor of 25.1 and A(0.23) has a factor of 31.6.

Figure 6.3.3.3(a) shows how the average value of the number of counts of the images (A(0)) is practically constant from 10 iterations. The iterations, after being reconstructed the object of interest, can be viewed as small rearrangements in the counts' distribution to "follow" the oscillations of the noise but keeping steady the total counts.

Figure 6.3.3.3(b) confirms what we observe in Figure 6.3.3.2. The amplitudes whose frequency corresponds to the basic morphology of the image (0.01 to 0.03 mm^{-1}) increase rapidly up to ~30 iterations and then remain steady. Amplitudes for (0.04 and 0.05 mm^{-1}) increase gradually to the stabilization which is reached at ~50 iterations. A(0.06) seems does not to stabilize. This behavior indicates that the structural details need more iterations than the global shape but not many more.

0.054 mm^{-1} at 25 cm. Higher frequencies do not contribute to the morphology of the detected object but they attempt to reproduce the random variations of the counts (noise).

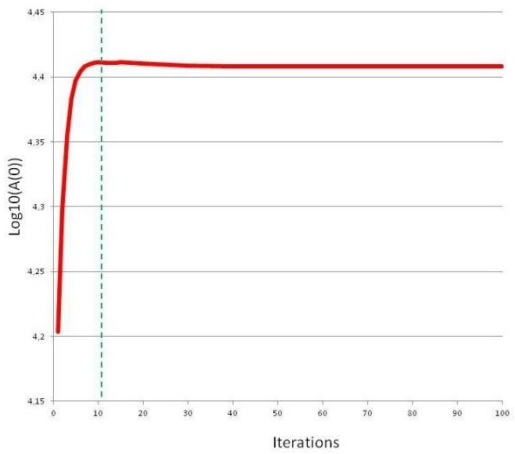

Fig.6.3.3.3(a): variation of the average number of counts(A(0)).

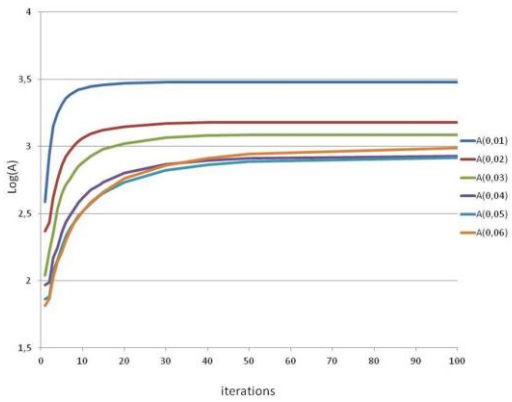

Fig.6.3.3.3(b): variation of amplitudes from 0.01 to 0.06 mm^{-1}

It is important to remember that noise is a perturbation of the "true" shape already obtained in previous iterations which remains despite the noise which justifies applying a smoothing post-filter to reduce its effects.

Using the observed frequency behavior of the iterative procedure and the maximum "valid" frequency for the object, perhaps it is possible to obtain a stopping rule in a "mixed algebraic-frequential" iterative reconstruction method.

6.4 Pre-filtering and Post-filtering

6.4.1 Pre-filtering

As has been explained above, the most common methods of reconstruction (2D) are based on breaking down in cuts ("slices") the volume which inside we would like to study. The reconstruction algorithm is then applied on each slice, turning the volume reconstruction (3D) in a succession of two-dimensional reconstructions to obtain the inside of each slice. The reconstruction of each slice separately causes the loss of the influence of neighboring slices, which to some extent decreases the accuracy of the result.

One way to overcome in some way this "independence" of the slices is to apply a filter before the reconstruction, called pre-filtering.The slices are obtained according to the rows of the projections, then, the natural way of "mixing" information between slices shall be to filter in the direction of the columns, that is, in the direction of the axis of the detector. The result is another study where the reconstruction is applied. The Figure 6.4.1.1 shows a projection without any

treatment and Figure 6.4.1.2 a slice obtained by reconstruction with the filtered-backprojection using a restoration filter. In Figure 6.4.1.3, you see the same projection after a pre-filtering is applied, and in Figure 6.4.1.4 the result of having reconstructed the prefiltered study.

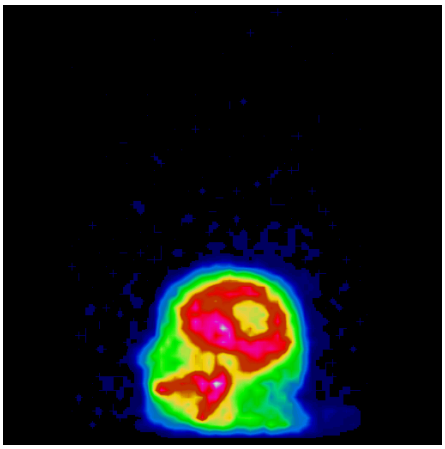

Fig.6.4.1.1: original projection

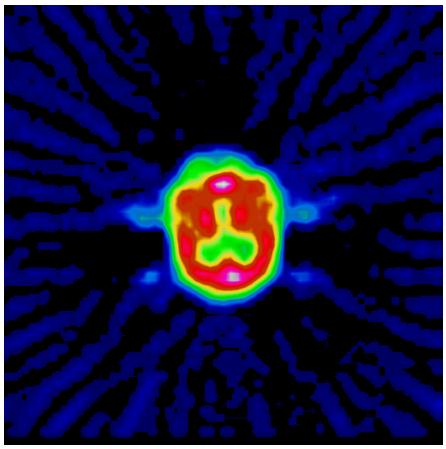

Fig.6.4.1.2: cross-sectional study

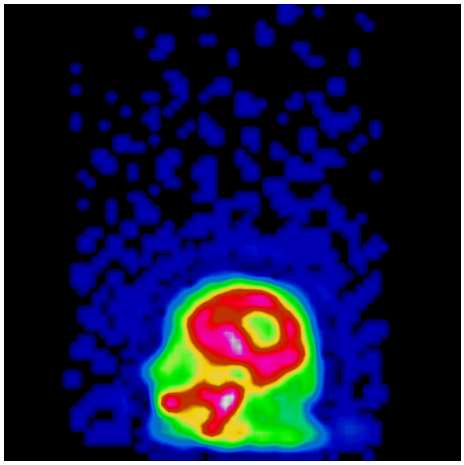

Fig.6.4.1.3: prefiltered projection.

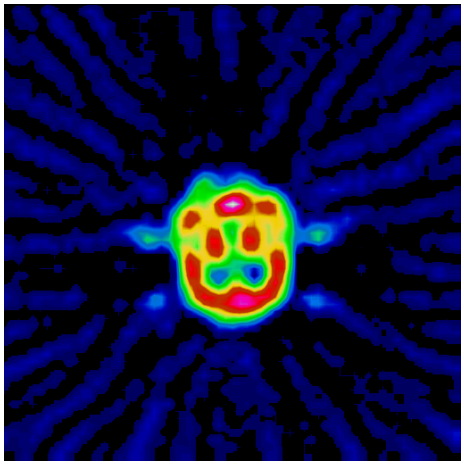

Fig.6.4.1.4: cross-sectional of prefiltered study

The image of the Figure 6.4.1.4 looks much sharper than the one in Figure 6.4.1.2, which shows the cumulative nature of the two filtered (the prior and the used in the reconstruction, which was the same that in Fig. 6.4.1.2).

6.4.2 Post-filtering

In Filtered-Back-Projection, it can be assumed that the post-filter is the second filter to reduce the effects of the ramp filter. In the iterative methods (MLEM or OSEM), the study is reconstructed in the first place, and a filter can be optionally applied later. These methods allow varying the number of iterations,

and consequently, it is possible to graduate the compromise between noise and spatial resolution knowing that frequencies greater than the maximum given by the inverse of the spatial resolution do not belong to the patient. In PET, the most common filter is a Gaussian function whose width is parameterized by its standard deviation and is generally applied by convolution in the spatial domain[29]. The Figure 6.4.2.1 shows the effect of applying a Gaussian filter in FBP and three iterative reconstructions using OSEM. It shows that as the number of iterations increases, the noise also grows and that the results came to be like in FBP. It also indicates that by increasing the width of the gaussian, the smoothness also increases.

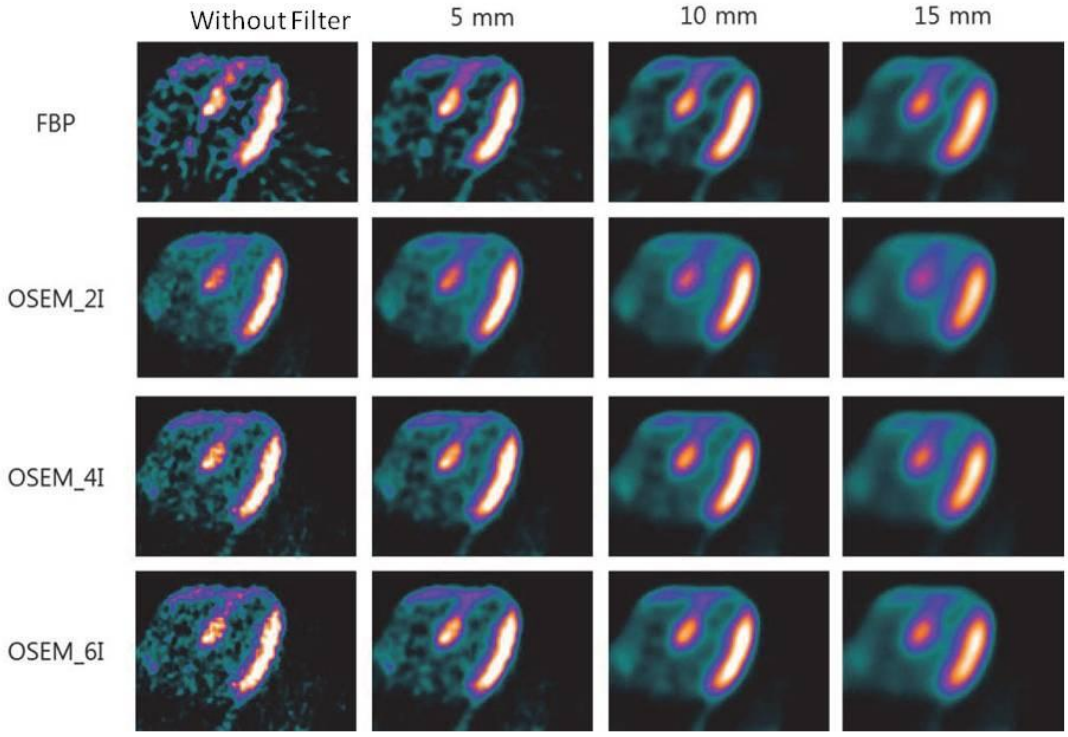

Figure 6.4.2.1: the effect of post-processing according to the method of reconstruction and the number of iterations and different widths of a gaussian filter. (Extracted from Kim et al., Asia Oceania J. Nucl. Med. Biol. 2014; 2(2):104-110.)

6.5 Quantitative aspects

The absolute quantification of the values of activity per unit volume (Bq/ml) is subject to multiple factors that make them enormously challenging to obtain in

[29] Some manufacturers insert filtering as an intermediate step between the iterations.

an accurate, reliable, and reproducible way. These factors are grouped into three origins.

6.5.1 Factors from the patient

The first factor is the source of radiation, that is to say, the own patient (accidental and physiological movements), the random nature of the radiation and its interaction with the patient (Compton scattering and attenuation). Nowadays, thanks to the hybrid techniques (PET/CT, SPECT/CT, PET/MRI) and iterative reconstruction algorithms, the attenuation is corrected in the clinical practice. It is essential to bear in mind that the images obtained through two different modalities can generate serious errors if they have registration errors (misplacements between different imaging modalities) as they assign incorrect attenuation coefficients. It is necessary, therefore, to have well-controlled the quality of the superposition of the images of both modalities. The more "exact" correction of the Compton effect is computationally complicated and currently left out of the clinical application[30]. However approximate methods are used, such as the acquisition with a double or triple window or by introducing changes in mathematical expressions of the iterative methods. The accidental movement of the patient is a problematic correction that must employ external methods of registration. The effects of the physiological movement are reduced using acquisitions synchronized (heart, chest).

6.5.2 Factors from the imaging devices

The second factor is the detection of radiation itself because the imaging systems have two significant limitations as are the dead time (so that the activity detected and the issued from the patient may not be proportional) and a low spatial resolution. These facts that limit the capacity to distinguish areas of small dimensions make the activity of these lesions to be determined erroneously due to partial volume effect[31]. Also, the spatial resolution is not the

---

[30] Klein-Nishima equation should be solved in each iteration to consider the relativistic Compton scattering.

[31] The partial volume effect occurs due to the PSF spreads the activity detected in a greater extension than the original. This dispersion causes the activity in the lesion to be less hot (effect "spill out") because it "moves" activity toward the outside and in cold lesions introduce activity from "around" inward. (effect "spill-in") causing the lesion appear less col

same throughout the field of view, both in gamma cameras as in PET scanners, which introduces a variation according to the location of the detections. In SPECT, a single average PSF is used because there is a more critical variation of the PSF with the distance to the patient due to the collimators than the change through the field of view[32]. On the other hand, the resolution in the PET tomographs depends on the distance to the center of the field of view. Currently, these defects or degradations are corrected in large part with the iterative reconstruction methods that incorporate them in the model of the imaging system.

6.5.3 Factors from processing

The third source of factors that influence uptake values is processing. The values depend on how they are derived, that is, the method of reconstruction, the filters, and the parameters used, the delimitation of areas of interest. Either you have sophisticated equipment or a basic one, it is important to bear in mind that the person who processes the studies has a great capacity to influence the outcome by altering, for example, the number of iterations and "subsets" if he is using OSEM and changing the filter of post-processing. If he uses the filtered backprojection, the effect of the smoothing filter or restoration is significant. Remember that all filters act, in short, by changing the values of the pixels and that each filter causes a variation in the number of counts in a different manner. Consequently, if studies use the comparison of numeric values of activities, areas, indexes, Standard Uptake Values (SUV), etc., the same method of reconstruction and the same filtering in all the scans must be used.

6.5.4 Dependence of values with filters. An example.

Filters can vary the extent of areas of interest and the number of counts without that their effects could be "canceled," as is shown in the following example, in which a single study of brain SPECT has been reconstructed with FBP and eight different filters. In each reconstruction the same cross-sectional has been selected, using the same areas of interest. 6 areas were selected: the brain

---

[32] In SPECT it is important to have obtained experimentally the tomographic spatial resolution in a scattering media (water) to use as a reference for the maximum useful frequency to be used when filtering.

(area 0), right parietal (area 1) and left parietal (area 2), front (3), occipital area (area 4) and background (area 5). With the average values of each area, different indexes were calculated:

I1: parietal right /left parietal
I2: right parietal/global
I3: right parietal/occipital
I4: frontal/occipital
I5:left parietal/background

The results are shown in Figure 6.5.1, in which the filters have the following numbering: 1= Restoration "A" , 2= Hann , 3= None (FBP reconstruction without a second filter), 4= Parzen, 5= Hamming, 6= Butterworth (4, 25%), 7= Restoration "B", 8=Shepp-Logan.

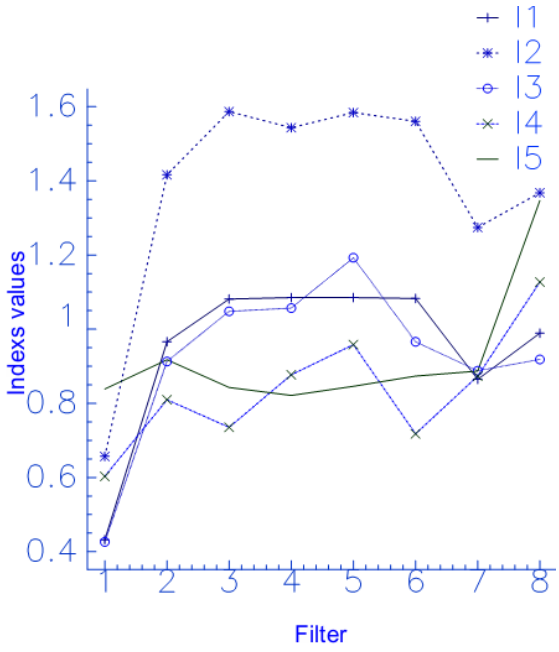

Fig. 6.5.1: variation in indexes due to the applied filter.

The restoration filters 1 and 7 have different behavior from the rest. Of note is the stability of the index I3 with filters 2,3,4,5 and 6 compared to the high variability that presents the index I5.

By grouping the average values of all areas, the variation of the number of counts in function of the filter (Figure 6.5.2) is obtained in which it is clear that the 1,3 and 7 filters behave differently than the rest, which is consistent

because 1 and 7 are restoration filters and 3 consists in not apply anything and the others are smoothing filters.

A usual way of generating areas of interest is using isocontours, that is to say, the automatic outline of regions of interest whose contour encompasses the pixels that are above a certain percentage of the maximum value. The results obtained in the average value when using this alternative method are illustrated in Figure 6.5.3. The curves show total parallelism with those of Figure 6.5.2, and again highlighted the alteration of the values for the filters.

This requires extreme caution in obtaining quantitative parameters and the comparison of results.

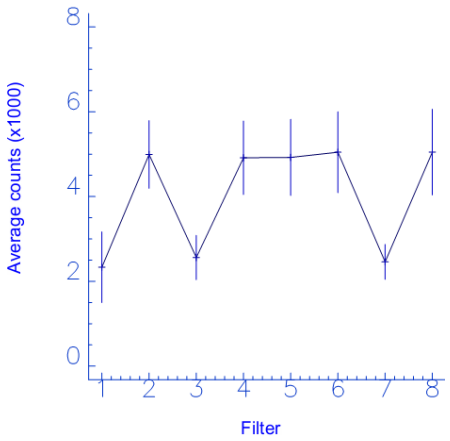

Fig. 6.5.2: variation, according to the filter (mean and standard deviation)

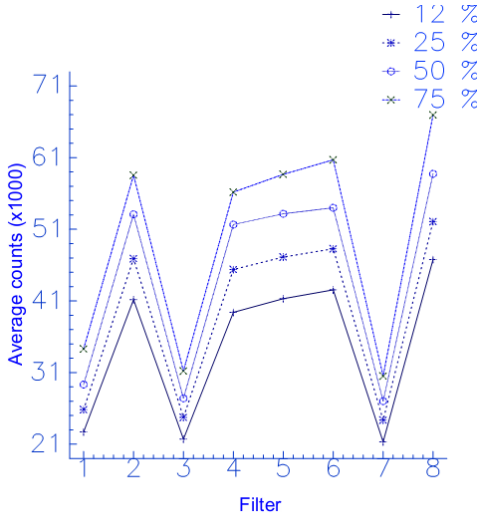

Fig.6.5.3: variation of the number of average counts with isocontours with 4 thresholds accordingto the filters.

PET, whose significant contribution is to be able to make a more reliable quantification than in SPECT, is also subject to the method of reconstruction, and with the filter used in the post-filtering. For example, Figure 6.5.4 shows how the process alters the values of SUV from OSEM to an improved iterative method.

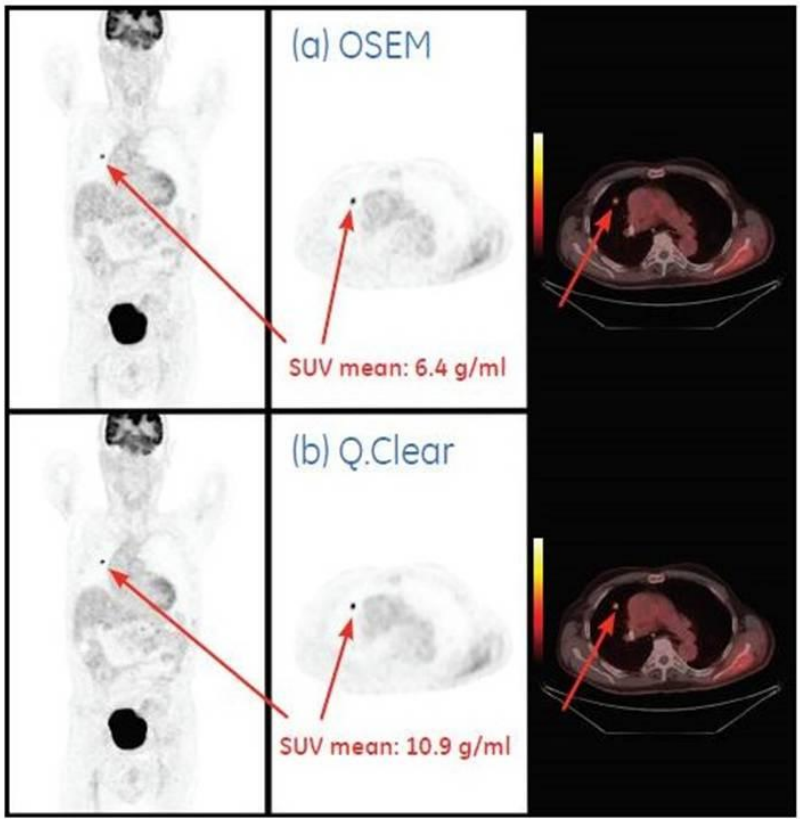

Fig.6.5.4 Variation of the values of SUV with the method of reconstruction (extracted from Steve Ross, Q.Clear, GE Healthcare)

The change of width of the gaussian parametrized by its standard deviation (σ) applied as post-filter also alters the values of SUV.

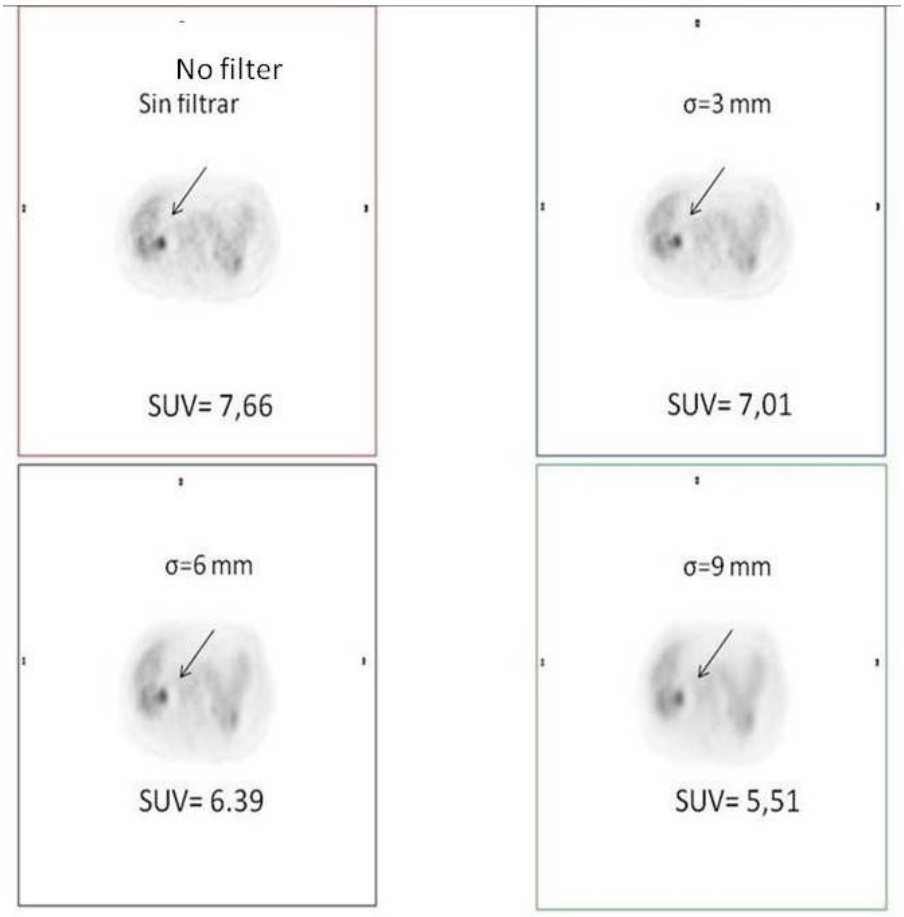

Figure 6.5.5: variation of the SUV according to the applied filter

One last comment: Given the extreme dependence of the results with the processing method, in both SPECT and PET, many times it is advisable to carry out a double process. One, systematic and unchanged for the quantification and comparison of numerical results and another to obtain images for a visual interpretation that facilitates the diagnosis.

Appendix 1: Filters implemented in SPECT and PET

The processing equipment in Nuclear Medicine allows the user to choose and design their filters. To have a reference for the assessment of the effects of a given filter on an image, below are the results of applying a series of filters to two images. One, the image of a bar-phantom to appreciate the variations of resolution that are implicit in the filtration, and another of a phantom of the brain that corresponds to a tomographic slice to observe these effects on a more clinical image.

Here are only their graphical representations for specific values of their parameters and their effect on the two test images.

There are four types of filters. The first one is common for filters with different names but with quite similar or almost identical behavior. It comprises the Hann, Hanning, Hamming, Shep-Logan and Parzen filters. The second one is the Gaussian filter, which is included due to the extensive presence in almost all computers, both in SPECT and PET. The third filter is the Butterworth, which is the more flexible one. The last one is the Metz filter as an excellent example of a restoration filter.

Due to changes in terminology between manufacturers, the filters are classified by their names. It is also indicated the parameters that define them. The images are in black and white to make them independent of the color table. Also, it has been considered appropriate to use a scale of frequencies (0-100) as a percentage of the Nyquist frequency. In this way, it is easily adaptable to the system of each manufacturer.

It is essential to note that with the filters, there is no total unanimity between the different brands of computers for Nuclear Medicine. Each manufacturer introduces variations that must be known in advance to be able to compare and reproduce results from other manufacturers or authors[33]. They also can use different ways of expressing the frequencies which are described in appendix 2.

[33] See, for example, Puchal R. Filtros de imagen en Medicina Nuclear -Apéndice 2 and Lawson R.S. et al. An audit of manufacturers' implementation of reconstruction filters in single-photon emission computed tomography. Nuclear Medicine Communications, 2013, 34:796-805, for their mathematical expression.

A1.1 Generic lowpass (Hamming, Hann, Parzen, Shepp-Logan)

Parameter: v_c (cutoff frequency).

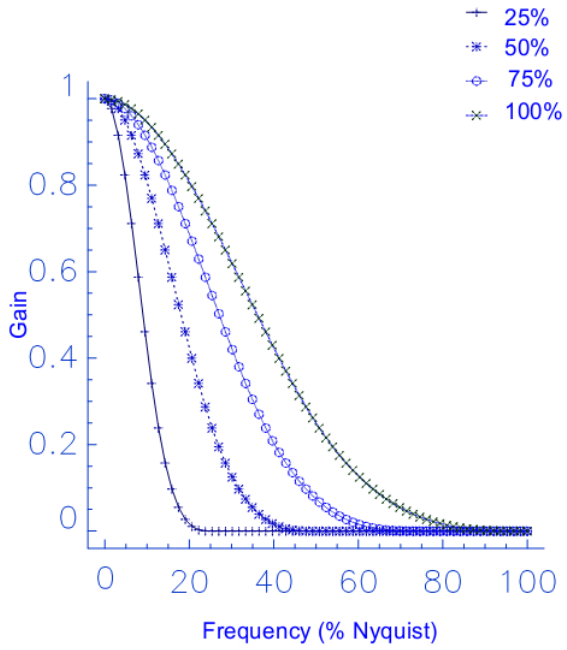

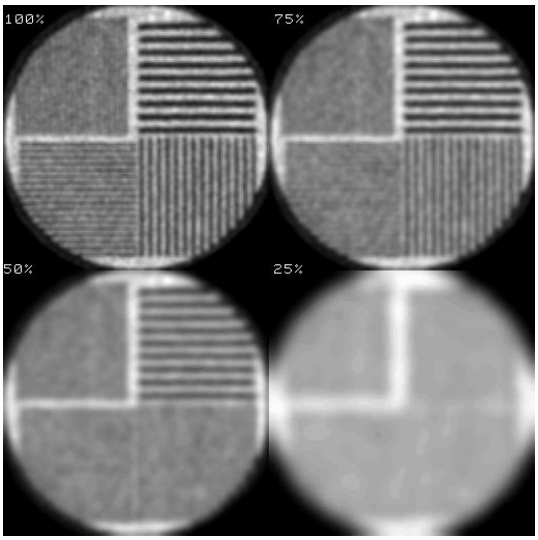

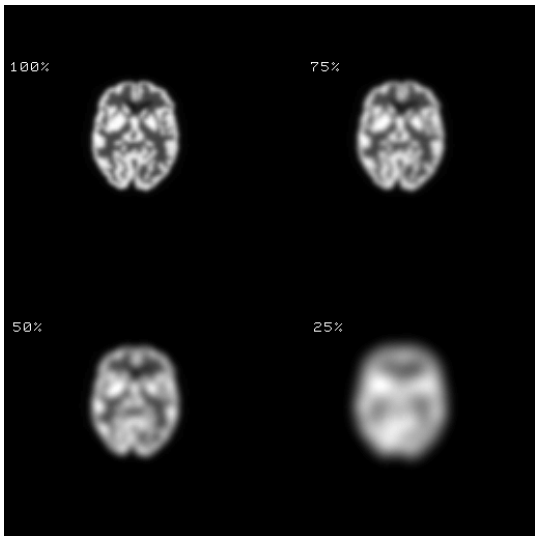

A1.2 Gaussian

Parameters: a (center), b (standard deviation)

<u>A1..2.1 dependence on the center:</u>

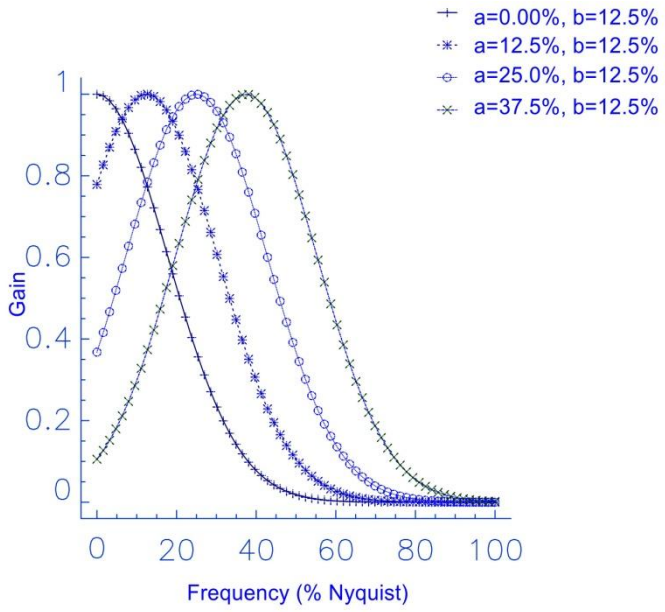

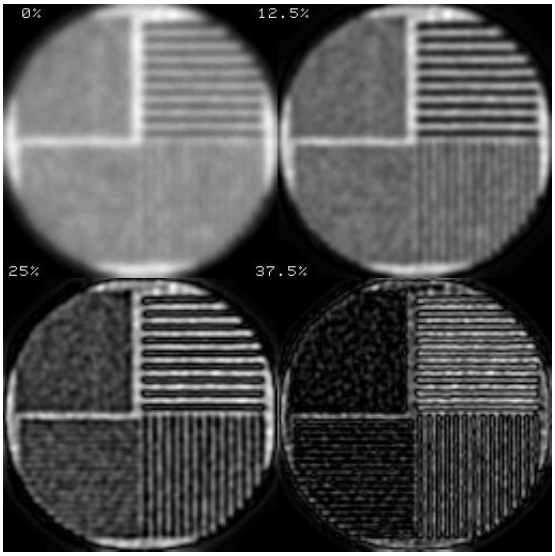

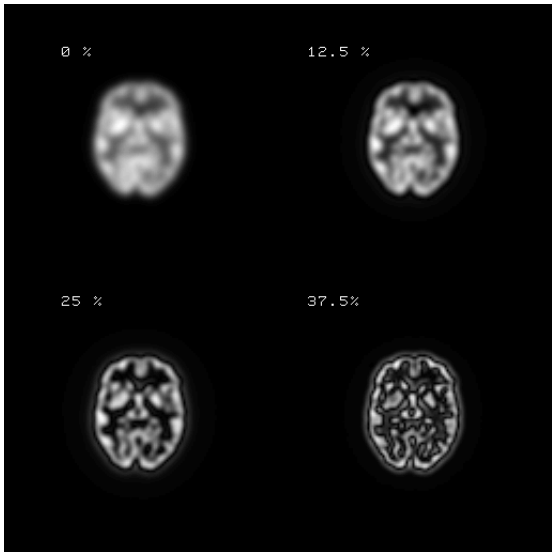

A1.2.2 Dependence on the standard deviation (b)

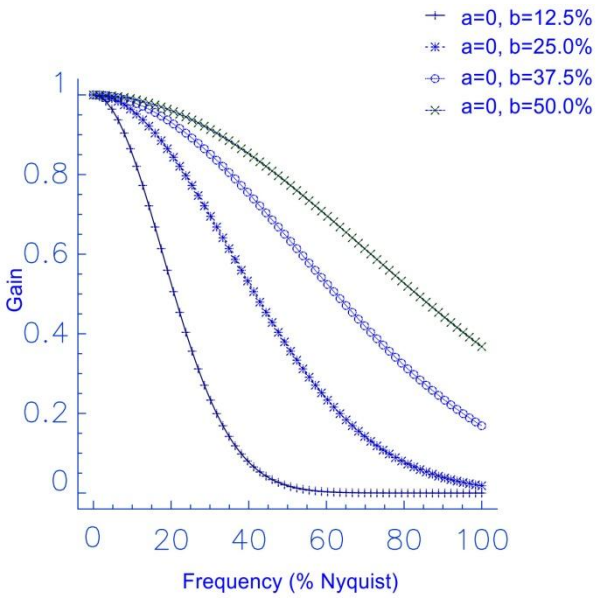

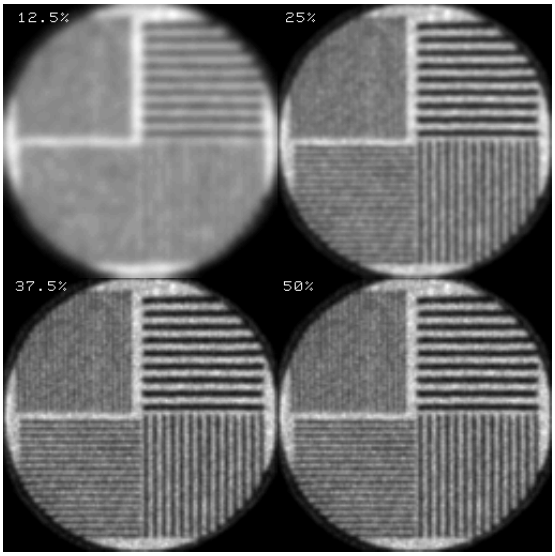

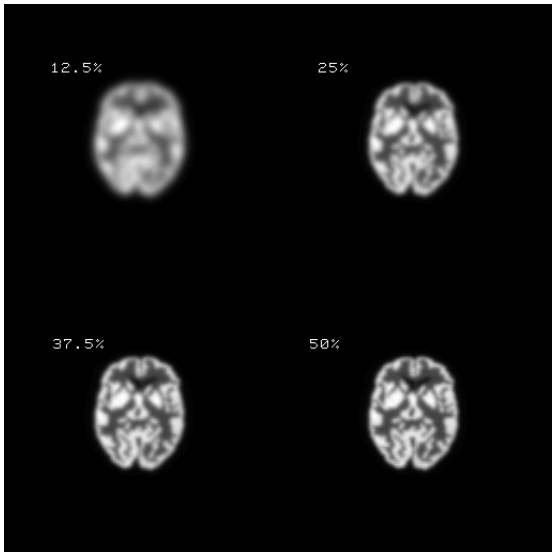

A1.3 Butterworth

Parameters: Order (n), v_c critical frequency

A1.3.1 dependence with the order (n)

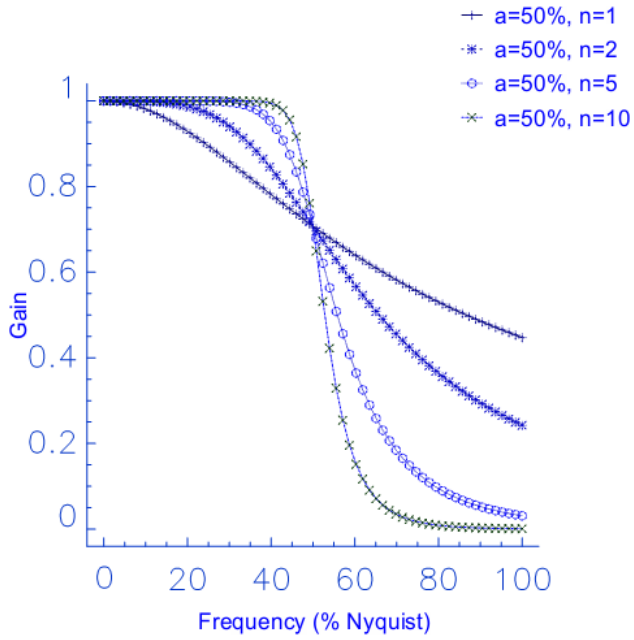

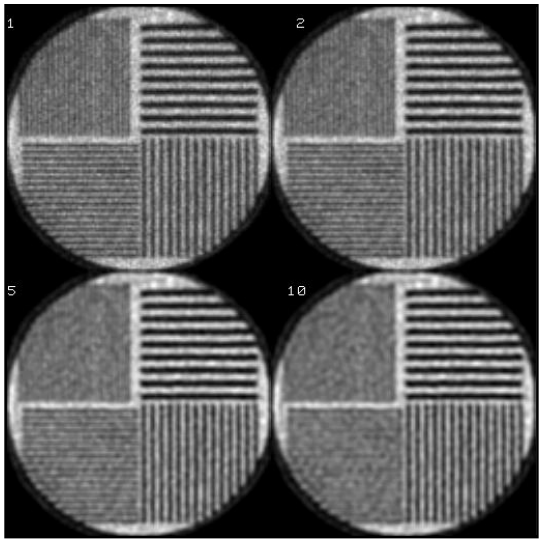

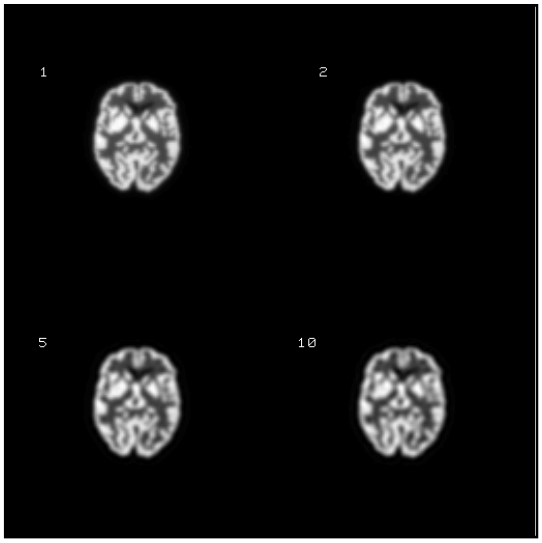

A1.3.2 dependence on critical frequency v_c

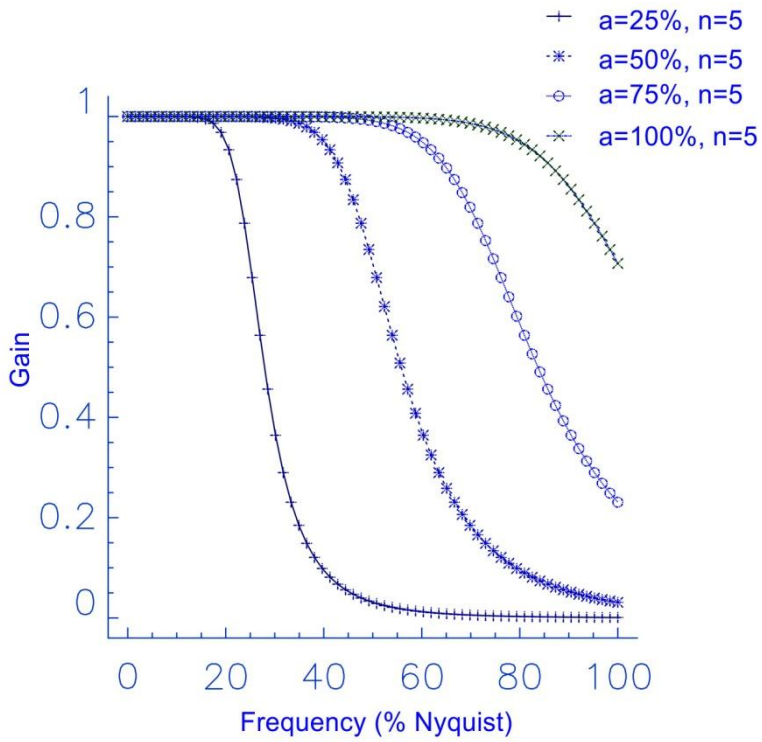

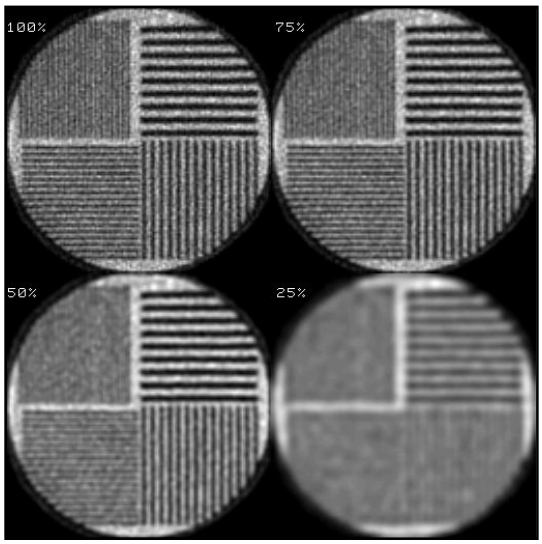

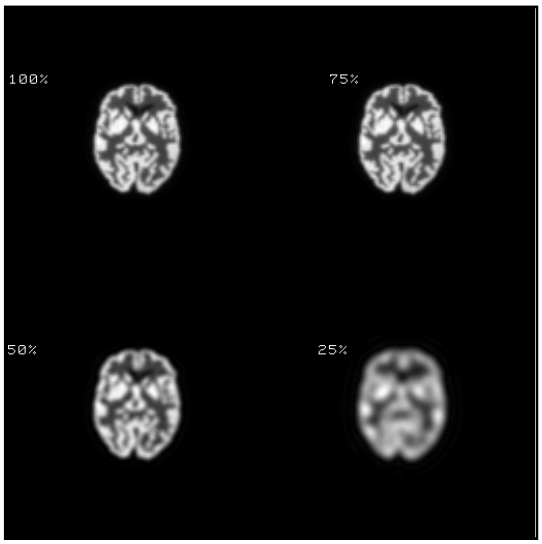

A1.4 Metz

Parameter: depending on the manufacturer there is one or two parameters: the FWHM, which depends on the distance and the collimator and the X factor of amplification that are to be entered by the user or only the X factor because the computer automatically identifies the collimator and the turning radius in SPECT.

A1.4.1Dependence with the X factor

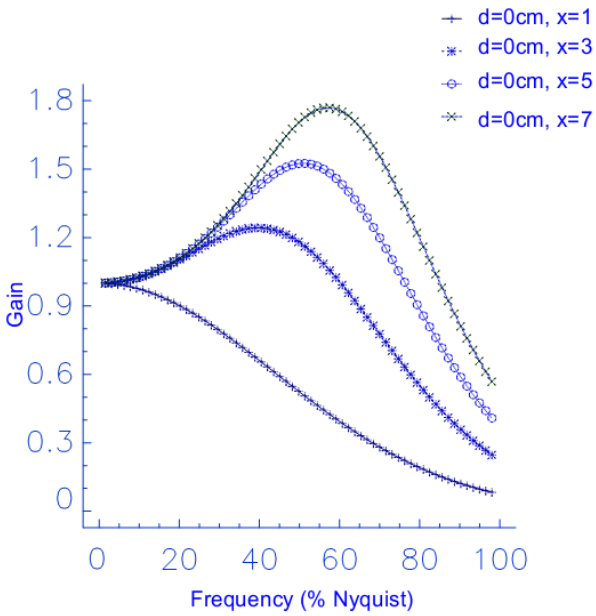

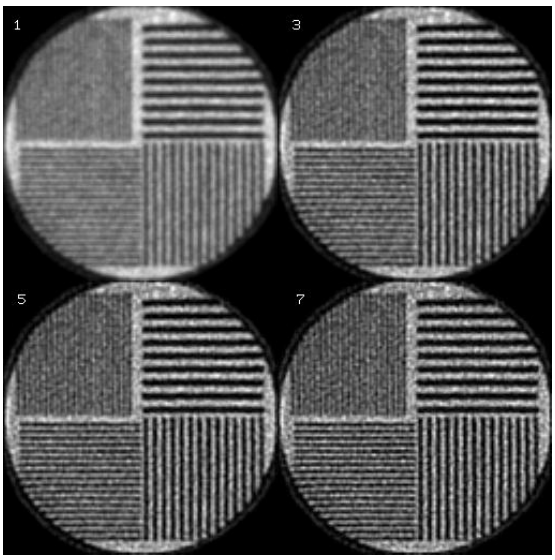

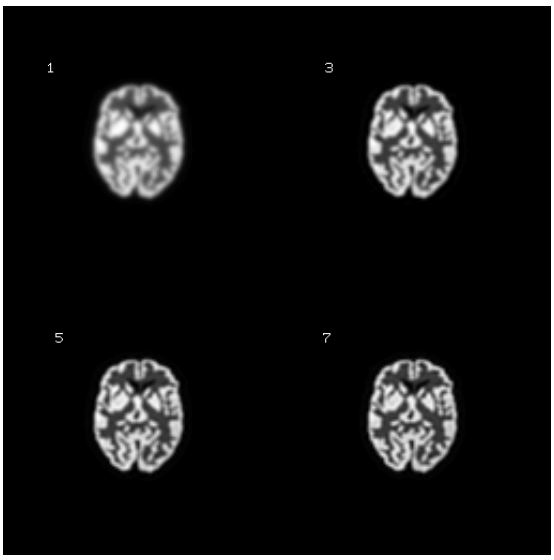

A1.4.2 dependence with distance

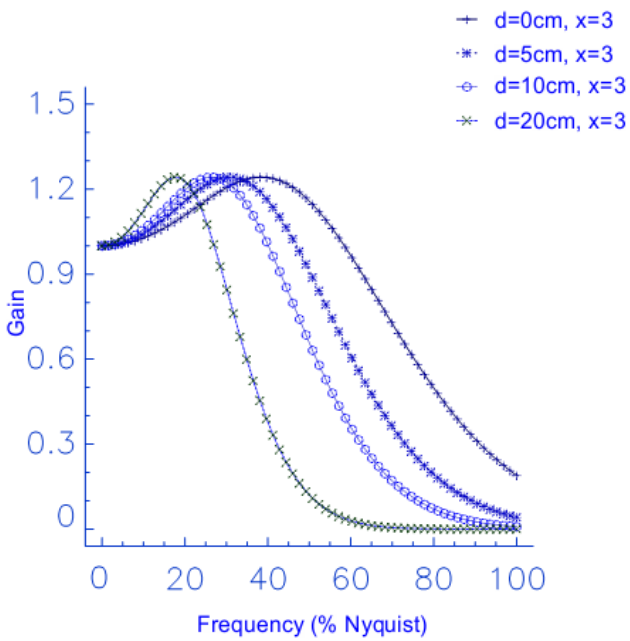

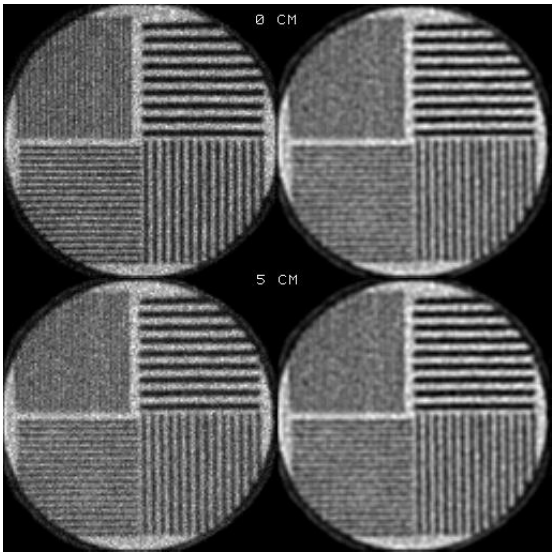

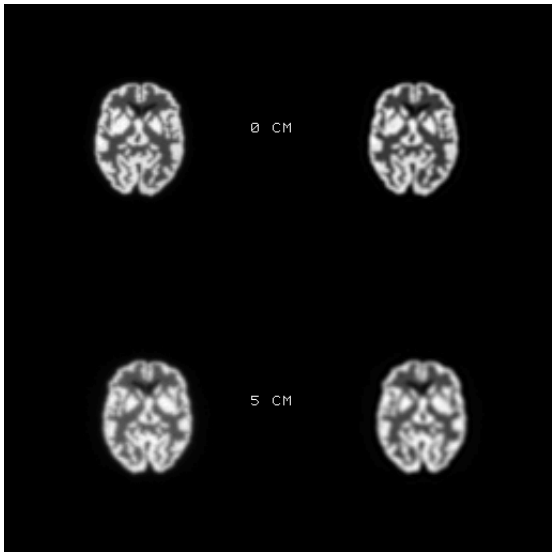

Appendix 2: Note on the units of frequencies

The units of frequency in [length^{-1}] as [cm^{-1}] or [mm^{-1}] is absolute, that is, applicable to all equipment. Unfortunately, several Nuclear Medicine computer manufacturers use other forms more simple but which can lead to confusion.

Remember that to achieve the same filtering in studies acquired with different pixel sizes or on separate computers, the parameters of the filter must inevitably be changed to maintain the same filtering.

Previous: The absolute frequency units can be given as 1/(unit of length) or as cycles /(unit of length) both being the same.

A) The pixel size is left "indicated" with what the real value of the frequencies will vary depending on the size of the pixel.

FNyq = 1/(2Px) = 0.5 cycles/pixel

Range of variation: 0 - 0.5

Just divide by the pixel size in cm to obtain the measurement in cycles/cm.

B) All frequencies are given as fractions of the Nyquist, assigning it the value 1:

FNyq = 1

Range of variation: 0 - 1

It is necessary to divide by the double the pixel size in cm or mm (2Px) to go to absolute units.

C) Directly employs the absolute units

FNyq = 1.5 cycles/cm (for example)

Range of variation: 0 - 1.5

Bibliography

- Abdallah Y.M.Y., Wagiallah E. Enhancement of Nuclear Medicine Images using Filtering Techniques.International Journal of Science and Research (IJSR) 3,8, 2014.

- ADAC Processing Applications. Rev A. 1995.

- Amersham Healthcare. Functional Brain Imaging with Ceretec and SPECT- a user's guide. Amersham International, 1994.

- Appledorn C.R., Oppenheim B.E., Wellman H.N. Performance measures in the selection of reconstruction filters for SPECT imaging. J.Nucl.Med .26(5)p.35, 1985.

- Apostol T.M. Análisis matemático. Ed. Reverté. S.A. 1960.

- Armstrong I.S., Kelly M.D., Williams H.A., Matthews J.C. Impact of point spread function modeling and time of flight on FDG uptake measurements in lung lesions using alternative filtering strategies. EJNMMI Physics 2014, 1:99

- Bailey D.L., Humm J.L., Todd-Pokropek A., van Aswegen A. Technical Editors. Nuclear Medicine Physics. A Handbook for teachers and Students. IAEA 2014.

- Barret H., Swindell W. Radiological Imaging vol.1, Academic Press, 1981.

- Behrenbruch C.P., Image filtering techniques in medical post-processing: an overview. Br. J.of Radiology 74: S126-132, 2004.

- Beis J.S., Celler A., Barney J.S. An Automatic Method to Determine Cutoff Frequency Based on Image Power Spectrum. IEEE Trans Nucl Sci, vol.42, no. 6, pp.2250-2254,dec 1995.

- Bieszk J.A., Hawman, E.G. Evaluation of SPECT Angular sampling effects: Continuous versus step-and-shoot acquisition. J Nucl Med 28:1308-1314, 1987.

-Budinger Th.F. Physical Attributes of Single PhotonTomography. J Nucl Med 21: 579-592, 1980

- Budinger Th.F., Derenzo S.E., Greenberg W.L., Gullberg G.T., Huesman R.H. Quantitative potentials of dynamic emission computed tomography. J Nucl Med 19:309-315, 1978.

-Buvat I. Quantification en imagerie SPECT et PET. Réunion APRAMEN - Irène Buvat - octobre 2002 - 1. http://www.guillemet.org/irene

-Buvat I. Principles of PET: reconstruction / simulations. International Workshop on Imaging, "Piero Caldirola" International Center for the Promotion of Science, Varenna, 7 septembre 2015.

-Camino JM, García MT, Puchal R. Método de control de calidad del registro de imágenes de SPECT y transmisión. Revista de Física Médica 2004;5:65-72

- Cao ZJ, Holder L-E., Chen Ch. C. Optimal number of views in 360º SPECt imaging. J Nucl Med 37:1740-1744, 1996.

- Cullom S.James, Principles of cardiac SPECT. En Cardiac SPECT Imaging, editado por E.G.DePuey, D.S. Berman y E.V. Garcia. Raven-Press 1995.

- Chesler D.A., Riederer S.J., Pelc N.J. Noise due to photon counting statistics in computed X-ray tomography. J Comput Assist Tomog 1, 64-74,1977.

- Cherry S.R., Sorenson J.A:, Phelps M.E. Physics in Nuclear Medicine. Fourth Edition. Saunders Elsevier, 2012

- Dikson, J. Positron Emission Tomography PET Physics. Module 15. Unit 29. Distance Assisted Training Programme for Nuclear Medicine Professionals. IAEA.

- Dubois F. Réconstruction des images tomographiques par rétroprojection. Revue de l´ACOMEN 1998, vol.4,nº 2.

- Domingo, A. Tratamiento digital de imágenes, Anaya 1993.

- Duarte D.D., Monteiro M.S., El-Hakmaoui F., Prior J.O., Vieira L., Pires-Jorge J.A. Influence of Reconstruction Parameters During Filtered Backprojection and Ordered-Subset Expectation Maximization in the measurement of the left-ventricular volumes and Function during Gated SPECT. J.Nucl.Med. Technol. 40:29-36, 2012.

- Dwivedi, S. Evaluating low pass filters on SPECT reconstructed cardiac orientation. Proc. SPIE, 7258, 2009.

- English R.J., Brown S.E. SPECT A primer. The Society of Nuclear Medicine 1986.

- Elser H., Henze M., Spierer F.J., Georgi P. Semiquantitative 99mTc-HMPAO-SPECT and dementia of the Alzheimer type: influence of the selection of reconstruction filter and reference region. Nuklearmed 1996;35:243-250.

- Elscint APEX SPECT Manual. August 1988.

- Erlandsson K, Buvat I, Pretorius P.H., Thomas B.A., Hutton B.F. A review of partial volume correction techniques for emission tomography and their applications in neurology, cardiology and oncology. Physics in Medicine & Biology, 2012, Volume 57, Number 21

- Evans A Ll. The evaluation of medical images. Medical Physics Handbooks, 10. Adam Hilger, 1981.

- Florez Pacheco E, Shigemi Furuie S. Variance Stabilizing Transformations in the Reduction of Poisson Noise in 3D Nuclear Medicine Images. Computing in Cardiology 2014; 41:949-952.

- Forstrom L.A., Dunn W.L., O'Connor M.K., Decklever T.D., Hardyman T.J., Howarth D.M. Technical pitfalls in image acquisition, processing and Display. Seminars in Nuclear Medicine, Vol. XXVI, No 4, 1996: PP 278-294.

- Fulton R, Hutton B.F. The computer and its application in nuclear medicine. Nuclear Medicine in clinical diagnosis and treatment. Vol.2 Ed. I.P.C. Murray, P.J. Ell. Churchill Livingstone 1994.

- Gilland D.R., Tsui B.M.W., McCartney W.H., Perry J.R., Berg J.. Determination of the optimum filter function for SPECT imaging. J.Nucl.Med. 29:643-650,1988.

- Gillen G.J. A simple method for the measurement of local statistical noise levels in SPECT. Phys.Med. Biol. 1992,37:1573-1579.

- Goris M.L., Briandet Ph.A. A clinical and mathematical introduction to computer processing of scintigraphic images. Raven Press, 1983.

- Harris F.J. On the use of windows for harmonic analysis with the discrete Fourier transform. Proc. IEEE 66: 51-83,1978.

- Huang S.Ch., Hoffman E.J., Phelps M.E., Khul D.E. Quantitation in Positron Emission Computed Tomography: 3. Effect of sampling. J.Comput. Assist Tomogr. 4:819-826, 1980.

- Huesman R.H. The effects of a finite number of projection angles and finite lateral sampling of projections on the propagation of statistical errors in transverse section reconstruction. Phys.Med.Biol,1977;22:511-521.

- Hutton B. Angular Sampling Necessary for Clinical SPECT. J Nucl Med. 1996;37:1915-1916.

- Hutton B.F., Braun M., Thurfjell L., Lau D.Y. Image registration: an essential tool for nuclear medicine**,** European Journal of Nuclear Medicine and Molecular Imaging April 2002, Volume 29, Issue 4, pp 559–577

- Hutton B.F., Braun M., Software for image registration: algorithms, accuracy, efficacy, Seminars in Nuclear Medicine Volume 33, Issue 3, July 2003, Pages 180-192

- Hutton B.F., Hudson H.M., Beekman F.J. A clinical perspective of accelerated statistical reconstruction. European Journal of Nuclear Medicine July 1997, Volume 24, Issue 7, pp 797–808

-Hutton B.F., Osiecki A. Correction of partial volume effects in myocardial SPECT. Journal of Nuclear Cardiology .July 1998, Volume 5, Issue 4, pp 402–413|

- Hutton B.F., Baccarne V.Efficient scatter modelling for incorporation in maximum likelihood reconstruction. European Journal of Nuclear Medicine December 1998, Volume 25, Issue 12, pp 1658–1665

- IAEA Health Records No. 9. Quantitative Nuclear Medicine Imaging: Concepts, Requirements and Methods. Vienna, 2014.

- IAEA Quality Control Atlas for Scintillation Camera Systems. Vienna 2003.

- IAEA Health Records No. 27. PET/CT Atlas on Quality Control and Image Artefacts. Vienna, 2014.

- IAEA. Nuclear Medicine Physics: A Handbook for Teachers and Students. Publication 1617. Vienna, 2014.

- Jarrit P.H., Kouris K. Instrumentation for brain SPET: guidelines and quantification. En New trends in Nuclear Neurology and Psychiatry. Ed. D.C.Costa, G.F.Morgan y N.A.Lassen. John Libbey & Company, 1993.

- Jarrit P.H., Whalley D.R., Skrypnuk J.V., Houston A.S. Fleming J.S., Cosgriff P.S. UK Audit of Single photon emission computed tomography reconstruction software using software generated phantoms. Nucl.Med. Communications 23, 483-491, 2002.

- Joseph P.M., Schultz R.A. View sampling requirements in fan-beam computed tomography. Med. Phys. 7: 692-702, 1980.

- Kak A.C., Slaney M. Principles of Computerized Tomographic Imaging. Classics in Applied Mathematics series 33. SIAM 2001

- Kessler R.M., Ellis J.R., Eden M. Analysis of emission tomographic scan data: Limitations imposed by resolution and background. J Comput Assist Tomogr 1984, 8(3):514-522.

-Kim HS, Cho SG, Kim JH, Kwon SY, Lee B, Bom HS. Effect of Post-Reconstruction Gaussian Filtering on Image Quality and Myocardial Blood Flow Measurement with N-13 Ammonia PET. Asia Oceania J Nucl Med Biol. 2014; 2(2):104-110.

- King M.A., Doherty P.W., Schwinger R.B., Jacobs D.A., Kidder R.E., Miller T.R.. Fast count-dependent digital filtering of Nuclear Medicine images: Concise communication. J.Nucl.Med.24:1039-1045,1983.

- King M.A., Doherty P.W., Schwinger R.B., Penney B.C. A Wiener filter for Nuclear Medicine images.Med.Phys.10:876-880, 1983.

- King M.A., Schwinger R.B., Doherty P.W., Penney B.C. Two-dimensional filtering of SPECT images using the Metz and Wiener filters. J.Nucl.Med. 25:1234-1240,1984.

- King M.A., Schwinger R.B., Penney B.C., Doherty P.W., Bianco J.A. Digital restoration of Indium-111 and Iodine-123 SPECT images with optimized Metz filters. J Nucl Med 27:1327-1336, 1986.

- King M.A., Penney B.C., Glick S.J. An image-dependent Metz filter for Nuclear Medicine images. J.Nucl.Med. 29: 1980-1989, 1988.

- King M.A., Long D.T., Brill B. SPECT volume quantitation: influence of spatial resolution, source size, shape, and voxel size. Med.Phys, 18:1016-1024,1991.

- King M.A., Coleman M., Penny B.C., Glik S.S. Activity quantitation in SPECT: A study of pre reconstruction Metz filtering and use of scatter degradation factor. Med.Phys 18(2) Mar/Apr 1991.

- King M.A., deVries D.J., Pan T-S, Pretorius P.H., Case J.A. An investigation of the filtering of TEW scatter estimates used to compensate for scatter with ordered subset reconstructions. IEEE Trans Nucl Sci, vol.44, no.3, pp:1140-1145, June 1997.

- Kotzki P.O., Mariano-Goulart D., Quiquere M., Lyonnet F., Zanca M., Rossi M.. Optimum tomographic reconstruction parameters for HMPAO brain SPET imaging: a practical approach based on subjective and objective indexes. Eur J Nucl Med 22: 671-677, 1995.

-Lawson R.S., White D., Cade S.C., Hall D.O., Kenny B., Knight A., Livieratos L. and Nijran. K. An audit of manufacturers' implementation of reconstruction filters in single-photon emission computed tomography. Nuclear Medicine Communications 2013, 34:796–805

- Lee S.W., Lee Ch. L., Cho, H.M., Park H-S., Kim D-H, Chor Y-N, Kim H.J. Effects of reconstruction parameters on image noise and spatial resolution in cone-beam computed tomography. Journal of Korean Physical Society 59,4:2825-2832, 2011.

- Lesiak J., Królicki L. Dependence of image quality on the type of filter and the "cut off" value in SPECT reconstruction using Filtered Back Projection (FBP) in examinations with Ga-67. Nowotwory Journal of Oncology vol.7,1, 19c-23c, 2007.

- Levi de Cabrejas M., Pérez A.M., Giannone C.A., Vazquez S., Marrero G. SPECT una guía práctica. ALASBIMN 1992.

-Levi de Cabrejas M. Edit. Tomografía en Medicina Nuclear. Comité de instrumentación y garantía de calidad del ALASBIMN 1999.

- Levi de Cabrejas M. Edit. Tomografía por emisión de positrones y CT. Mariana Lev de Cabrejas, 2011.

-Levin C.S. New Imaging Technologies to Enhance the Molecular Sensitivity of Positron
Emission Tomography. Proceedings of the IEEE. Vol. 96, No. 3, March 2008

- Levin C.S., Hoffman E.J. Calculation of positron range and its effect on the fundamental limit of positron emission tomography system spatial resolution. Phys. Med. Biol. **44** (1999) 781–799.

- Links J.M., Jeremy R.W., Dyer S.M., Frank T.L., Becker L.C. Wiener filtering improves quantification of regional myocardial perfusion with Thallium-201 SPECT. J Nucl Med 1990;31:1230-1236.

- Lyra M., Ploussi A. Filtering in SPECT image reconstruction. International Journal of Biomedical Imaging, article ID 693795, 2011.

- Lyra M., Ploussi A., Rouchota M., Synepia S. Filters in 2D and 3D Cardiac SPECT Image Processing. Cardiology Research and Practice, Article ID963264, 2014.

- MacIntyre W.J., Go R.T., O'Donnell J.K., Feiglin D.H.I., Houser T.S., Sufka B.J., Saha, G.B. Thallium-201 and Technetium-99m-pyrophosphate- single photon emission computed tomography. En "Effective use of computers in Nuclear medicine." Michael J. Gelfand, Stephen R. Thomas McGraw-Hill, 1988.

- Madsen M.T. A method for obtaining an approximate Wiener filter. Med.Phys. 17:126-130, 1990.

- Manthey N., Tausig A., Pachmayer F., Walser R., Slotty D., Knesewitsch P., Tatsch K., Hahn K. The influence of restorative and smoothing 3D filters on ECT measurements of an anthropomorphic heart phantom using nonuniform attenuation correction. Eur J Nuc Med. 1997;24: p.879 (A:15.3).

- Martí J.M., Puchal R. Optimización de la imagen de SPECT. Rev.Esp.Med.Nuclear,14,3 (111-115), 1995.

- Martín-Viera J.M., Carrasco P. , Ribas M. Control de calidad del registro intermodal de imágenes SPECT-CT con un maniquí no específico. Revista de Física Médica 2006; 7(3): 113-121

- Mazziotta J.C., Phelps M.E., Plummer D., Kuhl D.E. Quantitation in positron emission computed tomography:5. Physical-anatomical effects. J. Comput Assist Tomogr 5(5):734-743, 1981.

- McQuaid S.J., Hutton B.F. Sources of attenuation-correction artefacts in cardiac PET/CT and SPECT/CT. European Journal of Nuclear Medicine and Molecular Imaging, 2008, 35, 6, pp 1117–1123

- Mettler F.A., Guiberteau M.J. Single photon emission computed tomography. En Essentials of Nuclear Medicine Imaging. 3era Edición. W.B.Saunders Company, 1991.

- Metz Ch.E., Beck R.N. Quantitative effects of stationary linear image processing on noise and resolution of structure in radionuclide images. J Nucl Med 1974;15:164-170.

- Miller T.R., Sampathkumaran K.S. Design and application of finite impulse response digital filters. Eur J Nucl Med 7:22-27, 1982.

- Miller T.R., Sampathkumaran K.S. Digital filtering in Nuclear Medicine. J.Nucl.Med. 23:66-72, 1982.

- Miller T.R., Rollins E.S. A practical method of image enhancement by interactive digital filtering. J.Nucl.Med. 26:1075-1080,1985.

- Mishima S., Maruno H, Yui N, Kinoshita F., Kubota M., Berger KL., Uchida Y., Uno K., Arimizu N. Optimization of Butterworth filter for brain SPECT imaging. Annals of Nuclear Medicine 7(2):71-7,1993 (May).

- Montz H.R. Filtros y representaciones de las imágenes de SPECT cerebral. Rev.Esp.Med.Nuclear 14:261-266, 1995.

- Moses W.W. Fundamental limits of spatial resolution in PET. Nuclear Instruments and Methods in Physics Research A 648 (2011) S236–S240

-O'Connor Michael K. Instrument - and computer related problems and artifacts in Nuclear Medicine. Seminars in Nuclear Medicine, vol.XXVI,4,1996:pp256-277.

- Nuclear Medicine Software Quality Group. Institute of Physics and Engineering in Medicine (IPEM). Conversion of SPECT filters.

- Oppenheim B.E., Appledorn C.R. Single Photon Emission Computed Tomography. En. Effective use of Computers in Nuclear Medicine. En "Effective use of computers in Nuclear medicine." Michael J. Gelfand, Stephen R. Thomas McGraw-Hill, 1988.

- Pandey A.K., Pant G.S., Malhotra A. Standardization of SPECT filter parameters. IJNM 19(2): 30-35, 2004.

- Papoulis A. Sistemas digitales y analógicos, transformadas de Fourier, estimación espectral. Marcombo Boixareu Editores, 1978.

- Parker J.A. Quantitative SPECT: basic theoretical considerations. Seminars in Nuclear Medicine vol. XIX, 1989: pp 3-12.

- Pedroso de Lima J.J. Nuclear Medicine and Mathematics Eur J Nucl Med 1996;23:705-719

- Perez-Garcia H., Barquero R. The HURRA filter: An easy method to eliminate collimator artifacts in high-energy gamma camera images. Rev Esp Med Nucl Imagen Mol 2017;36:27-36

-Phelps M.E. Emission computed tomography. Seminars in Nuclear Medicine vol 7,1977 pp 337-365.

- Phelps M.E-Edt. PET: molecular imaging and its biological applications. Springer 2004

- Picker. SPECT processing reference. 1994.

- Pratt W.K., Digital Image Processing. John Wiley & Sons, 1979.

- Prince J.L., Links J.M. Medical Imaging Signals and Systems. Pearson Prentice Hall 2006.

- Puchal R. Restauración variante de imágenes en Medicina Nuclear. Tesis doctoral. Universidad de Barcelona 1988.

- Puchal R. Filtros de imagen en medicina nuclear. Ediciones Eurobook, S.L., 1997

- Ralston A. Introducción al análisis numérico. Editorial Limusa 1978.

- Rosenthal M.S., Cullom J., Hawkins W., Moor S.C., Tsui B.M.W., Yester M. Quantitative SPECT imaging: A review and -recommendations by the focus committee of the Society of Nuclear Medicine Computer and Instrumentation Council. J.Nucl.Med.36: 1489-1513,1995.

- Ross S. Q.Clear, GE Healthcare, 2014.

- Rossmann K. Point Spread Function, Line Spread Function and Modulation Transfer Function. Radiology 93:257-272, 1969.

- Saad W.H.M., Mahdi M.A., Saion E, Hashim S., Saripan M.I. Iterative Parameter Estimation for Metz Filter, based on the image Quality of Breast Cancer Imaging. Engineering Letters 20: 2, EL 20_2_20, 2012.

- Sadrmontaz A., Taherparvar P. The influence of filters on the SPECT image of Carlson phantom. J.Biomedical Science and Engineering, 6:291-297, 2013.

- Sadrmontaz A. Compensation effect of the implementation of filters in use of unsuitable collimator in SPECT images. International Journal of the physical sciences, 6(17) 4154-4160, 2011

- Sankaran S., Frey E., Gilland K.L., Tsui B. Optimum Compensation Method and Filter Cutoff Frequency in Myocardial SPECT. A human observer study. J.Nucl.Med. 43:432-438, 2002.

- Sayed I., Nasrudun W.M., Effect of cut-off Frequency of Butterworth Filter on detectability and Contrast of Hot and Cold Regions in 99m-Tc SPECT. International Journal of Medical Physics, Clinical Engineering and Radiation Oncology 5: 100-109, 2016.

- Seret A., Forthomme J. Comparison of Different Types of Commercial Filtered Backprojection and Ordered-Subset Expectation Maximization SPECT Reconstruction Software. J Nucl Med Technol 37:179-187, 2009.

- Serra I., Vilanova R., Introducció al tractament del senyal. Universitat Autònoma de Barcelona, 1995.

- Sharp P.F., Dendy Ph.P., Keyes W.I. Radionuclide Imaging Techniques. Academic Press, 1985.

- Sik Kim H., Cho S.-G., Kim J.H., Kwon S.Y., Lee B., H.-S. Bom. Effect of Post-Reconstruction Gaussian Filtering on Image Quality and Myocardial Blood Flow Measurement with 13-N Ammonia PET. Asia Oceania Journal of Nuclear Medicine & Biology 2(2):104-110, 2014.

- Sowa-Staszczak A., Lenda-Tracz W., Tomaszuk M., Glowa B., Hubalenska-Dydejczyk A. Optimization of image reconstruction method for SPECT studies performed using [99mTc-ZDDA/HYNIC] octreotate in patients with neuroendocrine tumors. Nuclear Medicine Review 16, 1:9-16, 2013.

- Siemens Medical Solutions. Inside Biograph TruePoint PET•CT.

- Siemens Brochure. Are you HD ready? Siemens Medical Solutions, 2007

- Siemens. Operating Instructions SPECT User´s Guide for microDelta/Maxdelta. 1992.

- Soliman S.S., Srinath M.D. Continuous and discrete signals and systems. Prentice-Hall International Editions, 1990.

- Sopha Medical systems. XT processing guide: Filter generation and selection. 1994.

- Sorenson J.A, Phelps M.E. Physics in Nuclear Medicine. 2ª Edición. W.B.Saunders Company, 1987.

-Streit R.L. Poisson Point Processes. Imaging, Tracking and Sensing. Springer 2010

- Takavar A., Samsipsour Gh., Sohrabi M., Eftekhavi M. Determination of optimum filter in myocardial SPECT: A phantom study. Iran J. Radiat. Res-1 (4):205-210, 2004.

-Taylor D. Filter choice for reconstruction tomography. Nuclear Medicine

Communications (1994) 15, 857-859.

- Thomson B., Cullis J., O'Brien J. Manufacturers and Filters. Is it all still a bit fuzzy? City Hospital, Birmingham

- Todd-Pokropek A. Theory of tomographic reconstruction. Tomographic Methods in Nuclear Medicine: Physical principles, instruments and clinical applications. Ed. Bhagwat D. Ahluwalia. CRC Press, 1989.

- Todd-Pokropek A., di Paola R.. The use of computers for image processing in Nuclear Medicine. IEEE Transaction on Nuclear Science 19:1299-1309, 1982.

- Todd-Pokropek A. Image processing in Nuclear Medicine. IEEE Transactions on Nuclear Science 27: 1080-1094,1980.

- Tsui B.M.W. Emission Computed Tomography and Image reconstruction methods. Division of Medical Imaging Physics. The Russell H.Morgan. Department of John Hopkins Radiology and Radiological Science.

- Varga S., Bettinardi V., Gilardi M.C., Riddel C., Castiglioni I., Rizzo G., Fazio F. Evaluation of pre and post-reconstruction count-dependent Metz filters for brain PET studies. Med. Phys. 24(9) September 1997.

- Vakhtangandze T., Hall D.O., Zanamiri F.V-, Rees M.R. The effect of Butterworth and Metz reconstruction filters on volume and ejection fraction calculations with 99m-Tc gated myocardial SPECT. Br J Radiology 78,nº 932, 2005.

- Verhoeff N.P.L.G., Buell U., Costa D.C., Kirsch G., Lottes G., Moretti J.L., Podreka I., Schober O., van Royen E.A. Basics and Recommendations for Brain SPECT. Nucl. Med. 31: 114-131, 1992.

- Webb S., Flower M.A., Ott R.J., Leach M.O., Inamdar R.. The spatial resolution of a rotating gamma camera tomographic facility. Br. J. Radiol. 56: 939-944, 1983.

- Webb S. Edit. The physics of medical imaging. Adam Hilger, 1988.

- Wells R.G., Sinkin, Judy P.F., King M.A., Pretorius P.H., Gifford H.C. Med Phys 26(7) July 1999.

- Wernick M.N., Aarsvold J.N. Edt. Emission Tomography: The fundamentals of PET and SPECT. Elsevier Academic Press 2004

- Wright G.A., McDade M., Martin W., Hutton I. Quantitative gated SPECT: the effect of reconstruction filter on calculated left ventricular ejection fractions and volumes. Phys.Med.Biol 47, N99-N 105, 2002.

- *Ye J., Song X., Durbin M. K., Zhao M., Shao L., Garrard J., Rollo F.D.* SPECT image quality improvement with Astonish software. Philips Medical Systems Nuclear Medicine Milpitas, CA

-Yokey T., Shinohara H., Onishi H. Performance evaluation of OSEM reconstruction algorithm incorporating three dimensional distance dependent resolution compensation for brain SPECT: A simulation study. Annals of Nuclear Medicine. February 2002, Volume 16, Issue 1, pp 11–18.

- Zaidi H. Edit. Quantitative Analysis in Nuclear Medicine Imaging. Springer 2006.